DEVELOPMENT OF NANO-ARCHITECTURE SYSTEMS FOR HIGH-EFFICIENCY TUMOR-TARGETED DRUG DELIVERY

A Dissertation
Submitted to the Graduate Faculty
of the
North Dakota State University
of Agriculture and Applied Science

By

Babak Mamnoon

In Partial Fulfillment of the Requirements
for the Degree of
DOCTOR OF PHILOSOPHY

Major Department:
Pharmaceutical Sciences

April 2021

Fargo, North Dakota

North Dakota State University
Graduate School

Title

DEVELOPMENT OF NANO-ARCHITECTURE SYSTEMS FOR HIGH-EFFICIENT TUMOR-TARGETED DRUG DELIVERY

By

Babak Mamnoon

The Supervisory Committee certifies that this ***disquisition*** complies with North Dakota State University's regulations and meets the accepted standards for the degree of

DOCTOR OF PHILOSOPHY

SUPERVISORY COMMITTEE:

Sanku Mallik
Chair

Sathish Venkatachalem

Kristine Steffen

Mohiuddin Quadir

Approved:

04/12/2021
Date

Jagdish Singh
Department Chair

ABSTRACT

Breast cancer is the most common malignancy and the second leading cause of death among women in the United States. The commonly used breast cancer treatment strategies include surgery, chemotherapy, radiation, and hormonal therapy. Since chemotherapeutic agents do not adequately differentiate between normal and cancerous cells, systemic toxicity and adverse effects associated with these anticancer drugs limit their therapeutic efficacy. In addition, uncontrolled cell proliferation and insufficient blood supply produce low oxygen partial pressure or hypoxia in almost all solid tumors. Hypoxia increases cancer cell survival through aggressiveness, metastasis, and resistance to chemotherapy, leading to poor clinical outcomes. Targeted drug delivery nanoparticles can significantly reduce off-target toxicity of chemotherapy by selectively targeting tumor tissues. Polymersomes are self-assembled drug-encapsulated polymeric nanoparticles in which an aqueous core is enclosed by a bilayer membrane. To attain the appropriate therapeutic efficacy, polymersomes need to rapidly release their anticancer drug at the tumor sites. To fulfill this requirement, stimuli-responsive polymersomes have been developed. Since most of the tumors have hypoxic areas inside, hypoxia-responsive polymersomes are one of the most effective drug delivery vehicles for cancer treatment. To prepare targeted drug delivery systems, functionalizing polymersomes with specific ligands intended to be recognized by the receptors of the cancer cells, is the most common strategy.

Herein, we designed three distinct hypoxia-responsive polymersomes for targeting breast cancer tissues. More than 80% of breast cancers express estrogen receptor (ER-positive), and about 15-25% of them do not express any receptors (triple-negative). Hence, we decorated our polymersomes with three different ligands including estradiol and endoxifen for targeting ER-positive breast microtumors, and iRGD peptide for targeting triple-negative breast tumors.

ACKNOWLEDGMENTS

I would like to express my sincere gratitude to my adviser Dr. Sanku Mallik for his everlasting support and guidance through my PhD studies in his laboratory. I would like to express my thanks to my advisory committee members Dr. Sathish Venkatachalem, Dr. Kristine Steffen, and Dr. Mohiuddin Quadir for providing me with their insightful suggestions and comments.

I would like to thank our department chair Dr. Jagdish Singh and the staff Janet Krom, Diana Kowalski, and Tiffany Olson for being supportive all the time.

I would like to thank Dr. Siju Mathew and Dr. Yagna Jarajapu for letting me use their laboratory instruments and Dr. Yongki Choi for his excellent collaboration in our projects.

I would like to thank my wife, Parinaz, for designing spectacular graphical illustrations to my projects along with her great patience, love, and support.

I would like to thank Dr. Li Feng for practical contribution to my work and my lab mates Dr. Matthew Confeld, Jessica Pullan, Jacob Shreffler, and my collaborators James Froberg and Lina Alhalhooli for their great supports.

I would like to thank the Department of Pharmaceutical Sciences, the college of Health Professions, The Graduate School, and North Dakota State University for providing all facilities and supporting my work.

Last but not the least, I would like to thank my parents, my brother, and my sisters for their continuous patience and support.

DEDICATION

To my dear mother, father, and my supportive wife

TABLE OF CONTENTS

LIST OF TABLES

LIST OF FIGURES

LIST OF SCHEMES

LIST OF ABBREVIATIONS

ACS.....American Chemical Society

AFM.....Atomic Force Microscopy

ANOVA.....Analysis of Variance

ATCC.....American Type Culture Collection

BC.....Breast cancer

C.....Centigrade

CendR.....C-end Rule motif

Cys.....Cysteine

CD.....Circular Dichroism

DLS.....Dynamic Light Scattering

DMAP.....Dimethylaminopyridine

DMEM.....Dulbecco's Modified Eagle's Medium

DPPE.....1,2-dipalmitoyl-*sn*-glycero-3-phosphoethanolamine

DOX.....Doxorubicin

EDC.....1-Ethyl-3-(3-dimethyl aminopropyl)-carbodiimide

END.....Endoxifen

EPR.....Enhanced Permeability and Retention

ER+.....Estrogen receptor positive

Em.....Emission

Ex.....Excitation

HEPES.....4-(2-hydroxyethyl)-1-piperazineethanesulfonic acid

HER2.....Human epidermal growth factor receptor 2

HPLC.....High Performance Liquid Chromatography

HRP.....Hypoxia responsive polymersome

iRGD.....Internalizing Arginine-Glycine-Glutamic acid

iPs.....iRGD-conjugated polymersomes

NADPH.....Nicotinamide adenine dinucleotide phosphate

NHS.....N-hydroxysuccinimide

MW .....Molecular weight

LR .....Lissamine rhodamine B sulfonyl, ammonium salt

mM.....Millimolar

mg .....Milligram

mL .....Milliliter

mmol .....Millimole

nm .....Nanometer

NHS.....N-hydroxysuccinimide

NMR .....Nuclear Magnetic Resonance

NRP-1 .....Neuropilin-1

PBD.....Polybutadiene

PBS .....Phosphate Buffered Saline

PCL .....Polycaprolactone

PDI .....Polydispersity Index

PDMS.....Polydimethylsiloxane

PEG.....Polyethylene glycol

PLA.....Polylactic acid

PMDETA .....N, N, N′, N′, N″-pentamethyldiethylenetriamine

PR+ .....Progesterone receptor positive

SERM.....Selective estrogen receptor modulator

TAM.....Tamoxifen

TEM .....Transmission Electron Microscopy

THF .....Tetrahydrofuran

TNBC .....Triple negative breast cancer

μL .....Microliter

μM .....Micromole

UV .....Ultraviolet

3D .....Three dimensional

LIST OF APPENDIX FIGURES

1. INTRODUCTION AND DISSERTATION ORGANIZATION

1.1. Breast cancer and biomarkers

Breast cancer is the most common malignancy and the second leading cause of death among women in the United States.[1] Breast cancer is curable if diagnosed at an early stage. However, breast cancer would be hardly treatable when it metastasizes to the lymph nodes and distant organs such as bone, lung, and liver.[2,3] Biomarkers are small molecules found in tissues, body fluids, and blood which are measurable indicators of a natural or abnormal process.[4,5] The invasiveness, metastasis, recurrence, and treatment of Breast cancer have been conducted by its tissue-based biomarkers for a long time.[5,6] There are 3 major biomarkers for the breast cancer including estrogen receptor (ER), progesterone receptor (PR), and human epidermal growth factor receptor 2 (HER2).[7,8] Breast tumors are divided into subgroups based on these biomarkers, i.e., ER+PR+HER2- (tumors with either ER or PR, but without HER2), ER+PR+HER2+ (tumors with all 3 biomarkers), ER-PR-HER2+ (HER2 positive tumors), and ER-PR-HER2- (tumors without 3 biomarkers or triple negative).[9] The clinical use of biomarkers is to determine the most appropriate therapy for the breast cancer patients.[8]

1.1.1. Estrogen receptor (ER)

ERs are classified as ERα and ERβ. ERα has an important role in mammary gland development.[10] However, elevated level of ERα demonstrates an increased risk of breast cancer.[11] ERα expression in breast cancer is used for anti-hormonal therapy, including selective estrogen receptor modulators and aromatase inhibitors.[12] ERβ is expressed in about 80% of normal breast epithelial cells and its role in breast cancer is not completely clear.[13] However, five ERβ variants have been identified, ERβ1-5, that are detected in both normal tissues and breast cancer tissues.[14,15] For instance, some studies reported that ERβ2 expression demonstrated

cellular proliferation,[16] while other studies indicated the role of ERβ5 in preventing breast cancer recurrence.[17]

1.1.2. Progesterone receptor (PR)

PR is a steroid hormone receptor that is expressed in around 70% of all ER-positive breast cancers.[18] PR has two different isoforms called PR-A and PR-B with different functions.[19] It has been observed that PR-B is stronger activator of the genes than PR-A in human breast cancer cells.[20] In addition, the proliferative effects of progesterone hormone in breast cancer is mainly mediated by PR-B.[21,22] PR is used as a predictive biomarker to determine the optimum endocrine therapy for breast cancer patients.[23]

1.1.3. Human epidermal growth factor receptor 2 (HER2)

HER2 is a member of epidermal growth factor (EGF) family. HER2 is highly expressed in 20% to 30% of breast tumors.[24] HER2 overexpression causes aggressiveness, disease relapse, and shorter survival rate of the patients.[25,26] One of the most productive goals of anticancer drug development is the research into targeting HER2 agents.[27] Overall, HER2 targeting is classified into two categories: the first one consists of the drugs targeting HER2 overexpressed tumor cells which includes antibodies. The second one includes the drugs that inhibit the signaling function of HER2 such as tyrosine kinase inhibitors.[28]

1.1.4. Triple negative breast cancer (TNBC)

Triple negative breast cancer (TNBC) is a subtype of breast cancer in which the cells do not express ER, PR, and HER2.[29] The incidence of TNBC is about 10% to 15% of all breast cancer cases.[30] Triple negative breast tumors are aggressive enough to metastasize and spread to different organs such as bone, liver, lung, and central nervous system. Quantification of TNBC

biomarkers is the most important process to predict a therapeutic response and the survival rate of the patients.[31]

1.2. Drugs for breast cancer treatment

Surgery, radiation therapy, chemotherapy, and hormone therapy are the most common treatment options for breast cancer.[32] Anticancer drugs can be categorized into different groups including chemotherapeutics, hormonal drugs, anti-vascular and antigrowth factors.[33] Doxorubicin (DOX) is a chemotherapeutic drug which is a member of anthracyclines for treating various cancers including breast cancer. However, DOX has adverse side effects such as gastrointestinal or cardiac toxicity.[34] Paclitaxel (PTX) is another chemotherapy drug which hinders microtubule depolymerization and acts as a mitotic inhibitor.[35] Capecitabine and cyclophosphamide are another chemotherapeutic drugs that act as an alkylating agent by inhibiting DNA synthesis.[36,37] Since about 75% of breast cancers express ER, hormonal drugs can be a good candidate for ER+ breast cancer therapy.[38] These hormonal drugs can be classified into two groups including the ones which inhibit estrogen production (aromatase inhibitors) and the second group which are ER antagonists (selective estrogen receptor modulators, SERMs).[39] Tamoxifen is the most commonly used SERM with antagonistic activity for treating ER+ breast tumors. Tamoxifen efficacy is attributed to its two active metabolites, 4-hydroxy tamoxifen and endoxifen.[40] Raloxifene is another SERM which reduces the incidence of invasive breast cancer compared to tamoxifen which is superior to raloxifene in treating noninvasive breast cancers.[41] Anastrozole and letrozole are both aromatase inhibitors for treating early-stage breast cancer. Anastrozole is a well-tolerated drug which usually administered after tamoxifen treatment.[42] Letrozole has potential efficacy for preventing distant breast cancer recurrence and increasing survival rate of the patients.[43] HER2 positive breast cancer consists of about 20% of all breast

cancer cases. Trastuzumab is a monoclonal antibody with anti-HER2 activity which has been the first-line therapy for the HER2 positive breast cancer.[44] HER2 signaling blockade by trastuzumab improves the survival outcome in metastatic breast cancer.[45] Microtubules have been studied as potential targets for anticancer drugs. Microtubules form the spindles during metaphase-anaphase transition of cell division. Any interruption in microtubule function will induce cellular apoptosis.[46] Combretastatin is an anti-vascular agent that inhibits microtubule polymerization and causes vascular destruction and tumor cell death.[47] Combretastatin has demonstrated significant reduction in breast tumor perfusion.[48]

1.3. Nanoparticle-mediated drug delivery for breast cancer treatment

A new compound that exhibits potent biological activity but poor half-life or solubility, will not have that much chance to develop as a new drug molecule. On the contrary, poor biologically active molecules with potent pharmaceutical characteristics might have the potential to develop.[49] Nanotechnology will use the nanosized materials to overcome the hurdles of low solubility, circulation half-life, drug release, and immunogenicity.[50] Nanomedicine, the collaboration of medical sciences and nanotechnology, has provided novel perspectives towards disease therapy. A great deal of nanoparticle-mediated therapeutics has been produced for cancer treatment during the last 30 years.[51] Several types of nanoparticles have been employed for breast cancer treatment including polymersomes, liposomes, quantum dots, metal and protein-based nanoparticles, mesoporous silica nanoparticles, carbon nanotubes and dots, and so more.[7,52–54] A list of nanoparticles that have been reported in the literature are included within Table 1.1. Nanoparticles have become spectacular carriers for chemotherapeutics due to increasing solubility and bioavailability of drugs.[55] In addition, nanoparticles can be modified with specific molecules called ligands that selectively interact with overexpressed receptors on

the surface of preferred cancer cells.[56] This phenomenon is called targeted drug delivery which increases drug accumulation within breast cancer tumors and reduces undesired side effects.[57]

Table 1.1. Nanoparticles (NPs) for breast cancer treatment.

Type of NP	Drug cargo	Type of BC cell	Reference
Dendrimer	Doxorubicin	MCF-7	[58]
Micelle	Docetaxel,	MDA-MB-231	[59]
	Paclitaxel,	MCF-7	[60]
	Doxorubicin,	4T1	[61]
	Dosatinib	MDA-MB-231	[62]
Liposome	Paclitaxel	MCF-7	[63]
	Doxorubicin	MDA-MB-231	[64]
	Docetaxel	SK-BR-3	[65]
Polymersome	Doxorubicin	MCF-7	[7,66]
Exosome	Doxorubicin	BT-474, SK-BR-3	[67]
Gold NPs	Tamoxifen	MCF-7	[68]
	Docetaxel	MCF-7	[69]
	Doxorubicin	MCF-7	[70]
SPIONs	Violamycine B1	MCF-7	[71]
	Doxorubicin	MDA-MB-231	[72]
Quantum Dots	Trastuzumab	SK-BR-3, BT-474	[73]
MSNs	Doxorubicin	MCF-7	[74]
Fullerene	Docetaxel	MCF-7, MDA-MB-231	[75]
CNTs	Doxorubicin	4T1	[76]
CDs	Cisplatin	MCF-7, MDA-MB-231	[77]
Viral NPs	Trastuzumab	SK-OV-3, SK-BR-3	[78]
	Doxorubicin	MDA-MB-231	[79]
SLNs	Tamoxifen	MCF-7	[80]
	Paclitaxel	MCF-7	[81]
	Docetaxel	MCF-7	[82]
	Doxorubicin	MCF-7/ADR	[83]

1.4. Polymeric nanoparticles (polymersomes)

Polymersomes are polymeric nanoparticles that are made from synthetic amphiphilic block copolymers.[84] Polymersomes have an aqueous core which is surrounded with a bilayer membrane. This membrane has a lipophilic middle section that is sandwiched between hydrophilic polymers. Many proteins, nucleic acids, and hydrophilic drugs can be encapsulated within the aqueous core of the polymersomes.[7,85] However, lipophilic drugs can be incorporated

into the polymersome bilayer.[52,53] The relative mass of the hydrophilic block to the total mass of the copolymers which is known as hydrophilic fraction (f) determines the morphology.[86] The hydrophilic fraction for the polymersome preparation ranges between 20-40%.[87] The membrane thickness is greater than 4 nm and the molecular weight is almost high in the polymersomes.[86] Incorporation of polyethylene glycol (PEG) as a hydrophilic block into the surface of polymeric nanoparticles will increase the circulation time of the polymersomes by diminishing steric repulsion and interfacial free energy.[88]

Polymersomes can be self-assembled by either solvent-exchange method or polymer dehydration method.[89] During the solvent-exchange method, block copolymers are first dissolved in an organic solvent. Then the hydration will be carried out by either injecting the organic copolymer solution into water or via slow insertion of water to the copolymer solution. Due to enhancing interfacial tension between water and lipophilic blocks, copolymers start self-assembling into the polymersomes.[90] The self-assembly of block copolymers to polymersomes can be rendered by hydrating of copolymer films during the polymer rehydration method. In this method, organic copolymer solution will be evaporated to prepare a thin-layer film by removing the organic solvent. The film is then hydrated by adding water which penetrates among polymer layers. This results in polymer swelling, protuberance production, and surface vesicular separation.[91]

Polymerization of a monomer or accumulation of chemically and physically similar monomers produces a block copolymer. Two or more block copolymers can self-assemble to polymersomes. Various combinations of non-biodegradable block copolymers such as polystyrene (PS), polybutadiene (PBD), polyethyl ethylene (PEE), and polydimethylsiloxane (PDMS), or biodegradable block copolymers including polytrimethylene carbonate (PTMC),

polylactide (PLA), and polycaprolactone (PCL) can be used for polymersome preparation.[92] Polyglutamic acid (PGA), polyacrylic acid (PAA), and PEG are commonly used as hydrophilic blocks in the structure of the polymersomes.[93–95]

Polymersome solutions can be characterized by dynamic light scattering (DLS) which is used to evaluate size distribution, nanoparticle size, charge, critical aggregation concentration, and nanoparticle disruption.[7,95,96] Optical microscopy such as scanning electron microscopy (SEM) and transmission electron microscopy (TEM) are high resolution techniques for visualizing polymersomes (Figure 1A).[97] Polymersomes can be labeled with fluorochromes and visualized by fluorescence microscope.[92] Confocal laser scanning microscopy (CLSM) is another tool for supplying three-dimensional z-stacked images from the polymersomes.[98] Atomic force microscopy (AFM) is a functional method for measuring the size and evaluating the topography of polymersomes which employs a microscopic tip for scanning nanoparticles (Figure 1.1.B).[99]

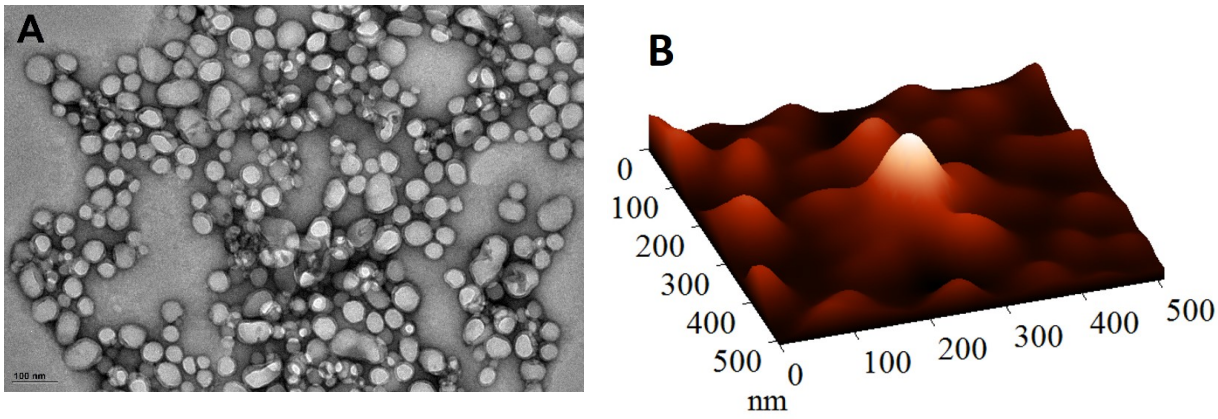

Figure 1.1. (A) TEM image (scale bar: 100 nm) and **(B)** AFM image of polymersomes.

1.4.1. Drug-encapsulation and release from polymersomes

Polymersomes are appropriate vehicles for drug delivery, diagnostics, and imaging. The amphiphilic and hydrophobic molecules, lipophilic drugs, membrane proteins, and dyes can be

incorporated into the polymersome's membrane.[52,100,101] However, the hydrophilic anticancer drugs can be encapsulated within the aqueous core of the polymersomes (Figure 1.2.).[7]

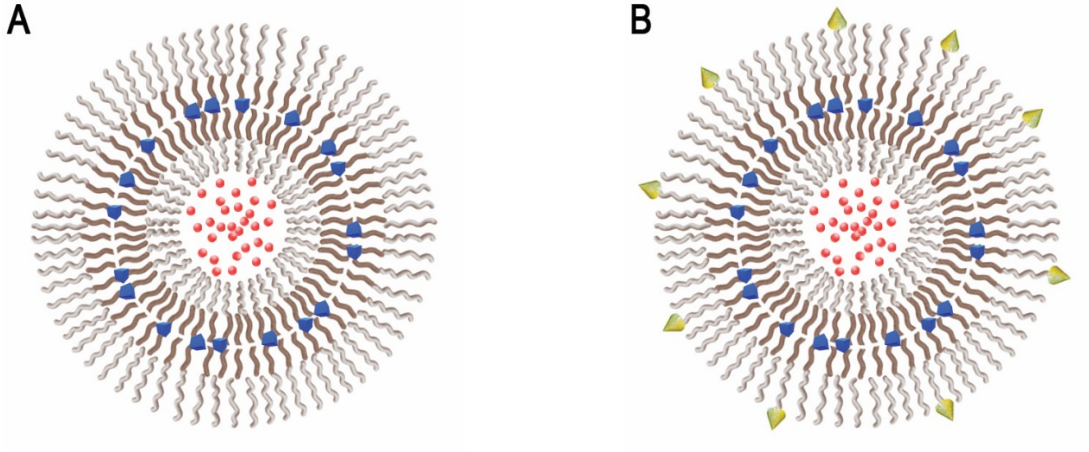

Figure 1.2. (A) Polymersomes with hydrophilic drugs (red circles) in the core and hydrophobic drugs (blue squares) in the bilayer. **(B)** Polymersomes with targeted ligands (yellow triangles).

Therapeutic drugs can be actively or passively loaded into polymersomes. In passive loading, the drug of interest is usually incorporated in the water or aqueous phase where the polymersomes form. In active loading or pH-gradient method, polar chemicals or low molecular weight drugs can pass through the polymersome membrane, ionize to get charge, and consequently are trapped inside the low or high aqueous pH of vesicle.[102] The membrane thickness of the polymersomes is robust enough to retain the encapsulated drugs for a prolonged circulation time before reaching the disease site.[103] Doxorubicin (DOX) is a potent anthracycline drug for the treatment of many types of solid tumors including breast cancer.[104–106] To reach a high DOX loading content within nanoparticles, previous studies demonstrated that generating a pH gradient (active loading) with lower pH level inside and higher level outside the membrane, enhances the amount of incorporated weak amines such as DOX into the aqueous core of the nanoparticles.[107]

Drug release from polymersomes occurs through diffusion from membrane via a driving force created from different drug concentrations between inner and outer sides of the membrane.[108] The size of the polymersome is a key factor for the drug release rate.[109] Based on the limitations related to the appropriate block copolymers used in the polymersome structure, the rate of drug release can only change within a limited range.[110]

1.4.2. Stimuli-responsive polymersomes

To optimize the polymersomes for the controlled drug delivery, some chemical and physical changes have been administered to the polymersome structure to be responsive to various stimuli. There are three types of stimuli which include chemical (i.e., pH, hypoxia, oxidation-reduction), physical (i.e., light, temperature, magnetic field), and biological (i.e., enzymes or glucose concentration) stimuli.[111–115] The pH-responsive polymersomes can carry the encapsulated drugs in blood circulation (pH 7.4) and release the drug within acidic tumor microenvironment. Hypoxia-responsive polymersomes are composed of an oxygen sensitive group such as nitroimidazole or diazobenzene which carry the encapsulated anticancer drugs in the bloodstream and release the drugs after translocating to the hypoxic niches of cancer cells.[7,116,117] Oxidation-reduction (redox)-responsive polymersomes have been made based on implementing disulfide bonds between hydrophilic and hydrophobic blocks which reversibly break under reductive environment within cells and release polymersomes' encapsulated drugs.[118] Light-responsive polymersomes are drug delivery systems that contain a photo-responsive linker such as spiropyran or diazonaphthoquinone between block copolymers which degrade by adjusting intensity of light wavelengths and release the drugs.[119] Temperature-responsive polymersomes contain a thermo-sensitive polymer block which is usually poly N-isopropylacrylamide (PNIPAAm). This polymer self-assembles into polymersomes above body

temperature to encapsulate drugs. PNIPAAm has a lower critical solution temperatire (LCST) of 32 °C which causes polymersome degradation by decreasing temperature with external stimuli and releasing encapsulated drugs.[120] Magnetic field-responsive polymeric vesicles are prepared by encapsulating paramagnetic or ferromagnetic iron oxide materials and drugs into polymersomes. An external magnetic field stimulus triggers polymersome disintegration and drug release within target tissues.[121] Enzyme-responsive nano-vesicles have been developed by incorporating an enzyme-sensitive substrate between block copolymers. Based on upregulation of some specific enzymes within disease sites, these polymersomes would disassemble and release the encapsulated drugs when subjected to the enzymes.[122] An example of enzyme-responsive polymersomes is the incorporation of Gly-Phe-Leu-Gly-Phe peptide between PEG and polylactide (PLA) copolymers which is degraded when exposed to upregulated cathepsin B lysosomal enzyme within tumor tissues.[123] Glucose-responsive polymersomes are a type of stimuli-responsive nanoparticles that are prepared by integrating various glucose-sensitive materials such as phenyl boronic acid or glucose oxidase into the polymersomes loaded with insulin.[124,125] Phenyl boronic acid is in a balance between charged/uncharged mood. When it reacts with glucose, it reversibly converts to hydrophilic form and releases encapsulated insulin from polymersomes.[126]

1.4.3. Tumor-targeted drug delivery polymersomes

Targeted drug delivery systems increase the therapeutic efficacy of anticancer drugs by selectively addressing therapeutics towards tumor tissues and reduce chemotherapy side effects. Two different types of tumor-targeted drug delivery include passive and active tumor targeting.[127] Enhanced endothelial cell proliferation and reduced amount of pericytes during angiogenesis in tumor microenvironment creates leaky vasculature.[128] In addition, impaired

lymphatic drainage present in tumor tissues along with increased vascular permeability causes an accumulation of nanoparticles within tumors via enhanced permeability and retention (EPR) effect (passive tumor targeting).[129] Cancer cells overexpress some receptors on their surfaces which are ideal traps for specific ligands incorporated into the surface of drug delivery nanoparticles. Through ligand-receptor mediated drug delivery systems, chemotherapeutic drugs can be directed to the ideal tumor destination (active tumor targeting).[57] Different types of ligands have been incorporated into the polymersomes to increase tumor penetration including peptides, nucleic acids, proteins, small molecules, and polysaccharides.[130] A list of ligand-decorated polymersomes for active targeting has been shown in Table 1.2.

Table 1.2. Ligands used for polymersome-based targeted drug delivery.

Type	Ligand	Target site	Cargo	Application	Reference
Protein	Trastuzumab	HER2	γFe_2O_3	Breast cancer imaging	[131]
Protein	Anti-EGFR	EGFR	Acridine orange	Breast cancer drug delivery	[123]
Protein	Transferrin	Transferrin receptor	Coumarin-6	Brain drug delivery	[132]
Peptide	PR_b peptide	$\alpha_v\beta_1$ integrin	TNFα	Prostate cancer drug delivery	[133]
Peptide	iRGD peptide	$\alpha_v\beta_3$ integrin	Doxorubicin	Breast cancer drug delivery	[104]
Peptide	iRGD peptide	$\alpha_v\beta_3$ integrin	Napabucasin and Gemcitabin	Pancreatic cancer drug delivery	[53]
Nucleic acid	A10-RNA aptamer	PSMA	Docetaxel	Prostate cancer drug delivery	[134]
Small molecule	Folate	Folate receptor	Doxorubicin	Cervix cancer drug delivery	[135]
Small molecule	Estradiol	Estrogen receptor	Doxorubicin	Breast cancer drug delivery	[7]
Polysaccharide	Hyaluronic acid particles	Hyaluronic acid receptor	Adamplatin	Breast cancer drug delivery	[136]

1.5. Pharmacokinetics and biodistribution of the polymersomes

The fate of drug-loaded nanoparticles is evaluated by calculating their pharmacokinetic properties. Blood clearance of nanoparticles depends on size, charge, and surface characteristics

of nanovesicles.[137–139] The concentration of surface PEG molecules and molecular weight of nanoparticles play an important role in the clearance process.[140] It has been demonstrated that polymersomes accumulate in the liver at the beginning step.[95] Kupffer cells (liver macrophages) digest the polymersomes.[139] It has been shown that slight charge on the polymersome surface will increase the circulation times of the vesicles, but highly charged polymeric nanoparticles will be rapidly cleared by the liver.[141,142]

The size of the nanoparticles affects the circulation time. PEGylated nanoparticles which are greater than 200 nm will be filtrated through phagocytosis in the spleen.[143] However, nanoparticle which are below 70 nm will be accumulated in the liver.[144] It has been demonstrated that the optimal polymersome size for the enhanced blood circulation and tumor accumulation would be below 200 nm.[92]

A reported study compared pharmacokinetic parameters between doxorubicin-loaded polymersomes and commercial liposomal doxorubicin administered on induced mammary carcinoma female rats.[145] According to this report, DOX-loaded polymersomes demonstrated longer circulation half-life (21.9 vs. 0.49 h), higher AUC (569 vs. 4 h*μg/mL), reduced volume of distribution (137.7 vs. 1091 mL/kg) and clearance (10.5 vs. 1579 mL/h/kg) compared to that of free DOX. Tissue distribution displayed an enhanced DOX accumulation within tumor and reduced accumulation in heart compared to that of free DOX. A comparison was also made between DOX-loaded polymersomes and liposomal DOX which showed lower circulation half-life (22 vs. 35 h) and AUC (568 vs. 2291 h*μg/mL) of polymersomes compared to liposomes. These results demonstrated that DOX-loaded polymersomes had better pharmacokinetics and biodistribution profiles compared to free DOX and had comparable efficacy to liposomal DOX.

1.5.1. Metabolism and clearance of doxorubicin

Doxorubicin is a member of anthracycline antibiotics with an extensive spectrum of application against neoplastic malignancies. DOX has a rapid distribution within the body with a volume of distribution between 20 to 30 L/kg followed by a slow elimination rate due to biliary and renal metabolism and clearance. The high volume of distribution creates an increased drug accumulation within liver, kidney, heart, and lung. The enhanced DOX accumulation causes severe side effects such as cardiotoxicity which restricts its therapeutic dosing in clinic.[146,147]

Although around half of DOX eliminates intact, the metabolism of DOX occurs through three different routes in hepatic and extrahepatic tissues including deglycosidation, one-electron, and two-electron reduction.[148] Two-electron reduction is the primary metabolic route by reduction of a carbonyl group that yields a secondary alcohol called doxorubicinol which is facilitated by different aldo-keto reductases in various cell types. One-electron reduction pathway forms a DOX-semiquinone radical by several oxidoreductase enzymes.[149] About 1-2% of DOX metabolism occurs through deglycosidation reaction by different enzymes such as xanthine oxidase, NADPH dehydrogenase, and cytochrome P450 reductase which results in the formation of hydroxyaglycone and deoxyaglycone metabolites.[150] The majority of final DOX metabolites, including doxorubicinol and aglycones, will be excreted in the bile within seven days and a small portion of excretion carries out by urine.[151]

The pharmacokinetics of DOX is linear in a range between 20 to 60 mg/m^2.[152] Based on DOX administration in different malignancies, DOX clearance varies among different individuals. Owing to wide distribution of DOX, the total clearance of DOX from the body has been reported to be 62.4 L/h.[153] According to a reported study, rapid elimination, terminal elimination, and distribution half-life of DOX has been 3.3 h, 29.6 h, and 12 minutes,

respectively.[154] Based on another study with 12 breast cancer patients, the total DOX clearance, renal clearance, hepatic clearance, and total clearance of doxorubicinol metabolite were reported to be 30.7, 0.66, 29.97, and 0.39 L/h, respectively.[155] Another study was performed on normal weight and obese lymphoma patients by infusing a dose of 50 mg/m^2 DOX. The results demonstrated an average clearance of 1935 and 1951 mL/min for DOX and doxorubicinol, respectively.[156]

1.6. Organization of the thesis

The aim of nanoparticle-based targeted drug delivery is to enhance the therapeutic efficacy of chemotherapeutic agents, reduce off-target side effects, increase the survival, and improve the quality of life for the patients suffering from cancer. I have designed, developed, and characterized three targeted drug-encapsulated, hypoxia-responsive polymeric nanoparticles (polymersomes) that release their chemotherapeutic cargo in response to low oxygen concentration (hypoxia) within tumor microenvironments. To demonstrate the efficiency of my drug-loaded nanoparticles, I have employed estrogen receptor positive and triple negative breast cancer cells as model systems. I have performed in vitro (two-dimensional and three-dimensional cell cultures) and in vivo (induced breast cancer animal models) studies to evaluate the efficacy of my drug-loaded nanoparticle formulation on breast cancer cells and solid tumors. Breast cancer is the second leading cause of death among women in the United States. The treatment of breast cancer is complicated due to rapid tumor growth from inside out, invasiveness, and metastasis to various organs within body. Thus, developing new cancer treatment options is of great importance to the survival of the breast cancer patients.

The following disquisition reports three independent studies. The second chapter has been published in the American Chemical Society ACS Molecular Pharmaceutics journal. The

results discussed in Chapter 3 will be published in a manuscript which is under revision by the American Chemical Society ACS Molecular Pharmaceutics journal. The fourth chapter has been published in the American Chemical Society ACS Applied Bio-Materials journal.

In chapter 2, HYPOXIA-RESPONSIVE POLYMERIC NANOCARRIERS FOR TARGETED DRUG DELIVERY TO ESTROGEN RECEPTOR POSITIVE BREAST CANCER CELL SPHEROIDS, we prepared estradiol-conjugated, hypoxia-responsive polymersomes. These polymeric nanocarriers encapsulate an anticancer drug, doxorubicin, for delivering to estrogen receptor positive breast cancer cells.

In chapter 3, ENDOXIFEN-CONJUGATED, HYPOXIA-RESPONSIVE POLYMERIC NANOPARTICLES FOR TARGETED DRUG DELIVERY TO BREAST CANCER MICROTUMORS, we incorporated endoxifen into the surface of polymersomes. Endoxifen acts as a ligand to distinguish and interact with estrogen receptors on the surface of estrogen receptor positive breast cancer cells. Subsequently, endoxifen-conjugated polymersomes selectively bind to the breast cancer cells, penetrate, and release their encapsulated drugs into the cells.

In chapter 4, TARGETED POLYMERIC NANOPARTICLES FOR DRUG DELIVERY TO HYPOXIC, TRIPLE-NEGATIVE BREAST TUMORS, we synthesized tumor-homing and penetrating iRGD peptide and conjugated this peptide to the surface of prepared polymersomes using cycloaddition reaction. These targeted iRGD-conjugated polymersomes selectively bind to neuropilin-1 receptors on the surface of triple negative breast cancer cells. Subsequently, polymersomes translocate into the cells, break, and release their chemotherapeutic payload to kill breast cancer cells.

2. HYPOXIA-RESPONSIVE, POLYMERIC NANOCARRIERS FOR TARGETED DRUG DELIVERY TO ESTROGEN RECEPTOR-POSITIVE BREAST CANCER CELL SPHEROIDS

2.1. Abstract

Uncontrolled cell growth, division, and lack of enough blood supply causes low oxygen content or hypoxia in cancerous tumor microenvironments. 17β-Estradiol (E_2), an estrogen receptor (ER) ligand, can be incorporated on the surface of nanocarriers for targeted drug delivery to breast cancer cells overexpressing ER. In the present study, we synthesized estradiol-conjugated hypoxia-responsive polymeric nanoparticles (polymersomes) encapsulating the anticancer drug doxorubicin (E_2-Dox-HRPs) for targeted delivery into the hypoxic niches of estrogen receptor-positive breast cancer microtumors. Estradiol-conjugated polymersomes released over 90% of their encapsulated Dox in a sustained manner within hypoxia (2% oxygen) after 12 hours. However, they released about 30% of Dox in normal oxygen partial pressure (21% oxygen, normoxia) during this time. Fluorescence microscopic studies demonstrated higher cytosolic and nuclear internalization of E_2-Dox-HRPs (targeted polymersomes) compared to Dox-HRPs (non-targeted polymersomes). Monolayer cell viability studies on ER-positive MCF7 cells showed higher cytotoxicity of targeted polymersomes in hypoxia compared to normoxia. Cytotoxicity studies with hypoxic three-dimensional spheroid cultures of MCF7 cells treated with targeted polymersomes indicated significant differences compared to normoxic spheroids. The novel estradiol-conjugated hypoxia-responsive polymersomes described here have the potential for targeted drug delivery in estrogen receptor-positive breast cancer therapy.

2.2. Introduction

Breast cancer is the most common malignancy and the second leading cause of death among women in the United States.[157] There are three significant biological markers in breast cancer: estrogen receptor (ER), progesterone receptor (PR), and human epidermal growth factor receptor 2 (HER-2). Based on these biomarkers, gene expressions, and molecular profiling, breast cancer is classified into different subtypes, including luminal A (ER+/PR+/HER2-), luminal B (ER+/PR+/HER2+), HER2 overexpression (ER-/PR-/HER2+), and basal-like tumors (ER-/PR-/HER2-).[158,159] About 83% of breast cancer cases are hormone receptor-positive (ER+/PR+) and are susceptible to hormonal therapy for suppressing tumor growth.[160]

Nanotechnology is an emerging field for targeted drug delivery in cancer therapy. Polymersomes are polymeric bilayer nanovesicles prepared from amphiphilic block copolymers.[161–163] They have several advantages compared to lipid-based nanocarriers, including controllable elasticity, permeability, and mechanical property that depend on the molecular weight of the hydrophobic block of the copolymers.[6] Polymersomes have an aqueous core surrounded by a bilayer membrane. This membrane has a hydrophobic part in the interior side and hydrophilic coronas on the outside and inside surfaces.[164] Polymersomes encapsulate hydrophilic therapeutics (such as proteins, peptides, nucleic acid fragments, anticancer drugs, and enzymes) in the aqueous core while hydrophobic molecules are integrated into the bilayer.[165–172] Polymersomes are rendered long circulating in the blood by the introduction of polyethylene glycol (PEG) as one of the main copolymers in their structure, or by conjugating PEG (PEGylation) on their surface.[173] The presence of PEG in polymersomes minimizes protein opsonization and protects the vesicles from degradation by dendritic cells or phagocytes.[173]

Uncontrolled and rapid cell proliferation along with insufficient blood supply produce low oxygen partial pressure or hypoxia in almost all solid tumors.[17] Hypoxia increases cancer cell survival through aggressiveness, metastasis to different organs, and resistance to chemotherapy and radiation therapy, leading to poor clinical outcomes.[174–176]

The chemotherapeutic agents are toxic or ineffective above or below their optimal plasma level, respectively. Hence, the carrier nanoparticles should release all of their anticancer payloads selectively at the targeted tumor sites. To reach this requirement, polymersomes are reported which respond to physical, chemical, or biological stimuli such as temperature, light, magnetic field, pH, redox, hypoxia, enzymes, inflammation, etc.[177–181] Since more than half of all tumors in breast cancer cases have less than 2.5 mm of Hg oxygen pressure,[182] hypoxia-responsive polymersomes are one of the favored nanocarriers for selective drug release in hypoxic niches of tumors.[178] Ligand-decorated polymersomes have been engineered for targeted drug delivery into microtumors to improve therapeutic efficacy and reduce cytotoxicity of the chemotherapeutic medicines.[10]

Estrogen is a hormone critical for the function of many organs such as bone, brain, cardiovascular, and reproductive systems. However, it is also associated with breast, ovarian, and uterine cancers.[183] 17β-Estradiol (E_2) is the predominant hormone among the three forms of estrogen hormones.[184] The cellular effects of estrogen are mediated by estrogen receptor α (ERα) and estrogen receptor β (ERβ), which are members of the nuclear hormone receptor superfamily of transcription factors. ERα expression is less than 10% in healthy breast cells but increases to 80% in breast cancer tissues.[185] To improve the cellular uptake of anticancer drugs and genes to ER-overexpressed cancer cells, estrogen conjugated liposomes have been developed. The reported liposomes encapsulated anticancer agents for targeted delivery to tumor tissues.[186–188]

In this study, we engineered estradiol conjugated hypoxia-responsive polymersomes loaded with doxorubicin for targeted drug delivery to hypoxic niches of ER-positive breast cancer microtumors. To our knowledge, this is the first report of receptor-mediated hypoxia-responsive polymeric drug carriers targeting breast cancer cells through the overexpressed estrogen receptors. With further developments, these ER targeted polymeric nanoparticles have translational potential for delivering chemotherapeutics to cancer tumor tissues.

2.3. Materials and methods

2.3.1. Materials

1-Ethyl-3-(3-dimethyl aminopropyl)-carbodiimide hydrochloride (EDC), N-hydroxysuccinimide (NHS), dimethylaminopyridine, tin (II) ethoxyhexanoate, $CuCl_2.2H_2O$, pentamethyl diethylenetriamine, tetrahydrofuran (THF), and 17β-ethynylestradiol were purchased from Millipore Sigma (St. Louis, MO, USA). Azobenzene, 3,3′-dicarboxylic acid was purchased from TCI America (Montgomeryville, PA, USA). mPEG-NH_2 (MW: 2000) was purchased from BiochemPeg (Watertown, MA, USA). The water used in experiments was prepared by a Millipore Sigma water purification system (Burlington, MA, USA). The NMR spectra were recorded using a Bruker Advance II HD instrument. Gel-permeation chromatography (GPC) was performed using a Tosoh Bioscience (King of Prussia, PA, USA) EcoSEC HLC-8320 instrument. THF was used as mobile phase in GPC, and polystyrene was the standard used for calibration.

2.3.2. Synthesis of the diblock copolymer PLA_{8500}-Azo-PEG_{2000}

Excess Azobenzene, 3,3′-dicarboxylic acid (27 mg, 0.14 mmol, TCI chemicals) was dissolved in 5 mL of pyridine in a round bottom flask wrapped in aluminum foil. 1-Ethyl-3-(3-dimethyl aminopropyl)-carbodiimide hydrochloride (EDC.HCl, 27 mg, 0.14 mmol), N-

hydroxysuccinimide (NHS, 11.5 mg, 0.14 mmol) and dimethylaminopyridine (DMAP, 0.6mg, 5%mol) were then added. The reaction mixture was stirred for 1 h under a nitrogen atmosphere. mPEG-NH_2 (MW: 2000, 100 mg, 0.05 mmol) was dissolved dropwise in 1 mL $CHCl_3$, added into this reagent mixture, and stirred overnight. Then, the solvent was removed under reduced pressure, the rest of the mixture was suspended in 50 mL water, and centrifuged at 2000 *g* for 10 min. The supernatant was filtered to remove the unreacted dicarboxylic acid, and the filtrate was dialyzed in 4 L water (molecular weight cut-off: 1000) for 2 days. The dialysate was dried under reduced pressure to obtain a yellow solid (yield: 62%). ^{1}H NMR (400 MHz, chloroform-d) δ ppm: 8.00-8.23 (aromatic C**H**=C**H**-CH, m, 8 H), 3.67 ((C$\mathbf{H}_2$-C$\mathbf{H}_2$-O), t, 4 H), 3.40 ((C$\mathbf{H}_3$-O), s, 3 H).

The synthesized PEG−diphenylazocarboxylate (50 mg, 0.023 mmol) was dissolved in pyridine (1.25 mL). To this solution, 1-ethyl-3-(3-dimethylaminopropyl)-carbodiimide hydrochloride (EDC.HCl, 6.7 mg, 0.0345 mmol), and N-hydroxysuccinimide (NHS, 4 mg, 0.0345 mmol) were added followed by excess 3-aminopropanol (9 μL, 8.75 mg, 0.116 mmol). The reaction mixture was stirred overnight. The solvent was then evaporated. The residue obtained was dissolved in 10 mL dichloromethane and washed with water three times. The bottom organic layer was dried under vacuum to obtain the PEG conjugate (yield: 51%). ^{1}H NMR (400 MHz, chloroform-d) δ ppm: 8.00-8.23 (aromatic C**H**=C**H**-CH, m, 8 H), 3.67 ((C$\mathbf{H}_2$-C$\mathbf{H}_2$-O), t, 4H), 3.40 ((C$\mathbf{H}_3$-O), s, 3 H), 0.88 ((NH-C$\mathbf{H}_2$-CH_2-CH_2-OH), m, 2 H).

For the synthesis of PLA_{8500}-Azo-PEG_{2000}, D, L-lactide (500 mg, 3.5 mmol) and tin (II) ethoxyhexanoate (3 μL, 0.009 mmol) were added to anhydrous toluene (5 mL) in a 35 mL high-pressure reaction vessel. The product (100 mg, 0.05 mmol) obtained from the previous step was then added to the reaction mixture. The high-pressure reaction vessel was purged with nitrogen

for 5 minutes and stirred at 120° C for 24 hours. After cooling to 25° C, the reaction mixture was added dropwise to cold ether. The top clear supernatant was decanted and the precipitate was washed again with ether and dried (yield: 65%). The resultant polymer was analyzed by ^{1}H-NMR spectroscopy and gel permeation chromatography for purity and molecular weight. ^{1}H NMR (400 MHz, chloroform-d): 5.19 ((-C**H**-C=O), q, 1 H), 3.67 ((C**H**$_2$-C**H**$_2$-O), t, 4 H), 1.59 ((C**H**$_3$-CH-C=O), d, 3 H). Polydispersity index: 1.17 (gel-permeation chromatography: M_n = 10,700; M_w = 12,500).

2.3.3. Synthesis of polymer PLA$_{17000}$-PEG$_{2000}$-Estradiol

Hydroxyl-PEG$_{2000}$-azide (100 mg, 0.05 mmol), D, L-lactide (800 mg, 5.6 mmol), and tin (II) ethoxyhexanoate (3 µL, 0.009 mmol) were added to anhydrous toluene (5 mL) in a 35 mL glass high-pressure vessel and then purged with nitrogen. The solution was stirred at 120° C under nitrogen for 24 hours. After cooling to 25° C, the reaction mixture was added dropwise to cold ether. The top clear supernatant was decanted, the precipitate was washed with ether and dried under vacuum (yield: 72%). To characterize the purity and molecular weight, the product was analyzed by ^{1}H NMR spectroscopy and gel permeation chromatography. ^{1}H NMR (400 MHz, chloroform-d): 6.70((C**H**=CH-C=O), d, 1 H), 6.52((CH=C**H**-C=O), s, 1 H), 5.18 ((-C**H**-C=O), q, 1 H), 3.94 ((C**H**$_2$-C=O), d, 2 H), 3.66 ((C**H**$_2$-C**H**$_2$-O), t, 4 H), 1.58 ((C**H**$_3$-CH-C=O), d, 3 H), 0.89 ((C**H**$_3$-C-), s, 6 H).

The ethynylestradiol was reacted with N$_3$-PEG$_{2000}$-PLA$_{17000}$ polymer using [2 + 3]-cycloaddition reaction (Scheme 2.1). Briefly, a solution of Cu^{2+} complex (0.053 M) was prepared by mixing 3 mL of $CuCl_2.2H_2O$ (90.3 mg, 0.53 mmol) and 3 mL of pentamethyl diethylenetriamine (PMDETA) (442 µL, 2.1 mmol) in water, diluting the mixture to 10 mL in water, and stirring for 2 hours. Ethynylestradiol (3 mg, 10 µmol) and N$_3$-PEG$_{2000}$-PLA$_{17000}$ (100

mg, 5 μmol) were dissolved in 5 mL tetrahydrofuran (THF). Then, 100 μL of fresh sodium ascorbate water solution (27 mg/mL) and 100 μL copper complex (0.053 M) were added to the solution and stirred at 25° C for 24 hours. The reaction mixture was added into 40 mL water and the precipitate was pelleted using a centrifuge at 2906 g for 10 minutes. The precipitate was washed three times with water, added to an ion exchange resin (100 mg, Dowex.HCR-W2) in 20 mL water (to remove any remaining Cu^{2+} complex or amine), and stirred for 2 hours. Then, the mixture was dried under vacuum. ^{1}H NMR (400 MHz, chloroform-d) δ ppm: 6.70((C**H**=CH-C=O), d, 1 H), 6.52((CH=C**H**-C=O), s, 1 H), 5.18 ((-C**H**-C=O), q, 1 H), 3.94 ((C$\mathbf{H}_2$-C=O), d, 2 H), 3.66 ((C$\mathbf{H}_2$-C$\mathbf{H}_2$-O), t, 4 H), 1.58 ((C$\mathbf{H}_3$-CH-C=O), d, 3 H), 0.89 ((C$\mathbf{H}_3$-C-), s, 6 H). Polydispersity index: 1.15 (gel-permeation chromatography; M_n = 16,400, M_w = 18,900). Percentage of estrogen attached: For 100% attachment of the estradiol, the integration of the ^{1}H NMR signals at 3.66 ppm (PEG) and 6.52 ppm (benzene ring in estradiol) should be 188:1. From the calculated ratio in the ^{1}H NMR spectrum, we estimate the attachment of estradiol to be 20%.

2.3.4. Preparation of Dox-encapsulated (non-targeted) polymersomes and Estradiol-conjugated Dox-encapsulated (targeted) polymersomes

PLA_{8500}-Azo-PEG_{2000} and PLA_{17000}-PEG_{2000}-Estradiol were separately dissolved in acetone (10 mg/mL). Doxorubicin hydrochloride was dissolved in deionized water (20 mg/mL) and 1,2-dipalmitoyl-*sn*-glycero-3-phosphoethanolamine (DPPE)-N-lissamine rhodamine B sulfonyl ammonium salt (LR) lipid was dissolved in chloroform (0.01 mg/mL). PLA_{8500}-Azo-PEG_{2000} (95%), LR dye (5%), and doxorubicin hydrochloride were used to prepare non-targeted Dox-encapsulated polymersomes. For making targeted polymersomes, a combination of LR (5%), PLA_{8500}-Azo-PEG_{2000} (93%) and PLA_{17000}-PEG_{2000}-Estradiol (2%) were used.

Doxorubicin was encapsulated in the nanocarriers with the pH gradient method.[178] Briefly, 1 mL LR solution was added into two glass vials and chloroform was evaporated to make a thin film. The thin film in each glass vial was hydrated with 1 mL citrate buffer (20 mM, pH 4). One of the glass vials was used to prepare non-targeted polymersomes by adding PLA_{8500}-Azo-PEG_{2000} polymer solution (100 µL) dropwise into the citrate buffer and stirring for 10 min at 25° C. The second glass vial was used for targeted polymersome preparation. The PLA_{8500}-Azo-PEG_{2000} polymer and PLA_{17000}-PEG_{2000}-Estradiol polymer solutions (100 µL and 3.6 µL, respectively) were added dropwise into the citrate buffer and stirred for 10 minutes at 25° C. Acetone in the resultant solutions was evaporated by passing air through the mixture for 45 minutes. Polymersomes were formed after sonicating the glass vials with polymer solution for 1 hour in a bath sonicator (Symphony 117V, 60 Hz, Level 9). The polymersomes were passed through a Sephadex G-100 gel filtration column to build the pH gradient across the membrane. Doxorubicin was added to these polymersomes (polymer: drug ratio 5:1) and the mixture was stirred for 4 hours at 25° C. The solutions were again passed through Sephadex G-100 column to remove unencapsulated drugs from the polymersomes. The drug encapsulation efficiency was determined by UV-vis spectroscopy at 480 nm.

2.3.5. Preparation of buffer-encapsulated polymersomes

Buffer-encapsulated polymersomes were prepared to assess the cytotoxicity of the vesicles without any doxorubicin. PLA_{8500}-Azo-PEG_{2000} solution and LR lipid dye were used in the molar ratio of 95:5. Briefly, the LR solution was evaporated into a glass vial. Then, PLA_{8500}-Azo-PEG_{2000} solution (10 mg/mL, 100 µL) was added into the vial and the mixture was added dropwise into another glass vial containing 1 mL HEPES buffer (25 mM, pH 7.4). The acetone solvent in the polymer solution was removed by passing the air through the vial for 45 minutes.

The mixture was then sonicated for 60 minutes and passed through Sephadex G-100 chromatography column to separate unencapsulated Dox-loaded polymersomes from encapsulated ones.

2.3.6. Characterization

2.3.6.1. Atomic Force Microscopy (AFM)

Polymersomes were prepared before and after 24-hour exposure to hypoxia. For the hypoxic condition, 100 μM NADPH solution, and 100 μL human liver microsomes were dispersed in 1 mL polymersome solution. Polymersome samples (1 mg/mL) were prepared by incubating 10 μL of each solution on silicon substrates (University Wafer) for 10 minutes in a sealed compartment. The samples were then rinsed with deionized water (Millipore) and dried under purified nitrogen flow. The imaging was performed using a commercial atomic force microscope (NT-MDT NTEGRA AFM). The samples were imaged under ambient conditions in semi-contact mode using an AFM tip with a resonant frequency of 190 kHz (Budget sensors).

2.3.6.2. Dynamic Light Scattering (DLS)

After polymersome preparation, the size and zeta potential of non-targeted and targeted Dox-encapsulated polymersomes were analyzed before and after 24-hour exposure to hypoxia (the same conditions as described for AFM imaging) by Dynamic Light Scattering (Malvern Zetasizer Nano-ZS90). Four measurements were carried out for each sample and an average of all measurements was recorded.

2.3.6.3. Transmission Electron Microscopy (TEM)

Polymersomes were prepared before and after 24-hour exposure to hypoxia (the same conditions as described for AFM imaging). To pretreat TEM grids, poly L-lysine (1%) was added on 300 mesh Formvar-carbon coated copper grids. After standing for 1 minute, grids were

air-dried. A drop of polymersome suspension (1% diluted, 10 μL) was placed on the grids for 30 seconds and a filter paper was used to absorb the liquid. Phosphotungstic acid (0.1%, pH 7.0) was added to the grids, allowed to stand for 2 minutes, and then wicked away from the grids. Images were obtained (when the grids were dried) in a JOEL JEM-2100 LB_6 transmission electron microscope (Peabody, Massachusetts, USA).

2.3.7. Drug loading and release from the polymersomes

The encapsulation efficiency and loading content of doxorubicin in Dox-encapsulated polymersomes were estimated by using a UV-vis spectrophotometer at 480 nm. A calibration curve was created by preparing different Dox concentrations dissolved in deionized water. To evaluate the hypoxia-mediated release behavior of the polymersomes, 1 mL of E_2-Dox-HRPs (2 mg/mL), NADPH (100 μM), and 100 μL human liver microsomes were dispersed in 1 mL HEPES buffer (pH 7.4, 25 mM) within a cellulose membrane tube (MWCO: 10 KDa). The tube was immersed in 20 mL HEPES buffer containing 100 μM NADPH within a hypoxia chamber (2% oxygen). For the normoxic condition (control), the tube was immersed in 20 mL HEPES buffer containing 100 μM NADPH at standard atmospheric conditions (21% oxygen) (both hypoxic chambers and normoxic incubators contained 5% CO_2 during all experiments). Each sample was gently shaken at 100 rpm. The release medium was withdrawn and replenished with the medium at predefined time intervals. Dox concentration was measured by absorption at 480 nm.

2.3.8. Cell culture

The MCF7 cell line (ER+ breast carcinoma) was purchased from American Type Culture Collection (ATCC, Manassas, VA). The MCF7 cells were cultured in Dulbecco's Modified Eagle Medium (DMEM) supplemented with 10% Fetal Bovine Serum (Avantar Seradigm) and

1% v/v antibiotics (Penicillin, Streptomycin, Amphotericin B solution, Corning). For normoxia, a humidified incubator containing 5% CO_2, 21% oxygen, 74% nitrogen, and 37° C was used. The Biospherix C21 hypoxic chamber supplemented with 2% oxygen, 93% nitrogen, and 5% CO_2 was used to induce hypoxia for the cells.

2.3.9. Cellular uptake study

The MCF7 cells were cultured in two twelve-well plates (starting with 5000 cells per well) and allowed to grow in normoxia (21% oxygen) and hypoxia (2% oxygen) separately for one doubling time. Both the plates were treated with buffer-encapsulated polymersomes (non-targeted and targeted, 30 µL each well) for 3 hours. Subsequently, the cells were washed with PBS for 3 times and cytoskeleton actin filaments and nuclei of the cells were stained using Phalloidin (Biotium) and DAPI (NucBlue, Invitrogen) dyes, respectively. To demonstrate the role of receptor-mediated endocytosis, another cellular uptake study was performed using 3 µM free estradiol, equivalent amount of targeted Polymersomes, and a combination of 3 µM free estradiol and targeted polymersomes. A fluorescence microscope (Leica, 20x objective) was used for imaging.

2.3.10. Cytotoxicity studies with plain polymersomes

Different concentrations of the HEPES buffer-encapsulated polymersomes (20 to 100 µg/mL) were used to treat the MCF7 cells. The cells were seeded into two 96-well plates (5000 cells per well) and grew in normoxia (21% oxygen) and hypoxia (2% oxygen) separately. Then, buffer-encapsulated polymersomes were used to treat the cells. After 3 days, the cell viability was measured by the Alamar Blue assay. Briefly, a mixture of DMEM and Alamar Blue reagent (9:1 ratio) was prepared and added into each well of 96-well plates. After 5 hours, the

fluorescence was recorded (excitation: 560 nm, emission: 595 nm), and the cell viability was calculated.

2.3.11. Monolayer cell viability assay

The MCF7 cells were seeded into two 96-well cell culture plates (5000 cells per well) and allowed to grow in normoxia (21% oxygen) and hypoxia (2% oxygen) (one plate under each condition). When the cells reached 85-90% confluency, they were divided into 4 different treatment groups: control (without treatment), Dox-encapsulated hypoxia-responsive polymersomes (Dox-HRPs, non-targeted polymersomes), estradiol-conjugated Dox-encapsulated hypoxia-responsive polymersomes (E_2-Dox-HRPs, targeted polymersomes), and free Dox. The cells were treated for 3 days with 5,10, and 15 μM of free Dox and the equivalent amount of Dox in both non-targeted and targeted polymersomes. Subsequently, the plates were washed with phosphate buffered saline (PBS) three times and the cell viability assessed by the Alamar Blue assay.

2.3.12. Three-dimensional spheroidal cell viability assay

Three-dimensional spheroids of MCF7 cells were prepared using a magnetic 3D cell culture kit (Greiner-Bio-one, Monroe, NC). Briefly, 200 μL NanoShuttle-PL magnetic nanoparticles were added into an 85-90% confluent MCF7 cell culture flask and incubated overnight. Unattached nanoparticles were removed by washing the flask with PBS. Then, the cells were detached from the flask by trypsin and added into each well (15,000 cells per well) in a 96-well 3D culture plate and placed on top of a magnetic spheroid drive to form spheroids within 15 min. The cells grew overnight in normoxia (21% oxygen) and hypoxia (2% oxygen) separately. Then, the cells were divided into 4 treatment groups (same as the monolayer cell culture) and treated for 3 days with the same concentrations of Dox (5, 10, and 15 μM) in both

normoxia and hypoxia. The spheroids were washed with PBS, dislodged from the plates by removing the magnetic spheroid drive, transferred into a new cell culture plate, and cultured overnight. The following day, the cell viability was measured using Alamar Blue assay. To evaluate the effect of the drugs on the growth rate of the three-dimensional cultures, a different group of the 6-day old spheroids were treated with 10 μM free Dox, non-targeted and targeted Dox-encapsulated polymersomes for 72 hours in both normoxia (21% oxygen) and hypoxia (2% oxygen). Then, the spheroids were washed with PBS and their growth was monitored until day 16. NIH ImageJ software was used to analyze and measure the percent growth rate of the spheroids.

2.3.13. Statistical analysis

OriginPro software (version 9.3, Northampton, Massachusetts) was used for statistical analysis. The results were presented as mean ± SD (n = 3). The significant statistical difference ($p < 0.05$) between normoxia and hypoxia with different drug concentrations and polymersome treatments was analyzed by a one-way ANOVA Tukey HSD test.

2.4. Results and discussion

2.4.1. Synthesis of the polymers and preparation of polymersomes

We synthesized the estradiol-conjugated polymer PLA_{17000}-PEG_{2000}-Estradiol from ethynyl estradiol and the azide polymer using [2 + 3]-cycloaddition reaction (Scheme 2.1). The hypoxia-responsive PLA_{8500}-Azo-PEG_{2000} polymer was synthesized by following an analogous protocol developed in our laboratory.[178]

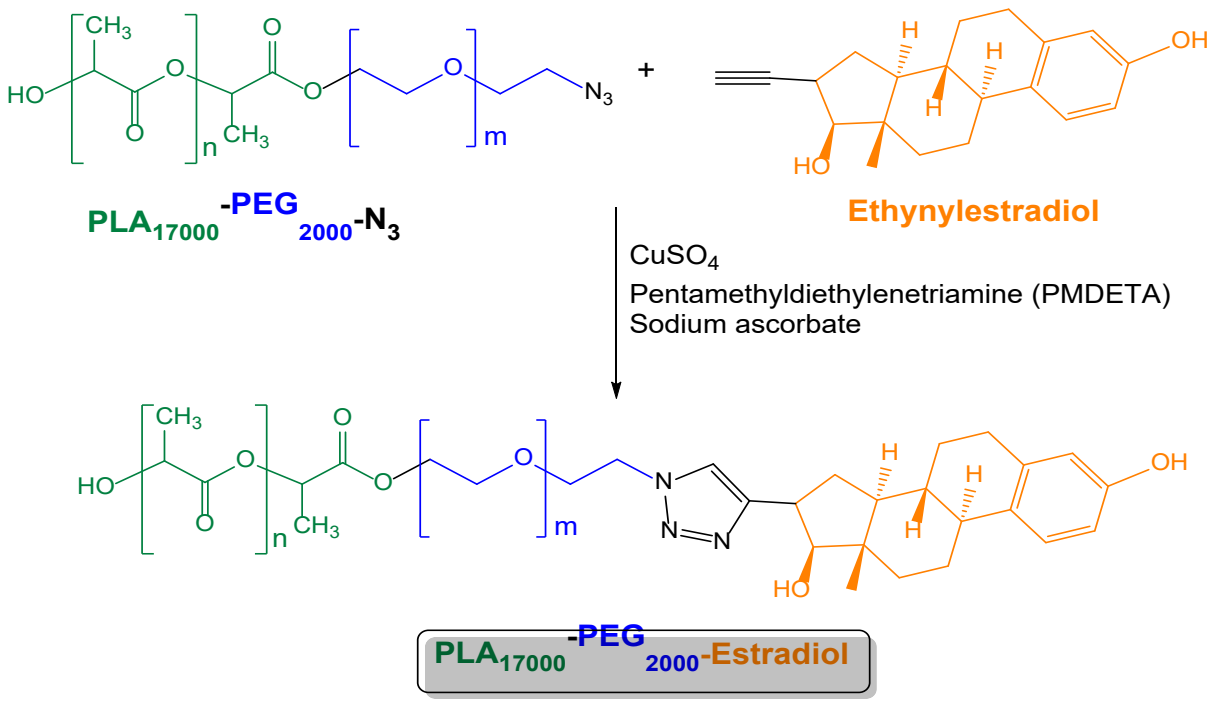

Scheme 2.1. Synthesis of the polymer PLA_{17000}-PEG_{2000}-Estradiol

The synthesized polymers were characterized by NMR spectroscopy and gel permeation chromatography (GPC). GPC analysis indicated the polydispersity indices to be 1.17 for PLA_{8500}-Azo-PEG_{2000} and 1.15 for PLA_{17000}-PEG_{2000}-Estradiol. We performed GPC for PLA_{8500}-Azo-PEG_{2000} polymer before and after exposure to hypoxia (Supporting Information A10, A11). The azobenzene linker group between PEG and PLA molecules is responsible for the polymersome disintegration in hypoxic conditions and acts as a hypoxia-sensitive moiety.[189] The surface PEG groups help in the prolonged blood circulation of the polymersomes. The ratio of molecular weights for the hydrophilic block to the whole polymer of 20-40% is critical for the polymersome formation.[190] In the synthesized polymers, this ratio was 20%. As it was mentioned in the polymer synthesis, the yield of estradiol attachment to PLA-PEG-N_3 polymer was around 20%. To prepare targeted polymersomes with high efficiency to bind the surface receptors, we optimized our polymersomes contain 2% PLA-PEG-Estradiol polymer in their combination (2% PLA-PEG-Estradiol, 93% PEG-Azo-PLA, 5% lissamine-rhodamine dye) (Figure 1).

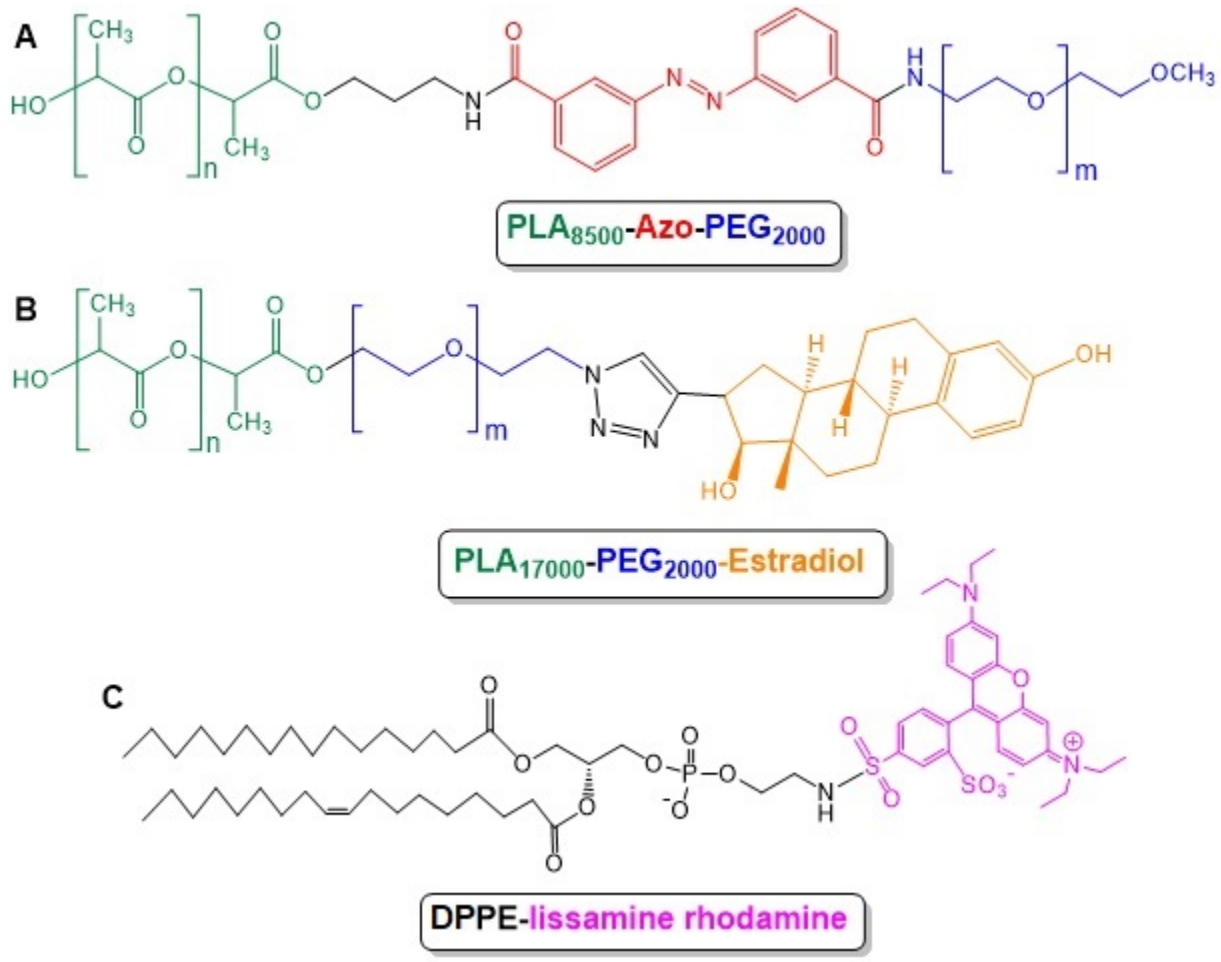

Figure 2.1. Chemical structures of polymers and fluorescent lipid used for polymersome preparation. **(A)** PLA_{8500}–Azo–PEG_{2000} polymer, **(B)** PLA_{17000}–PEG_{2000}–Estradiol polymer, and **(C)** 1, 2-dipalmitoyl-sn-glycero-3-phosphoethanolamine-N-lissamine rhodamine B sulfonyl ammonium salt.

Both non-targeted and targeted polymersomes accumulate within the tumors via enhanced permeability and retention (EPR) effect which is due to the leaky vasculature and impaired lymphatic drainage present in the solid tumors.[181] Subsequently, the targeted polymersomes enter the cells mediated by the interaction between estradiol groups of the polymersomes and estrogen receptors on the surface of breast cancer cells (Figure 2).[186]

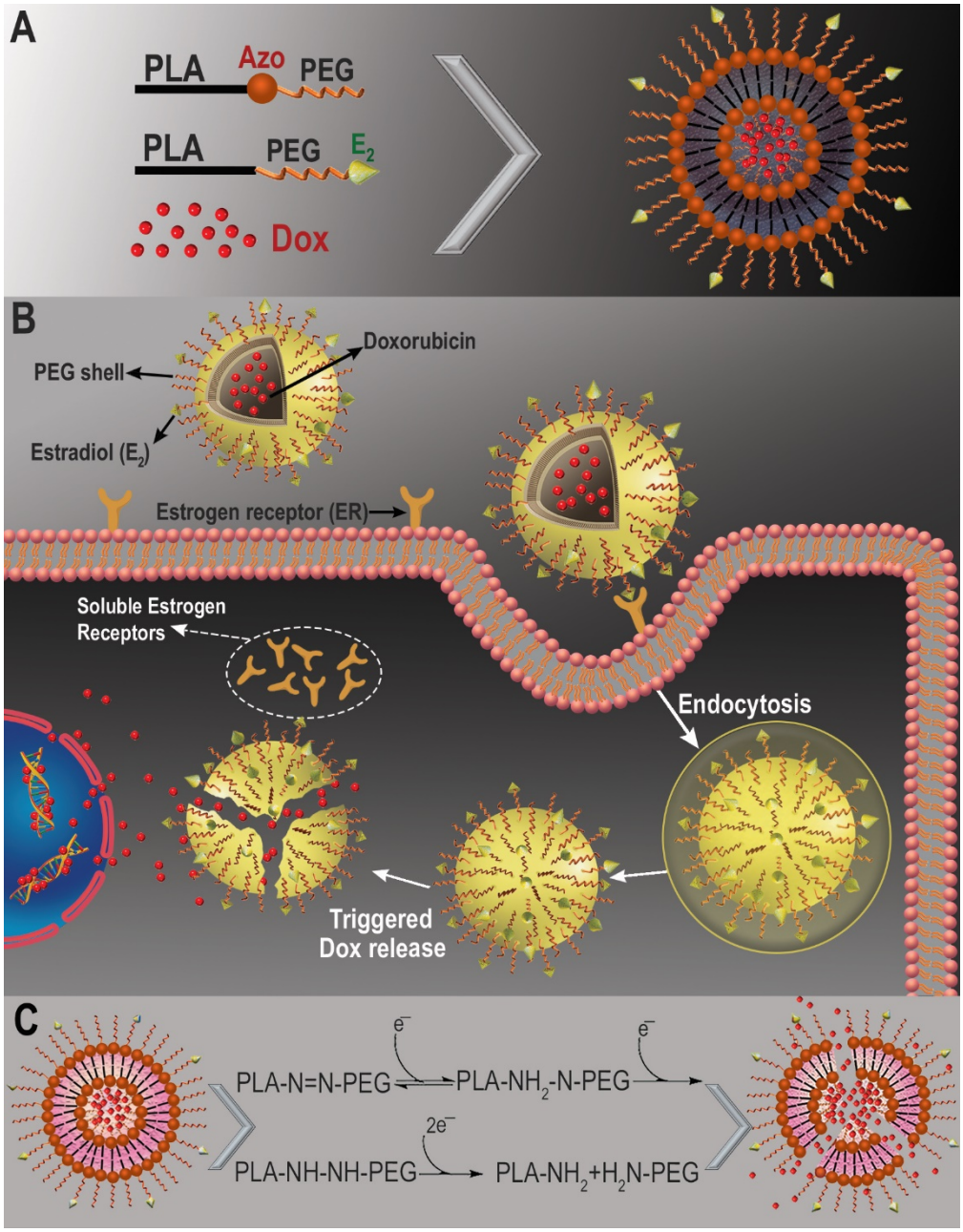

Figure 2.2. Schematic illustration of the targeted Dox-loaded polymersomes and internalization into ER-positive breast cancer cells. **(A)** Components of the ER targeted polymersomes; **(B)** ligand-receptor mediated endocytosis of ER targeted polymersomes into the cells.[29] **(C)** Mechanism of Dox release in hypoxia.

The polymersomes were prepared using the solvent exchange method[191] and characterized by dynamic light scattering, transmission electron microscopy, and atomic force microscopy. The average encapsulation efficiency and loading content of Dox within Dox-HRPs

were found to be 48% and 9 weight percent, respectively. The average encapsulation efficiency and loading content of Dox within targeted E_2-Dox-HRPs were 59% and 11.3 weight percent, respectively. The hydrodynamic diameter and zeta potential of the non-targeted and targeted polymersomes were measured before and after exposure to hypoxia. The zeta potential of the polymersomes was slightly positive and did not change significantly under normoxia and hypoxia (Table 1). We observed that the average hydrodynamic diameters of the non-targeted polymersomes changed from 126 ± 2 nm in normoxia to 41 ± 5 nm and 439 ± 25 nm in hypoxia (Figure 3A, Supporting information A12). However, the targeted polymersomes with 17β-estradiol on the surface were larger, likely due to the incorporation of the higher molecular weight PLA_{17000}-PEG_{2000}-Estradiol polymer conjugate (168 ± 3 nm in normoxia and 52 ± 6 nm and 695 ± 32 nm in hypoxia, respectively, Figure 3B, Supporting information A13, Table 2.1).

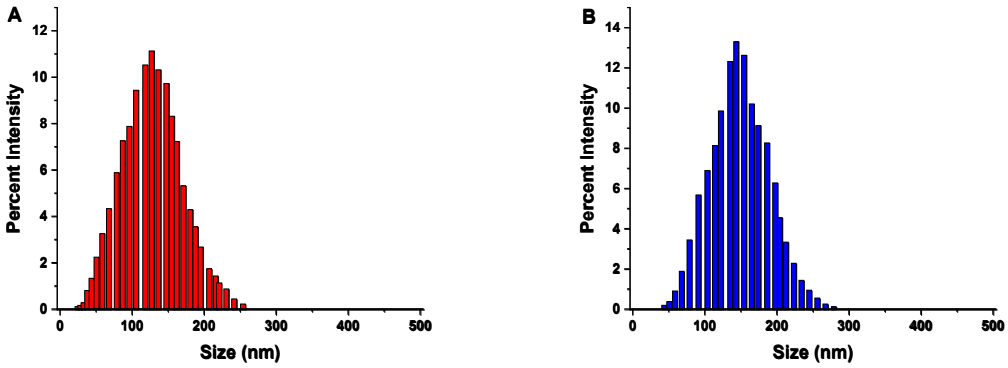

Figure 2.3. Hydrodynamic diameters of the polymersomes in normoxia. (**A**) Non-targeted, Dox-encapsulated and (**B**) ER-targeted Dox-encapsulated polymersomes.

Table 2.1. Hydrodynamic diameter and polydispersity index (PDI) of the polymersomes

Polymersome	Average diameter (nm)		Zeta potential (mV)		PDI	
	Normoxia	Hypoxia	Normoxia	Hypoxia	Normoxia	Hypoxia
Non-targeted	126 ± 2	41 ± 5, 439 ± 25	0.12 ± 0.12	0.23 ± 0.17	0.12 ± 0.03	0.71 ± 0.14
Targeted	168 ± 3	52 ± 6, 695 ± 32	0.21 ± 0.11	0.32 ± 0.14	0.13 ± 0.02	0.77 ± 0.18

2.4.2. Hypoxia-mediated drug release from polymersomes

The hypoxic microenvironment of solid tumors is rich in reductase enzymes and other reducing agents.[192] The azobenzene groups of the polymers undergo four-electron reduction under hypoxia to separate the hydrophobic PLA and the hydrophilic PEG blocks of the polymer. In fact, when reductase enzymes reduce the azobenzene moieties to separated aniline components, PEG and PLA polymers that are bound to opposite sides of azobenzene linker will break apart which causes polymersome disintegration. This phenomenon has been approved by various retrospective studies (Figure 2C).[193–195] Previously, we demonstrated that such reduction leads to the disintegration of the polymersome structure and release of the encapsulated drug.[178]

To test the release of drug under hypoxia, doxorubicin was encapsulated into the estradiol-conjugated hypoxia-responsive polymersomes (E_2-Dox-HRPs). Dox release was measured as a function of time in hypoxia and normoxia (Figure 4).

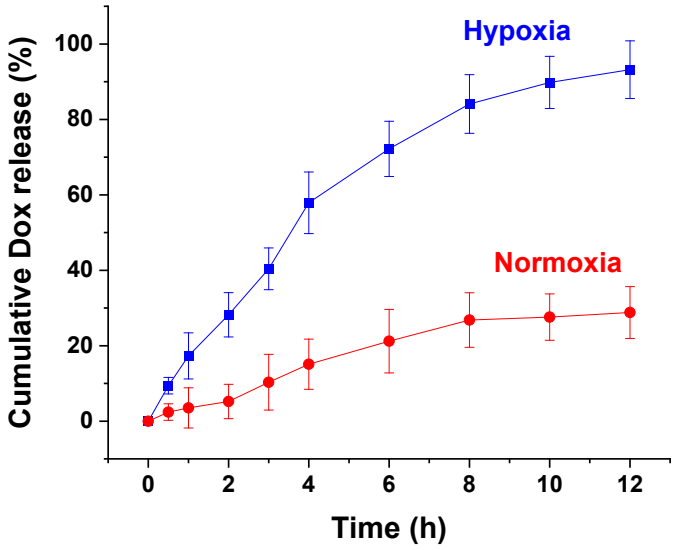

Figure 2.4. Cumulative release of encapsulated Dox from the targeted polymersomes under hypoxia (2% oxygen, blue squares) and normoxia (21% oxygen, red circles) (n = 3).

The release rate of Dox from polymersomes in hypoxia was significantly higher than Dox release in normoxia. The polymersomes released more than 90% of Dox in a sustained manner under hypoxia after 12 hours, while about 30% of Dox was released in normoxia during this time. The results demonstrated that hypoxia-responsive polymersomes preferentially release the encapsulated drug in hypoxic conditions due to the reduction of azobenzene moiety within the polymer structure (Figure 2C).[193,194] Polymersomes lost their spherical shape after exposure to hypoxic conditions, demonstrating vesicular disintegration (Figure 5A-D). Dynamic light scattering experiments showed a reduction in hydrodynamic diameter of the polymersomes and an increase in the polydispersity index under hypoxia (Table 2.1).

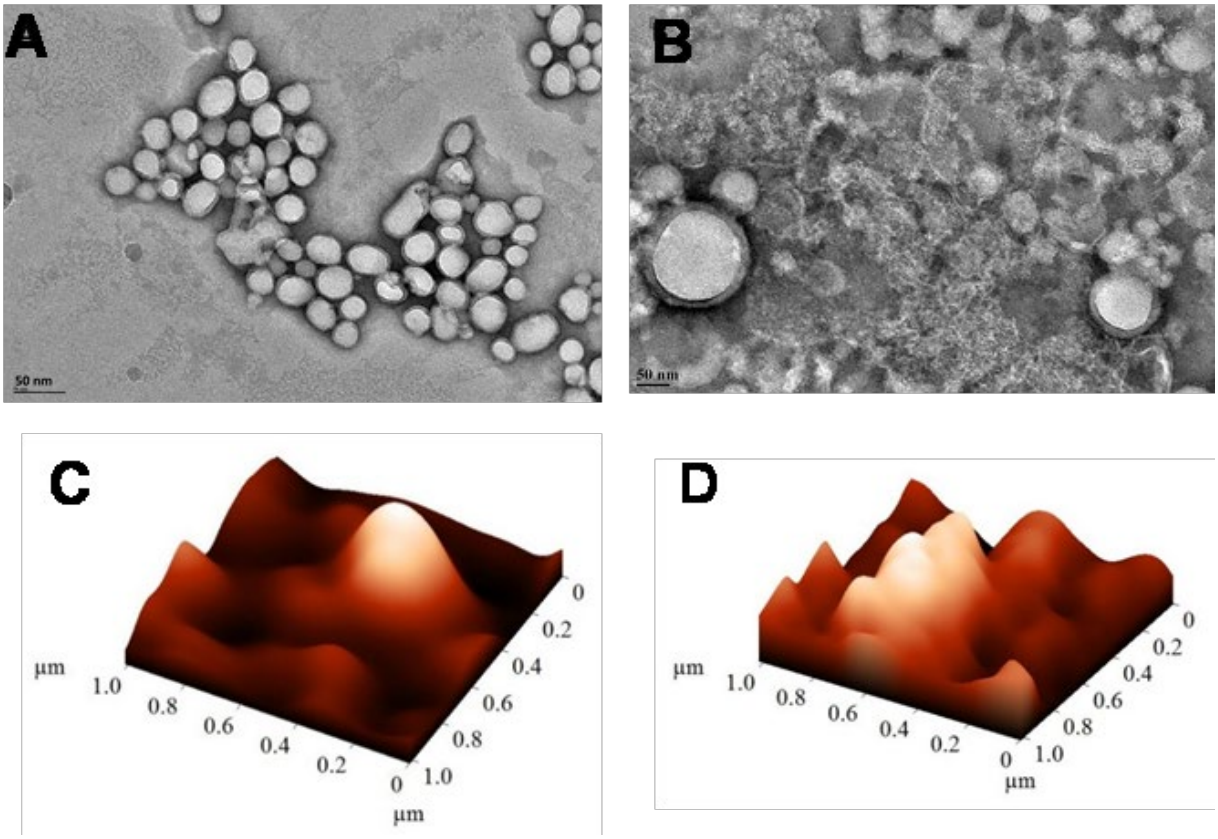

Figure 2.5. Transmission electron microscopic (TEM) and atomic force microscopic (AFM) images of estradiol-polymersomes under normoxia **(A, C)** and hypoxia **(B, D)**.

2.4.3. Cellular uptake study

To determine the internalization of the estradiol-conjugated polymersomes within ER-positive breast cancer cells, 5% DPPE-lissamine rhodamine (Figure 1C) was incorporated into the bilayer of the vesicles. The MCF7 cells were incubated with 3 µM targeted and non-targeted polymersomes (without Dox) for 3 hours under normoxia and hypoxia (Figure 6A). Cellular localization was observed after 3-hour treating the cells with the polymersomes. The fluorescence intensity of the microscopic images was normalized with respect to the number of the MCF7 cells. The images were analyzed using the NIH ImageJ software and the quantitative fluorescence integral density per unit area of targeted and non-targeted treatments in both normoxia and hypoxia were calculated (Figure 6B). The integral density of the targeted

polymersomes was 9.7 times higher compared to non-targeted vesicles under hypoxia and 3.5 times higher compared to targeted polymersomes in normoxia, respectively.

Nanoparticle retention within the cancer cells depends on various processes, including the size of nanoparticles, endo- and exocytosis, cellular homeostasis, and the degree and duration of hypoxia exposure. Based on previous studies, nanoparticle uptake in breast cancer cells changes in a dynamic way in hypoxia.[196] A prior study on MCF7 breast cancer cells demonstrated an elevated uptake of gold nanoparticles in hypoxia.[197] Since the MCF7 cells overexpress the estrogen receptors on surface, we anticipated that the targeted polymersomes would show increased cellular internalization compared to the non-targeted counterparts.[198] We observed that 3-hour exposure to hypoxia led to increased internalization of the E_2-targeted polymersomes in the MCF7 cells (Figure 6). To further demonstrate the role of receptor-mediated endocytosis, we performed another uptake study using 3 μM free estradiol, equivalent amount of targeted polymersomes (E_2-HRPs), and a combination of 3 μM both free estradiol and targeted polymersomes. The results demonstrated that estradiol decreased cellular uptake of the targeted polymersomes (Supporting Informations A8-9). This might be due to a competitive inhibition by free estradiol molecules to bind estrogen receptors. Thus, there would be less or no room for targeted E_2-polymersomes to bind estrogen receptors on the surface of the cells and pass through the membrane.

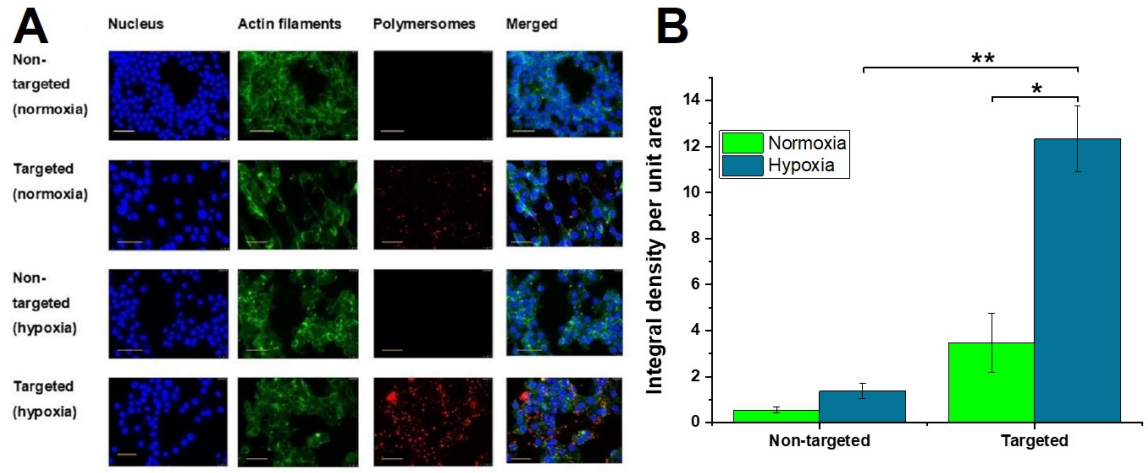

Figure 2.6. (A) Fluorescence microscopic images of cellular internalization of non-targeted and targeted polymersomes in monolayer cultures of MCF7 cells in normoxia and hypoxia (scale bar: 50 μm). **(B)** Quantitative fluorescence integral density indicating cellular uptake after treating the MCF7 cells with targeted polymersomes in normoxia and hypoxia (n = 3, *$p < 0.05$, **$p < 0.01$).

2.4.4. Cytotoxicity and cell viability in monolayer cultures

To determine the toxicity, we incubated MCF7 cells with varying amounts of the HEPES buffer-encapsulated estradiol-targeted polymersomes. The polymersomes showed minimal toxicity with more than 87% cell viability after 72 hours in both normoxic and hypoxic conditions up to a total polymer concentration of 100 μg/mL (Figure 7A). To determine the effectiveness of the drug-loaded polymersomes, we incubated the MCF7 monolayer cell cultures for 72 hours with four treatments: non-targeted Dox-encapsulated hypoxia-responsive polymersomes (Dox-HRPs), targeted estradiol-conjugated Dox-encapsulated hypoxia-responsive polymersomes (E_2-Dox-HRPs), free Dox, and control (no treatment) (Figure 7B). In hypoxic conditions, treating the MCF7 cells with 15 μM (Dox concentration) targeted E_2-Dox-HRPs reduced the viability to 14%. We also observed that non-targeted Dox-HRPs with 15 μM doxorubicin reduced the cell viability to 39% under hypoxia. There was a significant difference ($p < 0.05$) between normoxia and hypoxia when the cells were treated with targeted E_2-Dox-

HRPs. A substantial reduction in the viability was also observed when the cells were treated with non-targeted Dox-HRPs in hypoxia compared to non-targeted Dox-HRPs in normoxia.

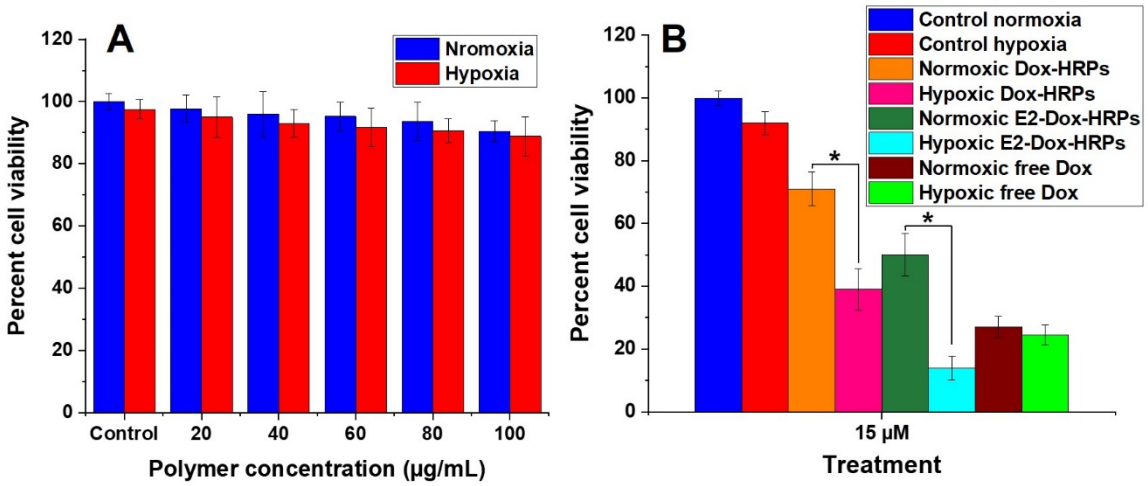

Figure 2.7. (A) Toxicity of the HEPES buffer encapsulated estradiol-polymersomes in normoxia and hypoxia for the MCF7 cells. **(B)** Viability of the MCF7 monolayer culture after 72 h treatment with free Dox, non-targeted Dox-encapsulated polymersomes (Dox-HRP) and targeted Dox-encapsulated polymersomes (E_2-Dox-HRPs) under normoxia and hypoxia ($n = 6$, $^*p < 0.05$).

The results demonstrated that both targeted and non-targeted polymersomes could lower the viability of the breast cancer cells in hypoxia compared to normoxia. However, the targeted Dox-polymersomes were more effective compared to the free drug (Figure 7B). Also, the targeted Dox-polymersomes were significantly more effective in killing breast cancer cells under hypoxia compared to normoxia. We did not observe such a trend for free doxorubicin. Based on the Dox release profile (Figure 4), the polymersomes will release about 40% of the encapsulated drug in 3 hours and about 80% after 8 hours. Hence, 72-hour treatment of the breast cancer cells with the polymersomes ensures enough time for the vesicles to enter the cells, undergo structural destabilization, and release the encapsulated drug in the cytosol.

2.4.5. Viability of breast cancer cells in three-dimensional spheroid cultures

Although the monolayer cultures offer valuable information about the cells, it does not mimic the three-dimensional structure of the tumors. To provide a better model system, MCF7 cells were cultured as three-dimensional spheroids. Hypoxic cells within the core of the spheroids can simulate hypoxic niches within tumors for in vitro hypoxia-responsive targeted drug delivery studies. The spheroids were treated for 72 hours with the two polymersome formulations and free drug the same as monolayer cell cultures (15 μM free Dox and equivalent amount of non-targeted and targeted Dox-encapsulated polymersomes) and the cell viability was determined (Figure 8A). Under hypoxia, treating the breast cancer cell spheroids with targeted E_2-Dox-HRPs (15 μM Dox) significantly ($p < 0.05$) reduced the cell viability to 21% compared to targeted E_2-Dox-HRPs in normoxia (55%). However, we did not observe significant differences in cell viability under hypoxia and normoxia when the cells were treated with non-targeted polymersomes or free Dox.

Due to the enhanced permeability and retention effect, both targeted and non-targeted polymersomes can pass through the leaky vasculature and reach the tumor site.[199] However, the targeted polymersomes will show enhanced tumor penetration and cytotoxicity based on receptor-mediated endocytosis. However, we note that some polymersomes may release their encapsulated Dox before cellular entry. In this case, free Dox will diffuse into the cell through the plasma membrane.[200] The passive diffusion would be less predominant when Dox is delivered to the cancer cells via the targeted hypoxia-responsive polymersomes. We observed that majority of the polymersomes internalized into the breast cancer cells in 3 hours under hypoxia (Figure 6), while less than 40% of the drug was released after 3 hours (Figure 4).

To further evaluate the efficacy of non-targeted and targeted polymersomes, the 6-day old spheroids were treated with 10 μM free Dox and equivalent amount of non-targeted Dox-HRPs and targeted E_2-Dox-HRPs for 72 hours in both hypoxia and normoxia and their growth was monitored until day 16 (Figures 8B, C).

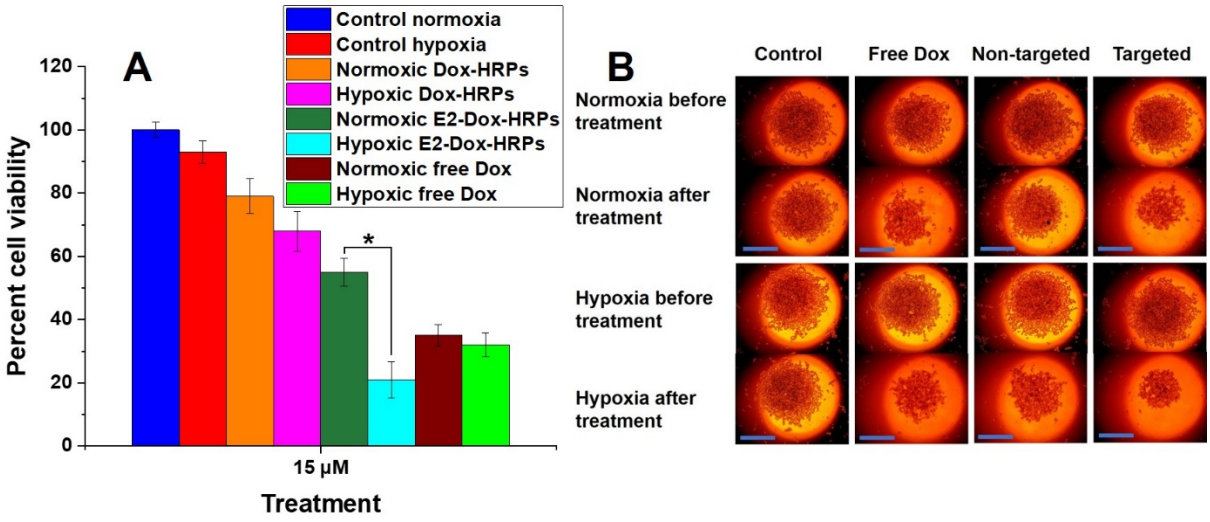

Figure 2.8. (A) Viability of MCF7 cell spheroids after 72-hour treatment with free Dox, non-targeted (Dox-HRPs) and targeted polymersomes (E_2-Dox-HRPs) under normoxia and hypoxia ($n = 6$, $*p < 0.05$). **(B)** Representative images of three-dimensional spheroid cultures of the MCF7 cells before and after 72-hour treatment with free Dox, non-targeted and targeted polymersomes in normoxia and hypoxia (scale bar: 100 μm).

We observed that targeted E_2-Dox-HRPs were more toxic to the MCF7 cells by shrinking the volume of the spheroids up to 68%, while non-targeted polymersomes reduced the volume of the spheroid by 24% in hypoxia (Figure 9A). The targeted polymersomes significantly reduced the spheroid volume compared to non-targeted Dox-HRPs ($p < 0.05$) and control group ($p < 0.01$) in hypoxia (Figure 9A). A significant difference ($p < 0.01$) was also observed between targeted E_2-Dox-HRPs and the control group in normoxia (Figure 9B), although not as pronounced as the cells under hypoxia. In addition, non-targeted polymersomes demonstrated less toxicity toward spheroids compared to free Dox in both hypoxia and normoxia. Overall, the results demonstrated that targeted polymersomes have the potential to shrink the microtumors in

hypoxia compared to non-targeted polymersomes. Targeted polymersomes could also shrink the spheroids compared to the control group in both hypoxia and normoxia.

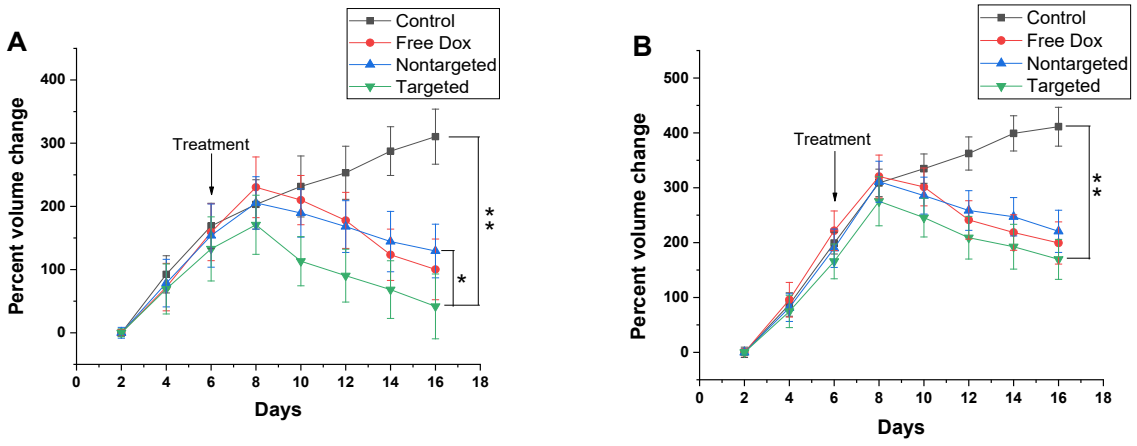

Figure 2.9. Growth curve for the MCF7 spheroids in hypoxia **(A)** and normoxia **(B)** treated with free Dox, non-targeted and targeted Dox-encapsulated polymersomes (n = 6, *p < 0.05, **p < 0.01).

2.5. Conclusion

The 17β-estradiol-conjugated polymersomes described here are the first reported targeted polymeric hypoxia-responsive drug delivery nanocarriers for reducing ER-positive breast cancer cell viability. Targeted polymersomes significantly reduced the volume of MCF7 spheroids in hypoxic conditions compared to non-targeted polymersomes and free drugs. Due to the presence of 17β-estradiol on the surface of targeted polymersomes, they can bind to the ER on the surface of the breast cancer cells and internalize. The targeted polymersomes encapsulated doxorubicin with an efficiency of 59%. The hypoxia-responsive group employed in polymer structure allowed the release of Dox within hypoxic breast cancer cells and enhanced doxorubicin therapeutic efficiency against ER-positive breast cancer cells. The merits of our targeted polymeric nanoparticles are: ability to selectively target the estrogen receptor-positive breast cancer cells, break in the hypoxic niches of microtumors, release the encapsulated anticancer drug, and reduce cancer cell viability. With further developments, the 17β-estradiol-conjugated

hypoxia-responsive polymersomes have the translational potential for targeted drug delivery in ER-positive breast cancer therapy.

2.6. Acknowledgements

This research was supported by NIH grant 1 R01GM 114080 (NIGMS) and a Ready-to-Go award from the DaCCoTA Center (NIGMS U54 GM128729) to SM. SM also acknowledges support from the Grand Challenge Initiative and the Office of the Dean, College of Health Professions, North Dakota State University. The authors thank Parinaz Ghanbari for designing all schematic illustrations in this manuscript.

3. ENDOXIFEN-CONJUGATED, HYPOXIA-RESPONSIVE POLYMERIC NANOPARTICLES FOR TARGETED DRUG DELIVERY TO BREAST CANCER MICROTUMORS

3.1. Abstract

Endoxifen is the major active metabolite of tamoxifen, a nonsteroidal selective estrogen receptor modulator (SERM). Endoxifen is widely used for the treatment of estrogen receptor positive (ER+) breast cancer. In this study, endoxifen was conjugated to the surface of polymeric nanoparticles (polymersomes) for targeted delivery of DOX to estrogen receptor positive breast cancer cells (MCF7). Rapid cell growth and insufficient blood supply results in low oxygen concentration (hypoxia) within the solid breast tumors. The polymersomes developed here are prepared from amphiphilic diblock polylactic acid (PLA) and polyethylene glycol (PEG) copolymers containing diazobenzene linker as the hypoxia-responsive moiety. We prepared two nanoparticle formulations: DOX-loaded hypoxia-responsive polymersomes (DOX-HRPs), and endoxifen-conjugated DOX-loaded hypoxia-responsive polymersomes (END-DOX-HRPs). Cellular internalization studies demonstrated 8 times higher cytosolic and nuclear localization after incubating breast cancer cells with END-DOX-HRPs (targeted polymersomes) in contrast to DOX-HRPs (non-targeted polymersomes). Cytotoxicity studies on monolayer cell cultures exhibited that END-DOX-HRPs were 3 times more toxic to ER+ MCF7 cells compared to DOX-HRPs and free DOX in hypoxia. The cell viability studies on three-dimensional cultures in hypoxia also demonstrated 2 times more toxic when the spheroids were treated with targeted polymersomes in contrast to the non-targeted polymersomes. The newly designed targeted endoxifen-conjugated, hypoxia-responsive polymersomes offered in this study might have translational potential for ER+ breast cancer treatment.

3.2. Introduction

Breast cancer (BC) is characterized by uncontrolled cell proliferation, angiogenesis, and metastasis to other organs.[201] Surgery and radiation therapy are effective treatment options for the localized disease.[202] Hormone therapy and chemotherapy are the most common regimen for the invasive BC.[203] Unfortunately, chemotherapeutic agents show various side effects that limit their administration in cancer therapy.[204–207] In addition, low solubility, high therapeutic dosage, reduced systemic blood circulation, and increased cytotoxicity are common drawbacks of anticancer drugs.[208,209] Uncontrolled cell proliferation and limited blood flow generate low oxygen concentration (hypoxic condition) in solid tumor tissues of various cancers including BC.[210–214] Hypoxia contributes to invasiveness, metastasis, and resistance against chemotherapeutic drugs.[215] Nanomedicine and nanotechnology are emerging fields in drug delivery, diagnosis, and development of nanoscale materials for cancer therapy.[216–219] Nanocarrier-based drug delivery systems have the possibility to address the shortcomings of traditional chemotherapy by improving circulation half-life, tumor penetration, and cellular internalization.[220,221] Among various types on nanoparticles, polymersomes show considerable promise to deliver drugs into cancerous tissues. They are self-assembled bilayer vesicles prepared from amphiphilic copolymers with hydrophilic and hydrophobic blocks.[222–224] Vesicle formation is fovored when the ratio of the hydrophilic block to the whole polymer is 20-40%.[210,222,225] Polymersomes carry hydrophilic drugs within the aqueous core and hydrophobic drugs within the bilayer simultaneously.[212,226] Polyethylene glycol (PEG) is commonly used as hydrophilic block due to its biocompatibility, reduction in protein adsorption, and the resultant prolonged circulation time of the polymersomes.[227] Because of the higher molecular weights of the polymers compared to lipids, polymersomes are more robust and stable compared to

liposomes.[226] However, enhanced stability requires a stimulus for releasing the encapsulated drugs.[227,228] The stimuli-responsive polymersomes are stable in systemic circulation and disintegrate within the disease sites by responding to physical, chemical, or biological stimuli.[229–232] Hypoxia-responsive polymersomes release therapeutic agents in response to the low oxygen partial pressure within solid tumors.[210–212] In addition, modifying polymersomes' surface with ligands for selective binding to overexpressed receptor on cancer cells facilitates tumor penetration and cellular internalization, reducing the off-target side effects of chemotherapeutic agents.[233–236]

Estrogen receptors (ERs) are overexpressed in about 80% of BC cases (ER+ BC).[237] ERs are divided into ERα and ERβ subclasses. A class of ERα (G-protein coupled receptors) are expressed on the membrane of BC cells.[238] Tamoxifen (TAM) is a pioneering medicine for ER+ BC treatment that belongs to selective estrogen receptor modulators (SERM).[239] TAM competes with estrogen for binding to ERs and reduces breast tumor growth.[240] TAM can be incorporated as a ligand into the surface of nanoparticles for targeting overexpressed ERs on the surface of BC cells.[241] However, TAM is a prodrug which converts to the active metabolites, such as 4-hydroxy TAM or endoxifen (END).[240] END is the most active metabolite of TAM. It binds to the ER about 100 times more strongly and about 30 times more potent in reducing the growth and proliferation of ER+ breast cancer cells compared to TAM.[242,243]

Herein, we conjugated to END to an amphiphilic block copolymer of polyethylene glycol (PEG) and polylactic acid (PLA). We prepared polymersomes from the END-conjugated and a hypoxia-responsive copolymer, encapsulating the anticancer drug doxorubicin inside. Due to the END ligands, the polymersomes selectively bind to overexpressed ERs on the surface of ER+ BC cells, translocate into the cells, disintegrate, and release their chemotherapeutic payload

selectively within hypoxic BC cells. This is the first report of employing END as a high affinity ligand to target ER+ breast cancer cells by polymersomes. We anticipate that these targeted nanoparticles have a potential for chemotherapeutic drug delivery to ER+ hypoxic cancer microtumors.

3.3. Materials and methods

3.3.1. Materials and reagents

Endoxiden hydrochloride was purchased from Selleckchem. Doxorubicin hydrochloride was purchased from Advanced Chemblocks. The chemicals for synthesizing the copolymers were from Millipore Sigma. The medium and antibiotics for the cell culture were purchased from VWR International. A humidified incubator (Thermo Scientific) containing 5% CO_2, and 21% O_2 at 37° C was used for normoxic condition. For all experiments, a hypoxia chamber containing 5% CO_2 and 2% O_2 was used.

3.3.2. Synthesis and characterization of copolymers

The polylactate-diazobenzene-polyethylene glycol (PLA_{8500}-Azo-PEG_{2000}) and polylactate- polyethylene glycol azide (PLA_{17000}-PEG_{2000}-N_3) polymers were synthesized and characterized according to the previously reported protocol (Supporting Information, Figures A1-5).[212] For the synthesis of endoxifen-hexynol, 5-hexyn-1-ol (11 µL, 100 µM) and triethylamine (0.1 mL) were dissolved in 5 mL of anhydrous dichloromethane. Then, N-(3-Dimethylaminopropyl)-N′-ethylcarbodiimide hydrochloride EDC.HCl (27 mg, 100 µM), N-hydroxysuccinimide (NHS) (11.5 mg, 100 µM), and dimethylaminopyridine (DMAP) (3 mg, 5% mol) were added and the mixture was stirred at 25° C for 1 h under nitrogen atmosphere. Endoxifen HCl (41 mg, 100 µM) was added to the reaction mixture and stirred overnight, followed by washing 3 times and drying under vacuum to get a solid compound (0.62 g, yield:

40%). ^{1}H-NMR (400 MHz, chloroform-d): 7.13-6.51 ((C**H**2=C**H**2), d, 13 H), 4.11 ((C**H2**-CH_2-N), t, 2 H), 3.99 ((C**H_2**-O-C=O), t, 2 H), 3.70 ((CH2-C**H_2**-N), t, 2 H), 3.59 ((C**H_3**-N), s, 3 H), 3.01 ((C**H**≡C-), s, 1 H), 2.51 ((CH≡C-C**H_2**), t, 2 H), 2.24 ((CH_3-C**H_2**), q, 2 H), 1.65 ((CH_2-C**H_2**-CH_2), m, 2 H), 1.28 ((CH_2-CH_2- C**H_2**), m, 2 H), 0.85 ((C**H_3**-CH_2), t, 3 H).

Endoxifen-hexynol (7 mg, 10 µmol) and azide polymer (100 mg, 5 µmol) were dissolved in 5 mL THF. The cycloaddition reaction between endoxyfen-hexynol and azide polymer was performed according to a protocol developed in our laboratory.212 The final product was dried under vacuum (7 mg, yield: 57%) and characterized by 1H-NMR and gel filtration chromatography (GPC). 1H-NMR (400 MHz, chloroform-d): 7.00 (C=CH-CH=C, s, 1 H), 5.19 ((-CH-C=O), q, 1 H), 3.67 ((CH2-C=O), d, 2 H), 2.29 ((CH3-NH), d, 3 H), 1.58 ((CH3-CH-C=O), d, 3 H), 0.89 ((CH3-C-), s, 6 H). GPC: Mw = 12k, Mn = 9.3k, and PDI = 1.29

3.3.3. Polymersome preparation

Polymers were dissolved in acetone (10 mg/mL) and lissamine rhodamine lipid dye (LR) was dissolved in chloroform (0.01 mg/mL). Plain (HEPES buffer-encapsulated) and non-targeted polymersomes were prepared by adding 95:5 molar ratio azobenzene polymer to LR. Targeted polymersomes were prepared by 85:10:5 molar ratios of azobenzene polymer, END-conjugated polymer, and LR dye. A consistent amount of doxorubicin HCl (0.2 mg/mL) was encapsulated into both non-targeted and targeted polymersome samples. Plain, non-targeted, and targeted polymersomes were all prepared according to the previously reported protocols from our laboratory.[212]

3.3.4. Characterization

Polymersomes were incubated in normoxic (21% O_2) and hypoxic (24 hours, 2% O_2) conditions. A mixture of NADPH (50 µM), microsomes (50 µL), and polymersomes (500 µL)

was used to prepare hypoxic samples. An atomic force microscope (AFM, NTEGRA) was used for AFM imaging, and transmission electron microscope (TEM, JOEL JEM-2100) was employed for TEM imaging using both normoxic and hypoxic polymersomes, as it was previously reported.[212]

Dynamic Light Scattering (DLS, Malvern Zetasizer) was used for determining the charge and size of the polymersomes under hypoxic and normoxic conditions by measuring each sample six times and recording the averages.

3.3.5. Release study

A series of DOX concentrations was used to create a calibration curve. The loading content and percent encapsulation of DOX within the vesicles were calculated by measuring the absorbance (480 nm). DOX release from the polymeromes was determined by preparing a combination of targeted nanoparticles, NADPH, human liver microsomes, and HEPES buffer (pH 7.4, 25 mmol) within a membrane, based on the reported protocol.[212]

3.3.6. Cellular internalization

The MCF7 ER+ and MDA-MB231 triple negative (ER-, PR-, HER2-) breast cancer cells were cultured in DMEM medium containing 10% FBS. The cells (5,000/well) were seeded in two cell culture plates and incubated in normoxic (21% O_2) and hypoxic (2% O_2) conditions overnight. Then, 5.5 μM END and the equivalent amount of non-targeted and targeted buffer-encapsulated nanoparticles, and a mixture of 5.5 μM END and END-conjugated nanoparticles were used for treating the cells for 3 hours. After washing, the cell nucleus and skeleton were stained with DAPI (Invitrogen) and Phalloidin (Biotium) dyes, and then washed again with PBS. The cells were imaged by 20x objective of a Leica DMi8 fluorescence microscope (Leica Microsystems Inc).

3.3.7. Polymer toxicity

The cells (5,000/well) were cultured in two plates and incubated in normoxia (21% O_2) and hypoxia (2% O_2) overnight. HEPES buffer-encapsulated END-polymersomes (20 to 100 μg/mL) were incubated with the cells for 72 hours. Then, a 1:9 volume ratio of Alamar Blue to cell culture medium was incubated with the cells for 5 hours. The cytotoxicity was calculated by measuring the fluorescence using an excitation wavelength of 560 nm and emission wavelength of 595 nm.

3.3.8. Toxicity of DOX-polymersomes in monolayer culture

The cells (5,000/well) were cultured in two plates and incubated in normoxic (21% O_2) and hypoxic (2% O_2) conditions overnight. When the cells were 80% confluent, they were divided into four treatments: control (without treatment), free DOX, non-targeted polymersomes (DOX-HRPs), and targeted polymersomes (END-DOX-HRPs). Subsequently, 2, 4, and 8 μM DOX within all doxorubicin-containing formulations were used to treat the cells for 72 hours. The plates were then washed with PBS and the cytotoxicity was calculated using Alamar Blue assay described in the previous paragraph.

3.3.9. Spheroid cytotoxicity study

The MCF7 cell spheroids were prepared by NanoShuttle three-dimensional kit (Greiner Bio one). NanoShuttle-PL magnetic nanoparticles (150 μL) were added into an 80% confluent MCF7 cell culture T-25 flask and incubated for 24 hours. The flask was washed to with PBS and the cells were then dislodged, counted, and 25,000 cells were added into each well, while placing the plates on a spheroid drive for 30 minutes. The plates were separately incubated in normoxia (21% O_2) and hypoxia (2% O_2) overnight. Subsequently, the cells were incubated with the same four treatments as monolayer cultures and treated with 2, 4, and 8 μM DOX in the formulations

for 3 days. The spheroid drives were removed to detach the spheroids. Then, the spheroids were moved into new plates and incubated for 24 hours. The cytotoxicity was evaluated by Alamar Blue assay. To further assess the effect of free drug, non-targeted, and targeted polymersomes on the growth of the spheroids, another plate of 6-day-old spheroids were incubated with 8 μM DOX, non-targeted DOX-HRPs, and targeted END-DOX-HRPs for 3 days under normoxic (21% O_2) and hypoxic (2% O_2) conditions. The spheroids were then washed, and their growth was monitored until day 16. The percent growth rate was analyzed by the NIH ImageJ software.

3.3.10. Statistical analysis

All statistical analyses were carried out by OriginPro 9.3 (Northampton, Massachusetts) and the results were shown as mean ± SEM. The significant difference among various drug-treated groups in hypoxic and normoxic conditions were evaluated by ANOVA.

3.4. Results and discussions

3.4.1. Polymer characterization and polymersome preparation

The PLA_{16000}-PEG_{2000}-Endoxifen polymer was synthesized by cycloaddition reaction between alkyne-endoxifen and PLA-PEG-N_3 (Scheme 3.1). The polymers were characterized by gel permeation chromatography (GPC) and ^1H NMR spectroscopy (Supporting Information, Figures B1-2). DOX was encapsulated within the polymersomes. Lissamine rhodamine lipid dye was incorporated into the polymersomes to visualize them while passing them through the gel filtration chromatography column to isolate the drug-encapsulated vesicles. The structures of the polymers used in polymersome preparation are shown in Scheme 3.2. Polymersomes are formed when the molar mass ratio of hydrophilic part to the total polymer is between 1:5 to 2:5.[244] For our studies, this ratio was 1:5. The surface PEG enhance the systemic half-life of the vesicles in blood circulation.[212] The targeted nanoparticles were optimized to contain 10% PLA-PEG-

Endoxifen polymer for efficient interactions with the membrane-associated estrogen receptors on the MCF7 cells.

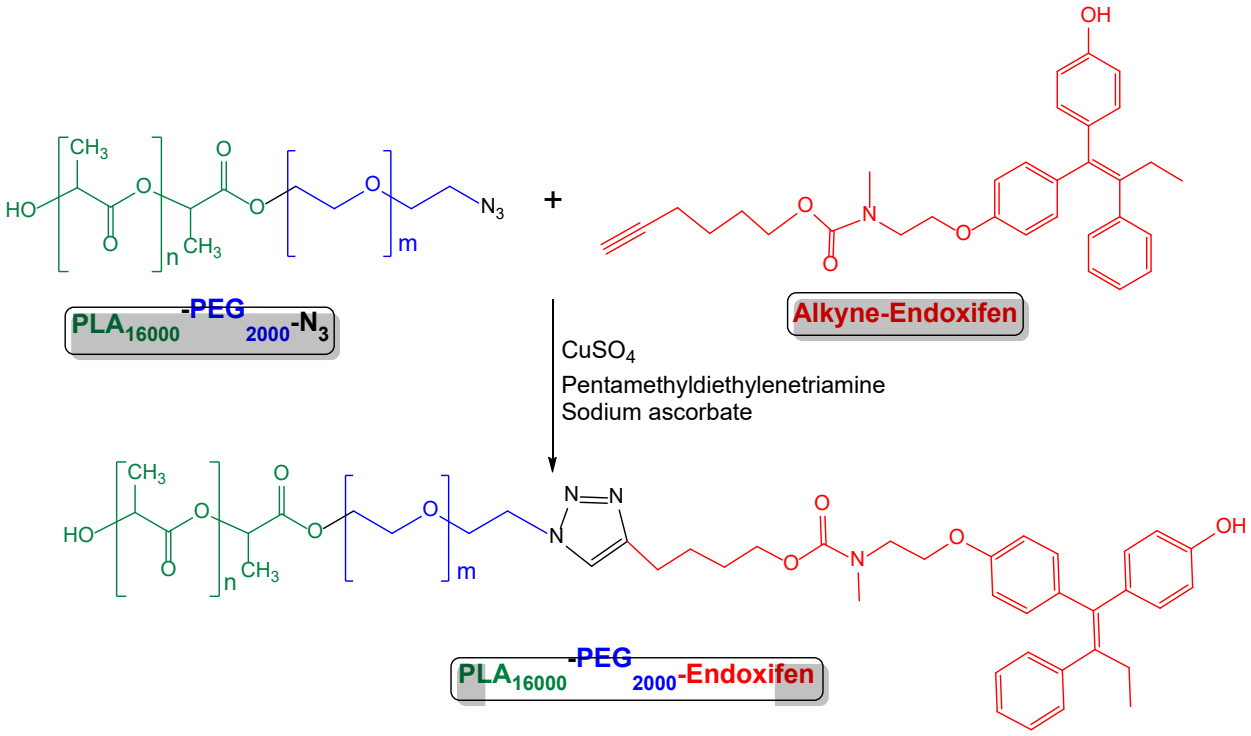

Scheme 3.1. Cycloaddition reaction between PLA-PEG-N_3 polymer and Alkyne-Endoxifen to prepare PLA-PEG-Endoxifen polymer.

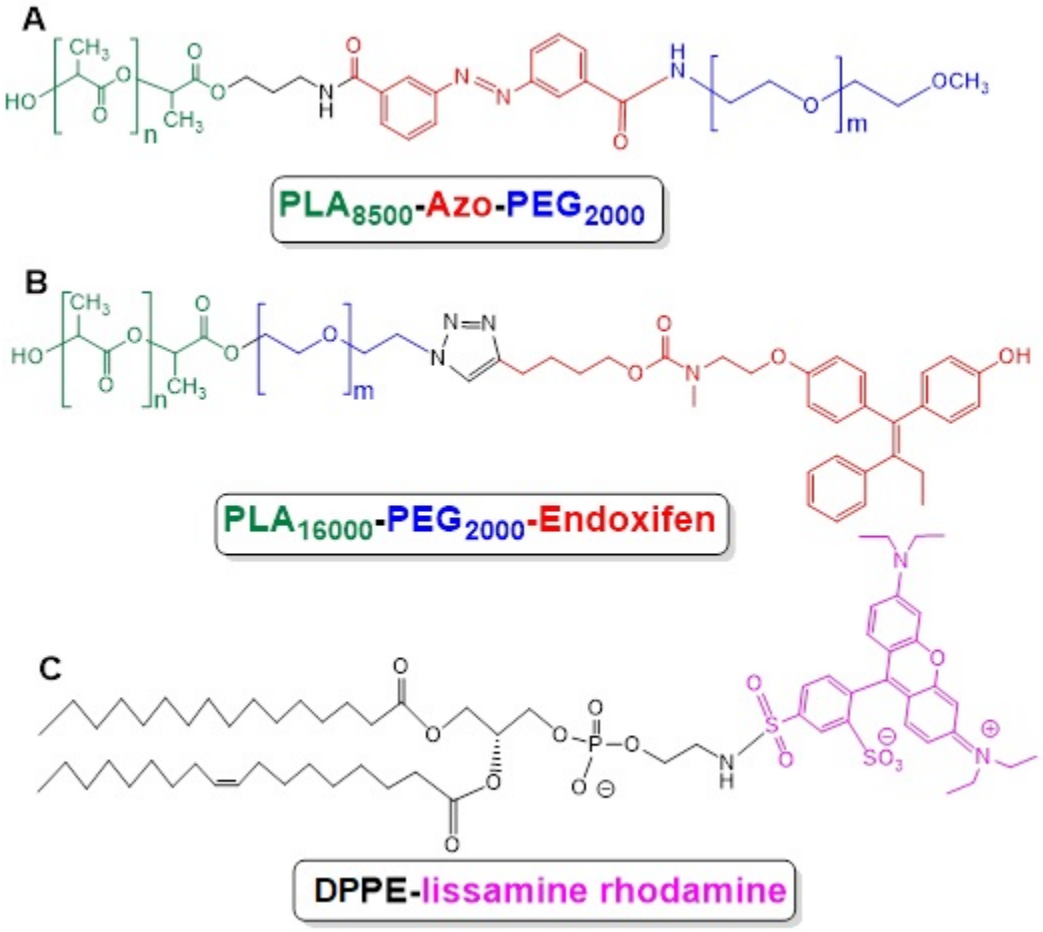

Scheme 3.2. Structures of synthesized polymers and fluorescent lipid dye. **(A)** PLA_{8500}-Azo-PEG_{2000} polymer, **(B)** PLA_{16000}-PEG_{2000}-Endoxiden.

We prepared both DOX-encapsulated non-targeted (DOX-HRPs) and targeted hypoxia-responsive polymersomes (END-DOX-HRPs). These nanoparticles are expected to passively accumulate within the tumors based on the EPR effect.[220] However, the functionalized polymersomes with targeting ligands not only accumulate within the tumor environment via EPR effect, but also selectively interact with the overexpressed surface receptors on cancer cells and enter the cells through active transport (Figure 1).[213,220]

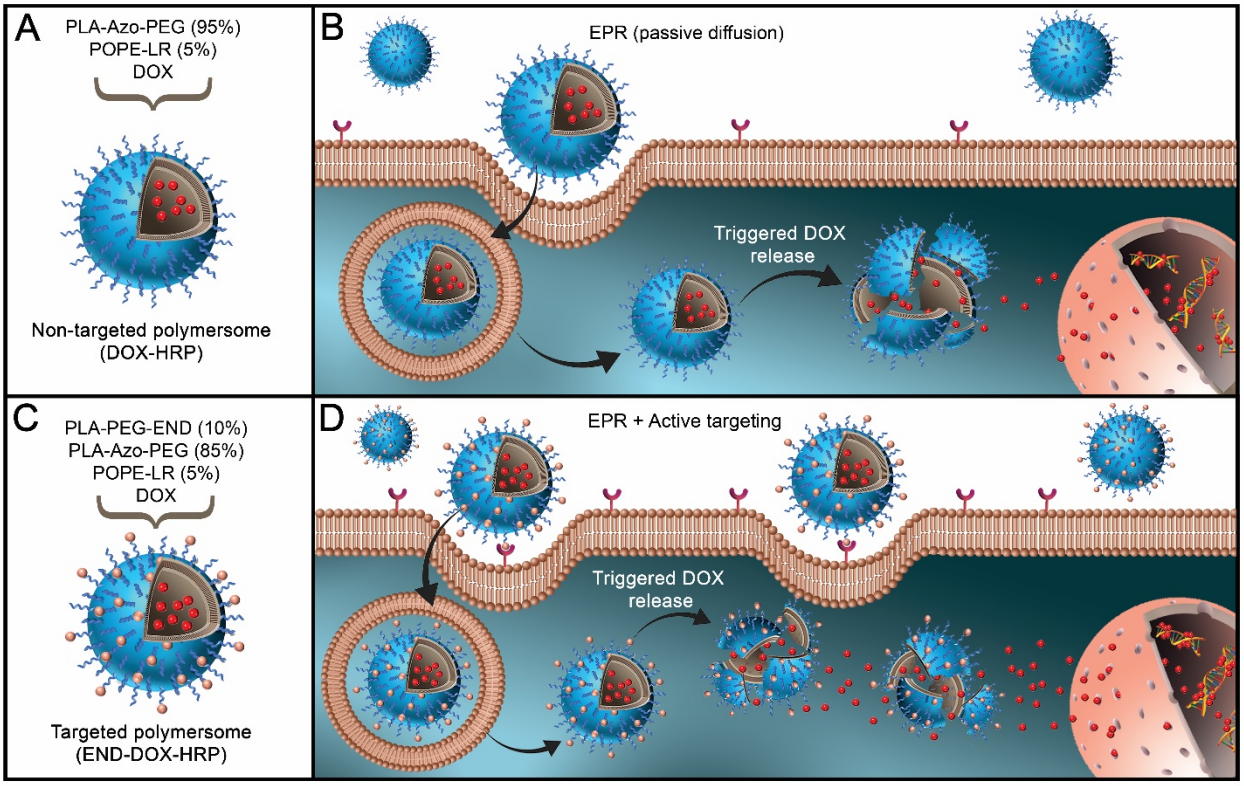

Figure 3.1. Illustration of non-targeted and targeted polymersomes containing doxorubicin. **(A)** Components of non-targeted polymersomes. **(B)** Internalization of non-targeted polymersomes in cancer cells via passive diffusion. **(C)** Components of targeted polymersomes. **(D)** Internalization of targeted polymersomes in cancer cells via receptor-mediated endocytosis.

The solvent exchange procedure was used to prepare the polymersomes[224] and subsequently characterized by DLS, AFM, and TEM imaging. The loading content and average percent encapsulation of doxorubicin within non-targeted and targeted polymersomes were calculated (Table 3.1). The average charge and hydrodynamic diameter of the nanoparticles were measured under hypoxic and normoxic conditions by dynamic light scattering (Figure 2, Table 3.2). We observed that the average diameter of the DOX-encapsulated targeted polymersomes (164 $\pm$ 7 nm) were larger compared to the non-targeted vesicles (122 $\pm$ 5 nm). The increased hydrodynamic diameter is likely due to the incorporation of the endoxifen conjugated polymer (PLA_{16000}–PEG_{2000}–Endoxifen, Scheme 3.2) with a higher molecular weight of the PLA block.

Table 3.1. Encapsulation efficiency (EE%) and loading content (LC%) of the polymersomes

Polymersome	Encapsulation efficiency (%)	Loading content (%)
Non-targeted (DOX-HRP)	46 ± 5	8.1 ± 1.29
Targeted (END-DOX-HRP)	68 ± 6	10.2 ± 2.13

Table 3.2. Average hydrodynamic diameter, ζ potential, and polydispersity index (PDI) of the DOX-encapsulated polymersomes

Polymersome	Average diameter (nm)		ζ potential (mV)		PDI	
	Normoxia	Hypoxia	Normoxia	Hypoxia	Normoxia	Hypoxia
Non-targeted	122 ± 5	41 ± 6, 425 ± 8	0.18 ± 0.03	0.32 ± 0.14	0.14 ± 0.06	0.66 ± 0.17
Targeted	164 ± 7	68 ± 8, 678 ± 9	0.27 ± 0.19	0.44 ± 0.18	0.15 ± 0.05	0.73 ± 0.16

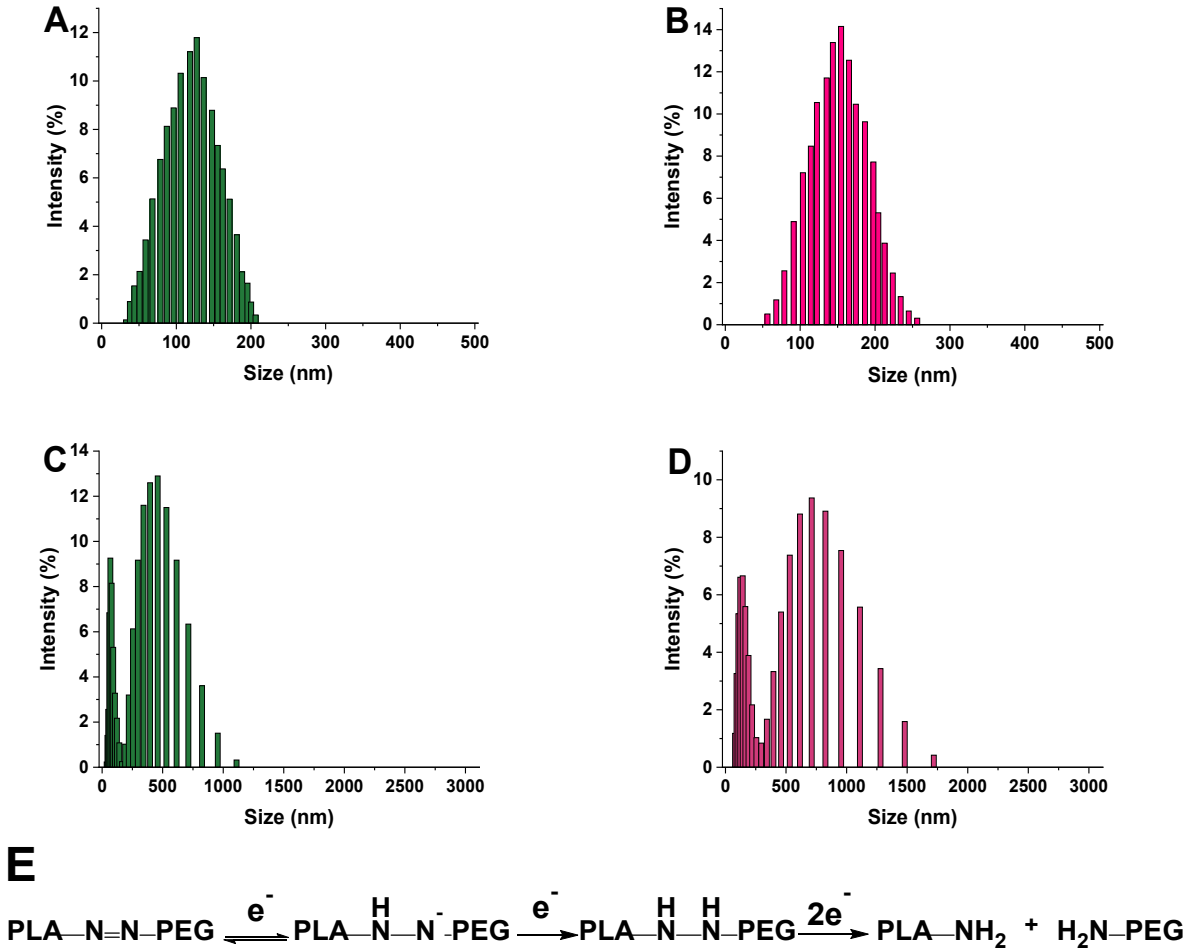

Figure 3.2. (A) Hydrodynamic diameter of non-targeted polymersomes under normoxia. **(B)** Hydrodynamic diameter of targeted polymersomes under normoxia. **(C)** Hydrodynamic diameter of non-targeted polymersomes under hypoxia. **(D)** Hydrodynamic diameter of targeted polymersomes under hypoxia. **(E)** Proposed mechanism of drug release under hypoxia in the presence of reducing agents.[245]

We observed that the size of the polymersomes changed substantially after exposure to hypoxia (Table 3.2, Figure 2). It is likely due to disintegration and coalescence to make smaller and larger vesicles with diameter ranges of 40-430 nm for non-targeted and 65-680 nm for targeted polymersomes (Figure 2C-D). Accordingly, the polydispersity indices (PDI) for the polymersomes increased under hypoxia (Table 3.2). TEM and AFM images corroborated these observations (Figure 3). The hypoxic tumor microenvironment is enriched in reductase enzymes.[246] For the in vitro studies, we simulated the reductive microenvironment with human liver microsomes (source of reductase enzymes) and NADPH (for enzyme activity).[212] Under hypoxia, reduction of the diazo linker of the hypoxia-responsive polymer separates the hydrophobic PLA and hydrophilic PEG blocks (Figure 2E).[211,245,247] The resultant structural collapse of the polymersomes facilitates the release of the encapsulated doxorubicin.[212] The ζ potential was positive under both normoxic and hypoxic conditions.

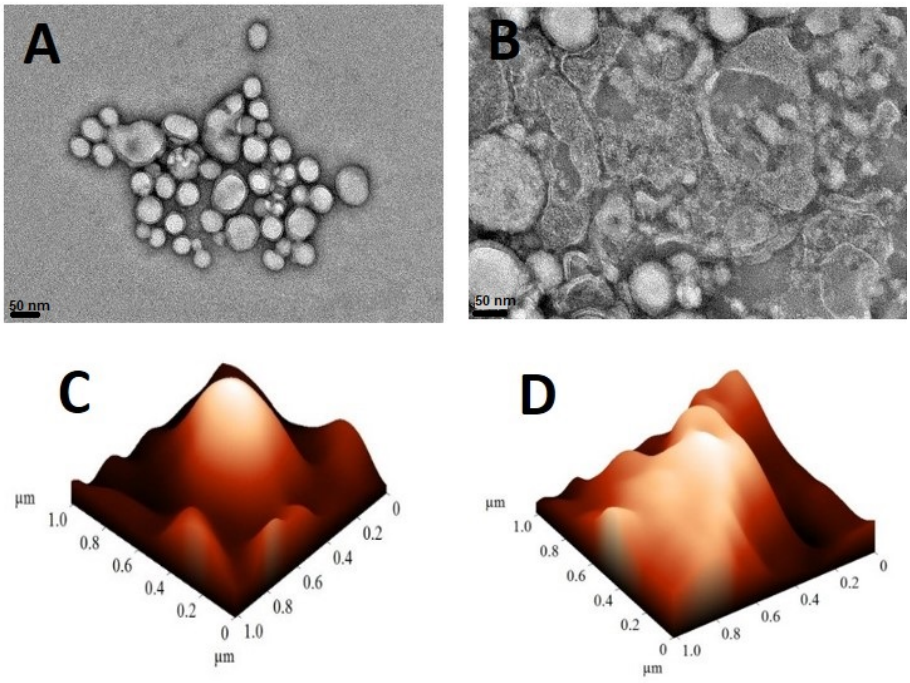

Figure 3.3. TEM and AFM images of endoxifen-nanoparticles under normoxic condition **(A, C)** and hypoxic condition **(B, D)**.

3.4.2. Doxorubicin release from polymersomes

To assess drug release from the polymersomes under hypoxic condition, DOX was encapsulated into the END-conjugated nanoparticles. These polymersomes were incubated under hypoxia (human liver microsomes, NADPH, 2% oxygen) and normoxia (human liver microsomes, NADPH, 21% oxygen) and drug release was evaluated for 12 hours (Figure 4).

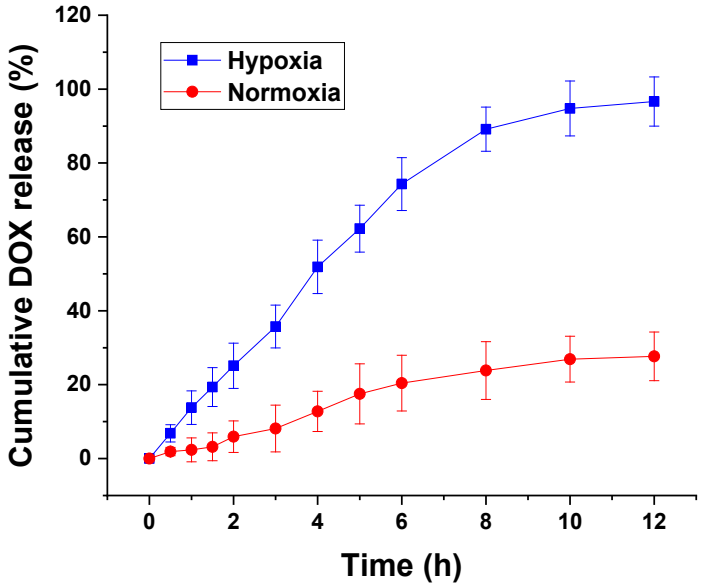

Figure 3.4. Cumulative release of doxorubicin from targeted hypoxia-responsive nanoparticles in hypoxic (2% oxygen) and normoxic (21% oxygen) conditions (n = 3).

We observed higher DOX release from the polymersomes under hypoxia compared to normoxia. Polymersomes released more than 96% of their cargo under hypoxia within 12 hours. However, less than 27% of DOX encapsulated in polymersomes was released in normoxia during the same time. The results indicated that the reduction of hypoxia-responsive benzene linker leads to the release of the encapsulated drug under hypoxia.

TEM and AFM images demonstrated that polymersomes maintained their normal shape under normoxia, while disrupting their vesicular structure under hypoxia (Figure 3).

3.4.3. Cellular internalization

To evaluate cellular internalization, the ER+ breast cancer cells (MCF7) were treated with 5.5 µM free END, equivalent amount of non-targeted and targeted buffer-encapsulated nanoparticles, and a mixture of 5.5 µM END and END-conjugated polymersomes under hypoxia and normoxia for 3 hours. Lissamine rhodamine dye was incorporated into the polymersome bilayer to follow the cellular uptake using a fluorescence microscope (Figures 5A, B).[212] The fluorescence density of the images was normalized based on the number of breast cancer cells. NIH ImageJ was used for calculating the fluorescence intensity of all treatment groups under hypoxic and normoxic conditions (Figure 5C).

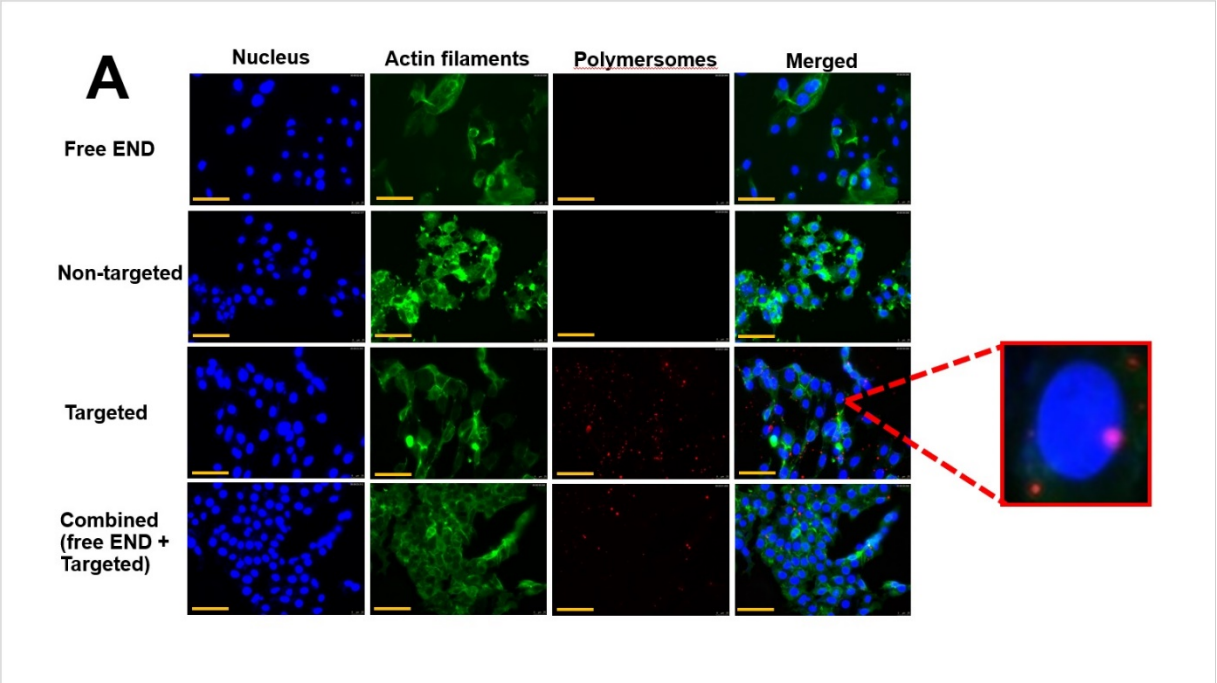

Figure 3.5. Fluorescence images of cellular uptake in MCF7 cells. Free endoxifen (free END), non-targeted and targeted polymersomes, and the combination of END and targeted polymersomes after 3 hours under normoxia **(A)** and hypoxia **(B)** (scale bar: 50 µm). **(C)** Quantitative fluorescence intensity of the cells under normoxia and hypoxia (n = 3).

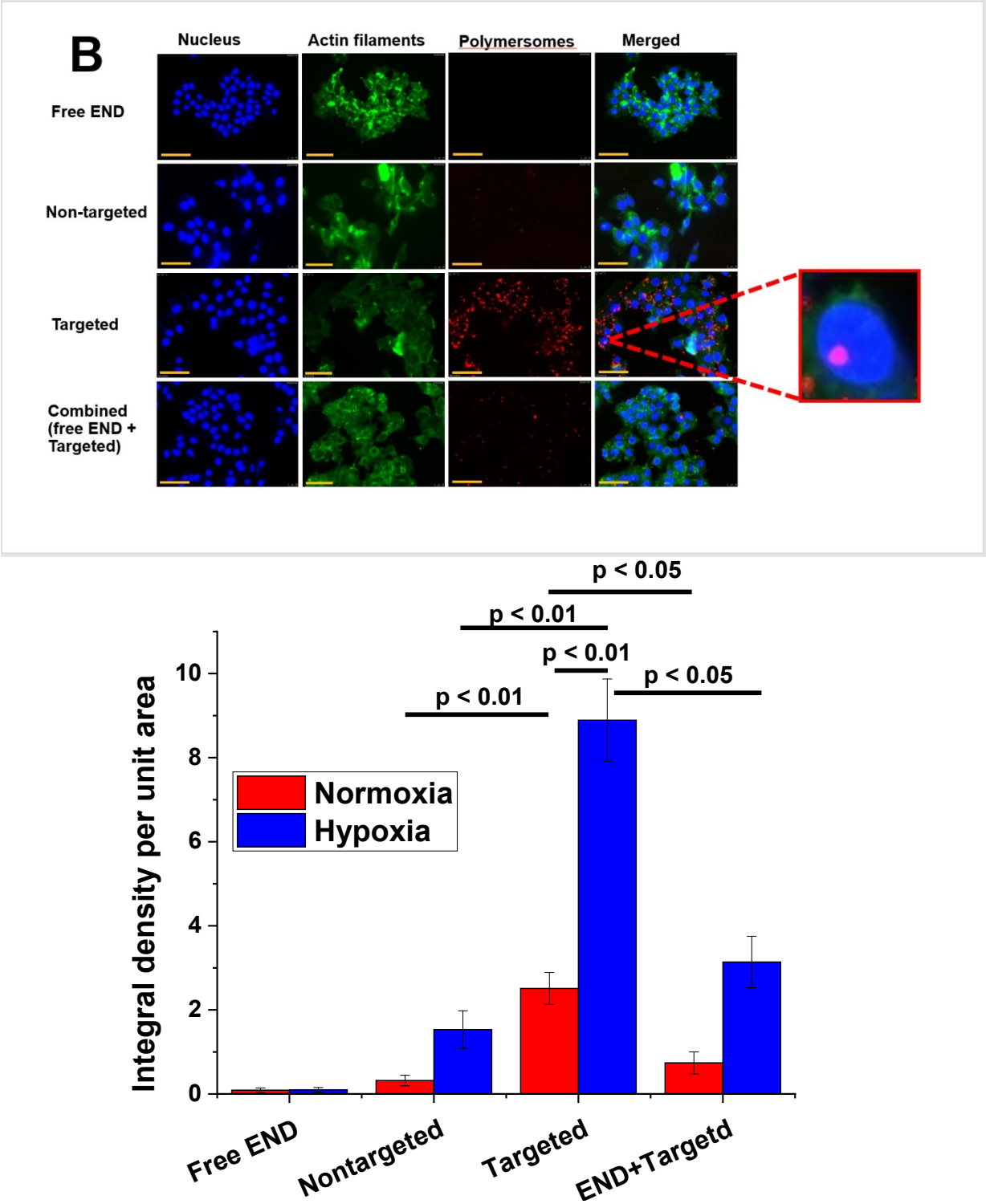

Figure 3.5. Fluorescence images of cellular uptake in MCF7 cells (continued). Free endoxifen (free END), non-targeted and targeted polymersomes, and the combination of END and targeted polymersomes after 3 hours under normoxia **(A)** and hypoxia **(B)** (scale bar: 50 μm). **(C)** Quantitative fluorescence intensity of the cells under normoxia and hypoxia (n = 3).

It was observed that targeted END-conjugated polymersomes penetrated to the breast cancer cells under both normoxia and hypoxia due to increased ligand-receptor interaction between endoxifen and estrogen receptors (insertions within Figures 5A, B). It was shown that the density of targeted polymersomes within the cells in both normoxia and hypoxia was higher than the combination of targeted polymersomes and END treatment ($p < 0.05$), and higher than non-targeted polymersomes ($p < 0.01$). We also observed that the fluorescence density of targeted polymersomes was 7.8 and 6 times higher than non-targeted polymersome-treated groups in hypoxia and normoxia, respectively. The fluorescence density in hypoxic targeted polymersomes was also higher than normoxic targeted polymersomes ($p < 0.01$).

Various factors are involved in retaining nanoparticles inside cancer cells such as the size and concentration of the nanoparticles, the duration of cellular exposure to hypoxia, and uptake or efflux of the nanovesicles from the cells. According to a recent study on breast cancer cells, nanoparticle penetration into the cells increased under hypoxia in comparison to normoxia.[248] Another study on ER+ breast cancer cells indicated an enhanced internalization of gold nanoparticles into the hypoxic MCF7 cells.[249] We observed that exposing the ER+ MCF7 cells to hypoxic condition for 180 minutes led to enhanced uptake of the targeted endoxifen-conjugated polymersomes into the cells (Figure 5B). It was observed that targeted END-polymersomes could penetrate more to the cancer cells compared to non-targeted vesicles likely due to the overexpression of membrane-bound estrogen receptors on the surface of breast cancer cells (Figure 5).[241] To evaluate the potency of END-polymersomes for cellular internalization, we conducted another experiment by treating a group of ER+ MCF7 cells with free END, and another group of the cells with a combination of END-polymersomes and free END. We observed that free END could not penetrate to the cells. However, when we treated the cells with

a combination of free END and targeted END-polymersomes, free END particles inhibited END-polymersome internalization into the cells. This was observed because free END binds to estrogen receptor and competitively inhibits END-polymersomes to interact with the receptors and penetrate to the cells.

To probe the role of ER in cellular internalization, we incubated the triple-negative breast cancer MDA-MB-231 cells with the same polymersome formulations and imaged them using a fluorescence microscope (Figures 6A, B). We observed a weak fluorescence intensity from both targeted and non-targeted polymersomes (deshed-line insertions in Figures 6A, B). Moreover, the intensities were not significantly different in hypoxia ($p = 0.124$) and normoxia ($p = 0.251$) and in the absence and presence of added endoxifen (Figure 6C). We chose the same treatment options for triple negative breast cancer cells as we did for ER+ cells to compare ER- and ER+ breast cancer cells together. It was clear that, owing to the lack of estrogen receptors on the surface of MDA-MB-231 cells,[214] endoxifen could not have any effect on nanoparticle uptake when the cells were incubated with a combination of END-polymersomes and free END (Figure 6C).

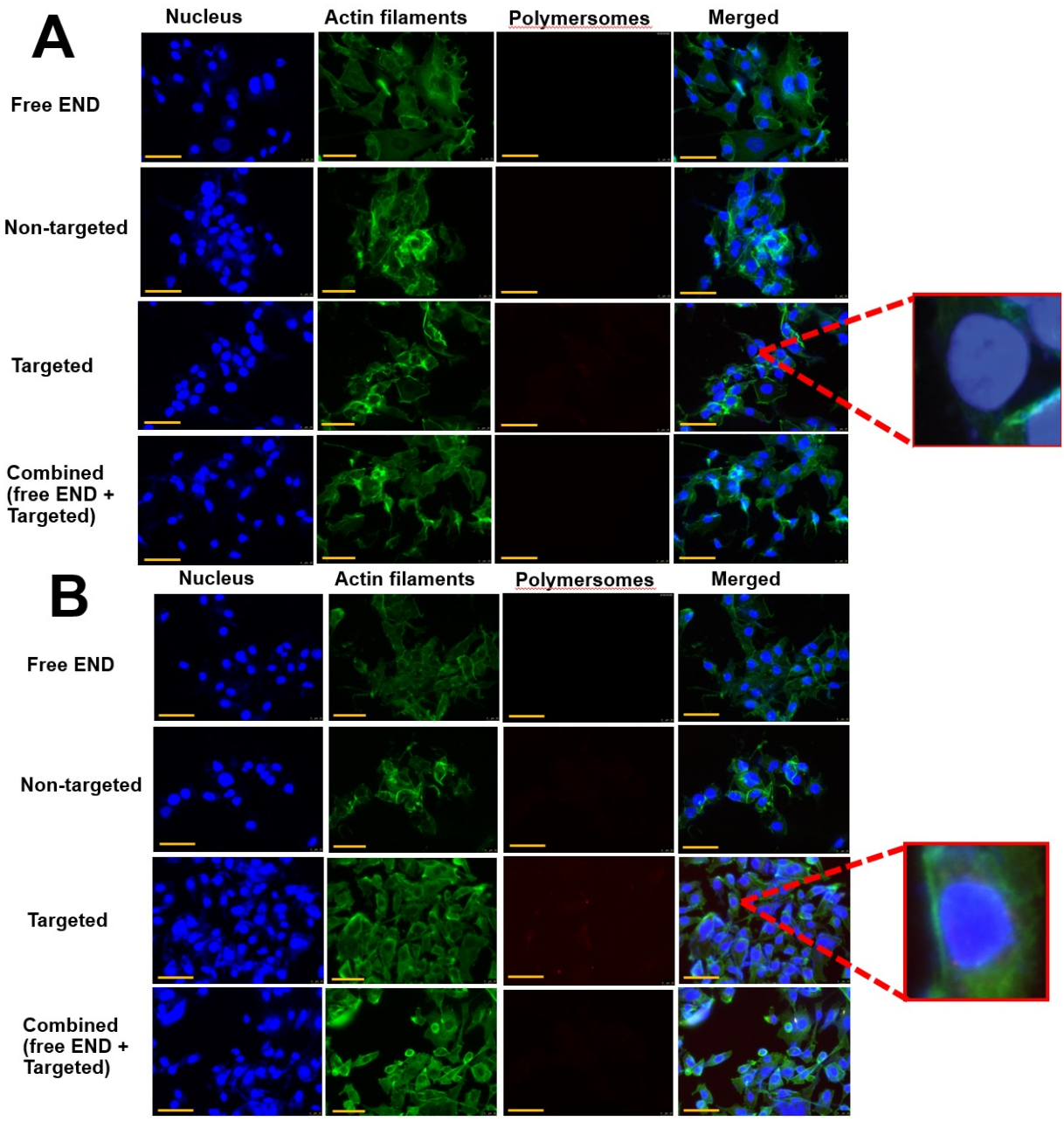

Figure 3.6. Fluorescence images of cellular uptake in triple-negative MDA-MB-231 cells. Free endoxifen (free END), non-targeted and targeted polymersomes, and the combination of END and targeted polymersomes after 3 hours under normoxia **(A)** and hypoxia **(B)** (scale bar: 50 µm). **(C)** Quantitative fluorescence intensity of the cells in normoxia and hypoxia (n = 3).

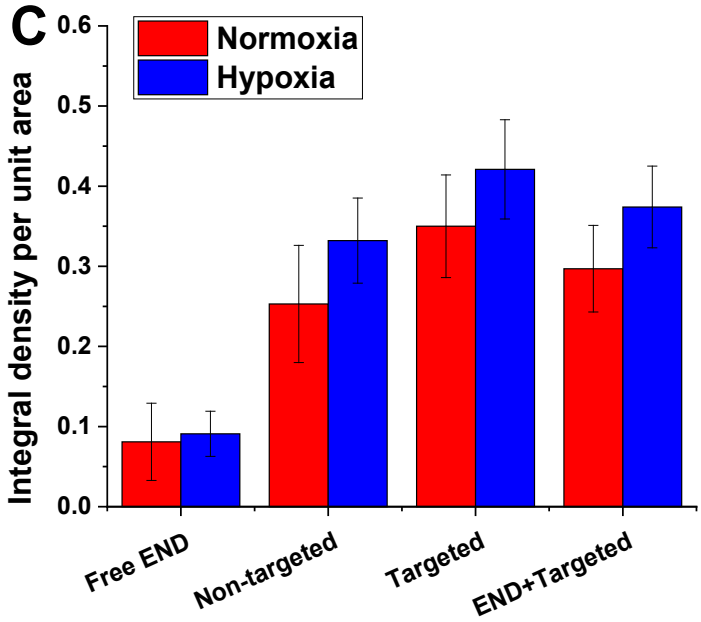

Figure 3.6. Fluorescence images of cellular uptake in triple-negative MDA-MB-231 cells (continued). Free endoxifen (free END), non-targeted and targeted polymersomes, and the combination of END and targeted polymersomes after 3 hours under normoxia **(A)** and hypoxia **(B)** (scale bar: 50 μm). **(C)** Quantitative fluorescence intensity of the cells in normoxia and hypoxia (n = 3).

3.4.4. Cytotoxicity in monolayer and spheroid cultures

To evaluate the toxicity, MCF7 cells were incubated with different concentrations of buffer-encapsulated END-polymersomes for 3 days. The cells were more that 85% viable with the highest amount of polymer concentration (100 μg/mL) tested in normoxia and hypoxia (Figure 7). For the subsequent experiments, we used 1 mg/mL of total polymer in preparing the polymersomes. To determine the efficacy of DOX-loaded polymersomes, the MCF7 monolayer and three-dimensional spheroid cell cultures were incubated for 72 hours with four treatments: non-targeted nanoparticles (DOX-HRPs), targeted END-conjugated nanoparticles (END-DOX-HRPs), control (buffer only), and free DOX (Figure 8A-B).

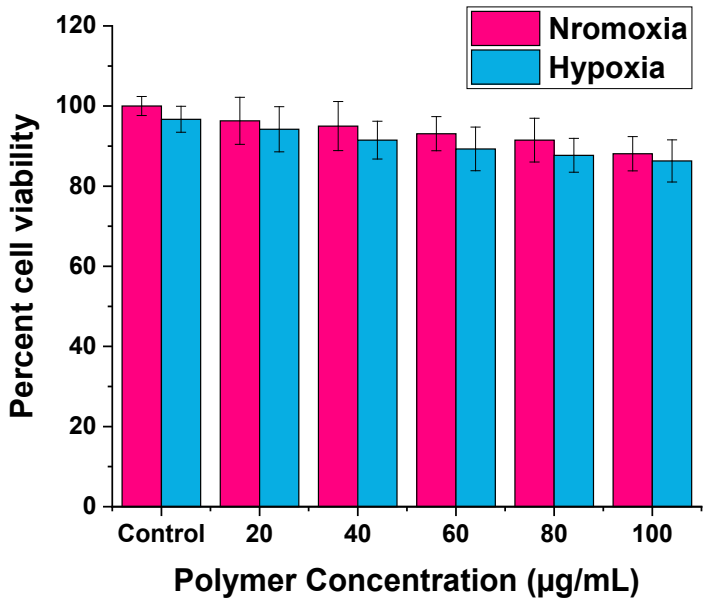

Figure 3.7. Toxicity of buffer-encapsulated endoxifen-conjugated polymersomes on MCF7 breast cancer cells under normoxic and hypoxic conditions (72 hours, n = 3).

The MCF7 cells were treated with various DOX concentrations within a range from 1 to 15 µM. The minimum drug concentration which made significant differences in most of treated cell cultures was 8 µM. It was observed that treating the MCF7 monolayer and spheroid cultures under hypoxia with non-targeted polymersomes (DOX-HRPs; [DOX] = 8 µM) reduced the cell viability to 50% and 65%, respectively. The reduced cell viability is likely due to passive diffusion of the polymersomes inside the breast cancer cells and subsequent release of doxorubicin in the cytosol. However, treating the monolayer and spheroids under hypoxia with the targeted polymersomes (END-DOX-HRPs; [DOX] = 8 µM) decreased the viability of the cells to 18% and 31%, respectively. The targeted nanoparticles show higher cellular internalization compared to the non-targeted counterparts, and this effect is enhanced in hypoxia (Figure 5). Hence, the higher cell death with the targeted polymersomes in hypoxia is likely due to more efficient internalization and subsequent DOX release.

We observed that the cell viability in treated microtumor-like spheroid cultures was higher than monolayer cultures likely due to the dense structure of the spheroids. A significant difference ($p < 0.05$) was shown between hypoxia and normoxia when the monolayer and spheroid cultures were incubated with targeted polymersomes. It was demonstrated that under hypoxia, targeted polymersomes decreased the viability of the monolayer and spheroid cultures to 18% and 31%, respectively (Figures 8A, B, brown bars). We also observed a significant difference ($p < 0.05$) between targeted and non-targeted treatment groups under hypoxia within both monolayer and spheroid cell cultures (Figures 8A, B, purple and brown bars) which should be caused by enhanced targeted receptor-mediated cellular uptake.[210] There was a significant difference ($p < 0.05$) between hypoxia and normoxia only in monolayer cultures when they were incubated with non-targeted treatment group (Figure 8A, green and purple bars). The cell viability decreased about 30% between these two groups. The reason why we observed a significant difference just in monolayer cultures should be due to their penetrable structure compared to the spheroids.

The polymersomes release 35% of their cargo within 3 hours and 90% after 8 hours in hypoxia (Figure 4). This ensures that 72-hour treatment is enough for the vesicles to pass through the cancer cells, disintegrate, and release their encapsulated DOX. According to EPR effect (passive diffusion), both non-targeted and targeted polymersomes can accumulate into the tumor.[220] However, in addition to passive diffusion, targeted vesicles demonstrate enhanced cellular uptake and toxicity regarding to estrogen receptor-mediated endocytosis.

According to overexpression of the surface estrogen receptors on ER+ breast cancer cells,[241] we expect to observe an increased receptor-mediated nanoparticle internalization into the cells. Even though staining the membrane-associated estrogen receptors demonstrated that

expression of surface estrogen receptors did not change between hypoxia and normoxia in breast cancer cells,[250]due to general overexpression of estrogen receptors and remaining unchanged under all conditions, we can expect to observe an enhanced ligand-receptor mediated cellular uptake of targeted nanoparticles.

To further estimate the efficacy of the polymersomes, the 6-day old spheroids were treated with 8 μM free DOX, non-targeted, and targeted nanoparticles for 72 hours in hypoxia and normoxia and their growth was monitored for 16 days (Figure 8C-D).

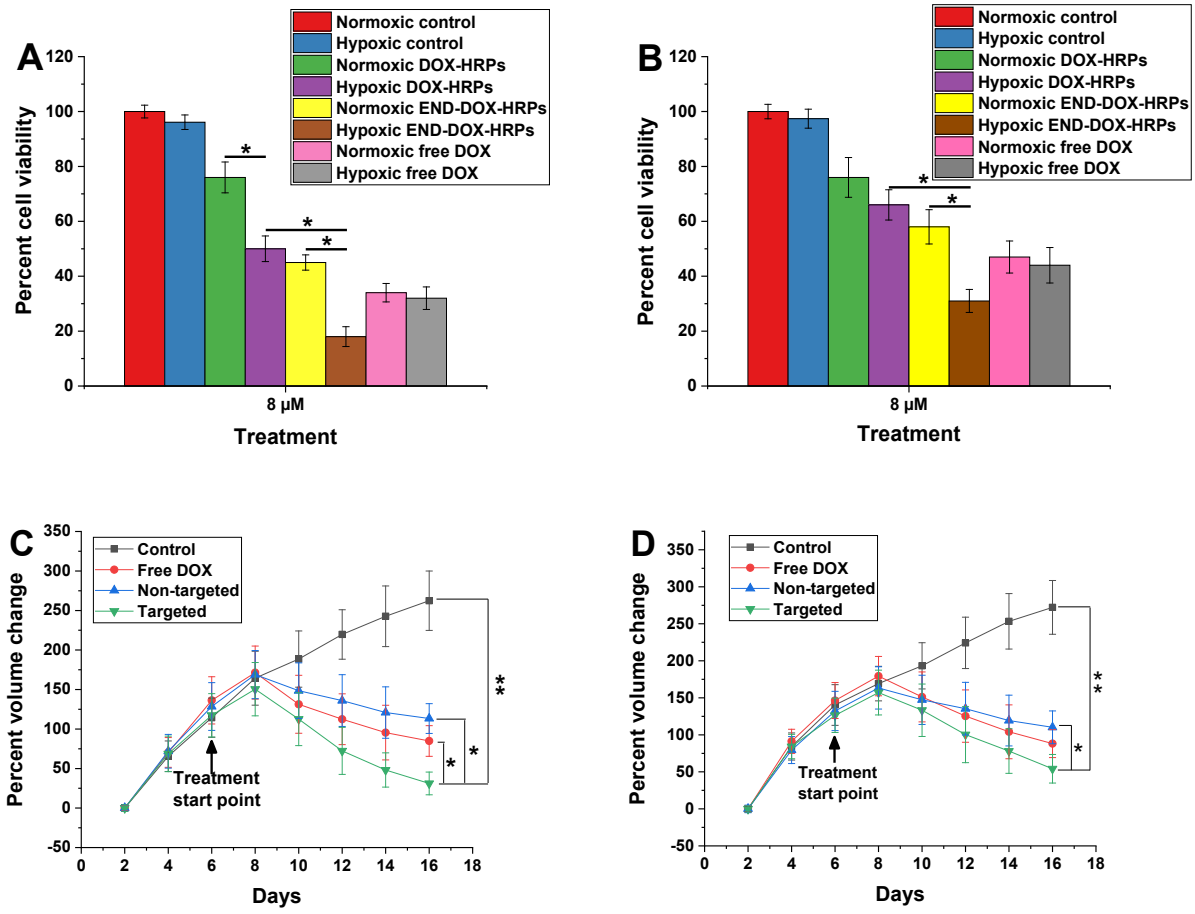

Figure 3.8. Viability of MCF7 cells under normoxia and hypoxia after 72-hour treatment in monolayer **(A)** and three-dimensional spheroid cultures **(B)** (n = 3, *p < 0.05). Growth curves of MCF7 spheroid cultures in hypoxia **(C)** and normoxia **(D)** (n = 3, **p < 0.01, *p < 0.05).

It was shown that targeted polymersomes were more toxic toward breast cancer cells in hypoxia by shrinking the spheroid volume up to 73%, while non-targeted polymersomes reduced this volume by 32% in hypoxia (Figure 8C). The results of spheroid growth curve in hypoxia confirms higher toxicity of targeted polymersomes compared to non-targeted vesicles on spheroid cultures under hypoxia (Figure 8B). We also observed that targeted polymersomes in normoxia decreased the spheroid volume up to 52%, while non-targeted polymersomes only shrink this volume by 20% (Figure 8D). The targeted polymersomes could enter the MCF7 cells easier than the non-targeted vesicles. This is based on surface END ligands that selectively interact with the ERs on the breast cancer cells and shrink microtumor volume. In addition, targeted polymesomes significantly decreased the volume of spheroids compared to free DOX ($p < 0.05$), non-targeted polymersomes ($p < 0.05$), and control group ($p < 0.01$) in hypoxia (Figure 8C). Overall, we observed that targeted polymersomes have a great potency to shrink the breast microtumors compared to non-targeted polymersomes and control group in all conditions.

3.5. Conclusion

The END-decorated doxorubicin-encapsulated polymersomes described in this study are targeted polymeric hypoxia-responsive nanoparticles for drug delivery to ER+ breast microtumors. These vesicles act as a dual-functional polymersomes. On one hand, they selectively bind to overexpressed ERs on the surface of breast cancer cells by the aid of surface-anchored END molecules and enter the cytosol. In addition, they sustainably release their anticancer drug within hypoxic niches of tumor microenvironment by the help of their hypoxia-responsive diazobenzene moieties. We note that some drug release from the nanocarriers can occur in the extracellular matrix also under hypoxia. Under hypoxia, targeted polymersomes demonstrated higher cytotoxicity on ER+ breast cancer monolayer and spheroid cultures

compared to non-targeted polymersomes and free drugs. In addition, targeted polymersomes shrank the breast microtumor volume more efficiently than non-targeted polymersomes in both hypoxia and normoxia. Based on the survey of previously published literature, this is the earliest use of targeted END-conjugated polymersomes with doxorubicin in treating ER+ breast cancer monolayer and spheroid cell cultures. Overall, the merits of our targeted polymersomes are the ability to specifically interact with estrogen receptors, disintegrate in the cancer cells under low oxygen partial pressure, selectively release their encapsulated drug in hypoxic breast cancer microtumors, diminish the cancer cell viability, and enhance therapeutic efficacy of anticancer drug. Most importantly, targeted END-conjugated DOX-loaded nanoparticles will have potential for delivering chemotherapeutic drugs and treating breast cancer.

3.6. Acknowledgements

The NIH grant 1 R01GM 114080, NSF EPSCoR Track-1 Cooperative Agreement OIA #1946202, and DaCCoTA Center award (NIGMS U54 GM128729) supported this study. Any opinions, findings, and conclusions or recommendations expressed in this material are those of the author(s) and do not necessarily reflect the views of the NSF. The authors thank Parinaz Ghanbari for designing all graphics of this manuscript.

4. TARGETED POLYMERIC NANOPARTICLES FOR DRUG DELIVERY TO HYPOXIC, TRIPLE-NEGATIVE BREAST TUMORS

4.1. Abstract

High recurrence and metastasis to vital organs are the major characteristics of triple-negative breast cancer (TNBC). Low vascular oxygen tension promotes resistance to chemo- and radiation therapy. Neuropilin-1 (NRP-1) receptor is highly expressed on TNBC cells. The tumor-penetrating iRGD peptide interacts with the NRP-1 receptor, triggers endocytosis and transcytosis, and facilitates penetration. Herein, we synthesized a hypoxia-responsive diblock PLA–diazobenzene–PEG copolymer and prepared self-assembled hypoxia-responsive polymersomes (Ps) in an aqueous buffer. The iRGD peptide was incorporated into the polymersome structure to make hypoxia-responsive iRGD-conjugated polymersomes (iPs). Doxorubicin (DOX) was encapsulated in the polymersomes to prepare both targeted and non-targeted hypoxia-responsive polymersomes (DOX-iPs and DOX-Ps, respectively). The polymeric nanoparticles released less than 30% of their encapsulated DOX within 12 hours under normoxic conditions (21% oxygen), whereas under hypoxia (2% Oxygen), doxorubicin release remarkably increased to over 95%. The targeted polymersomes significantly decreased TNBC cells' viability in monolayer and spheroid cultures under hypoxia compared to normoxia. Animal studies displayed that targeted polymersomes significantly diminished tumor growth in xenograft nude mice. Overall, the targeted polymersomes exhibited potent anti-tumor activity in monolayer, spheroid, and animal models of TNBC. With further developments, the targeted nanocarriers discussed here might have the translational potential as drug carriers for the treatment of TNBC.

4.2. Introduction

Breast cancer is a challenging disorder for women, regardless of the treatment strategy used.[251] A high recurrence rate and metastasis to different organs (e.g., lung, bone, liver, and lymph nodes) contribute to adverse outcomes.[252] Metastatic breast cancer claims about 40,000 lives in the US annually.[253] Triple-negative breast cancer (TNBC) is marked by the loss of all biomarker expression[254] and includes about 15% of all diagnosed breast malignancies.[255] Based on the gene expression profiles, there are four subtypes of TNBC.[256] Effective therapies are available for the estrogen, progesterone, and human epidermal growth factor receptor positive subtypes. However, no promising treatment exists for TNBC other than systemic chemotherapy.[257] This is partially due to rapid cell proliferation and inadequate blood flow, which creates a low oxygen concentration (hypoxia) in tumors.[258] Notably, hypoxia is a primary driver of metastasis and aggressiveness in TNBC, which hinders treatment.[259–261]

Due to the lack of specific targeting, chemotherapeutic drugs for TNBC inflict severe damage to healthy tissues. Besides, low solubility, decreased bioavailability, and accelerated clearance of drugs from the bloodstream make it challenging to achieve the desired clinical outcomes.[262] To address these problems, nanotechnology has emerged as a rapidly developing field to design drug carriers for TNBC treatment.[263,264] Drugs encapsulated in nanocarriers have several advantages compared to the free molecules. For instance, polymeric nanoparticles help increase the solubility of lipophilic drugs by carrying these drugs within their bilayer.[265–268] Polyethylene glycol (PEG) on the outer layer extends the nanoparticles' circulation time and allows passing of cancer tissues through enhanced permeability and retention (EPR) effect.[269] Nanoscale carriers with targeting moieties for the overexpressed surface receptors target the disease site, thus minimizing off-target side effects.[270,271] In addition, stimuli-responsive

nanoparticles respond to specific triggers for releasing anticancer drugs only in the presence of a stimulus.[272]

Polymersomes are nanoparticles prepared from amphiphilic copolymers. Several properties render polymersomes more advantageous than other nanoparticles, including membrane stability, tunable molecular weight of the polymers, ligand conjugation capacity, and more.[273,274] Hydrophobic molecules are encapsulated within the polymer bilayer, whereas hydrophilic drugs are incorporated into the aqueous core of the polymersomes, thereby carrying both types of drugs simultaneously.[275]

The tumor-penetrating iRGD peptide (CRGDKGPDC) contains the RGD motif for specific interaction to overexpressed $\alpha_v\beta_3$ integrins on endothelial cancer cells.[276] Subsequent cleavage of iRGD peptide exposes the CendR (RGDK) motif with a higher binding affinity to the neuropilin-1 (NRP-1) receptor. This ligand-receptor Binding promotes transcytosis and endocytosis, leading to tumor penetration.[277] Hence, surface conjugation of iRGD peptide to the drug-encapsulated polymersomes allows them to penetrate solid tumors [278] (Figure 1).

Doxorubicin (DOX) is a common anthracycline drug used for treating various cancers, particularly TNBC.[258,279] DOX can be encapsulated into biocompatible nanocarriers to increase therapeutic index and sustained release.[280] In this study, we synthesized DOX-encapsulated, iRGD-conjugated, hypoxia-responsive, polymersomes (DOX-iPs) as targeted drug delivery vehicles to deliver DOX into solid tumors of TNBC. The targeted polymersomes offered here are dual-functional nanoparticles that bind specifically to the surface NRP-1 receptors and translate into TNBC cells. Then, the diazobenzene linker of the PLA-PEG polymer undergoes reduction within hypoxia, disintegrates the polymersome membrane, and releases encapsulated

DOX in the tumor microenvironment. We also prepared non-targeted polymersomes (DOX-Ps) to evaluate their efficacy along with targeted polymersomes.

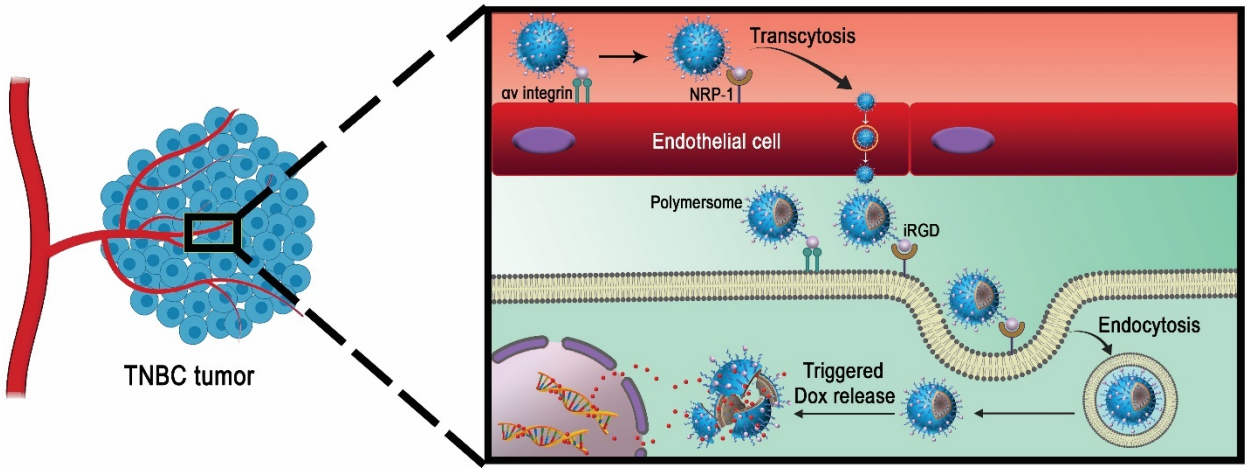

Figure 4.1. Schematic illustration of the iRGD peptide-mediated targeting and penetration into the solid TNBC by the polymersomes.

4.3. Materials and methods

4.3.1. Materials

The amino acids were purchased from Alfa Aesar. DPPE- lissamine rhodamine lipid dye was prepared from Avanti Polar Lipids. $mPEG_{2000}$-NH_2 was prepared from Biochempeg. All other chemicals for polymer synthesis were purchased from Millipore Sigma. The complete cell culture medium was prepared from VWR International. The antibiotic-antimycotic (Penicillin-Streptomycin-Amphotericin B) solution was purchased from Corning.

4.3.2. Synthesis and characterization of copolymers and peptide

The PLA_{8500}-Azo-PEG_{2000} polymer was synthesized in our laboratory, as previously reported.[258] The ^{1}H NMR, ^{13}C NMR, and gel permeation chromatography (GPC) were used to analyze the final product (Supporting Information, Figures A2-4). A peptide synthesizer (Liberty Blue) was used for synthesizing Hex-iRGD in our lab, as previously reported.[267] The product

(145 mg, 64%) was characterized by mass spectrometry and circular dichroism (Supporting Information, Figures C1-2).

4.3.3. Synthesis of PLA_{8500}–PEG_{2000}–iRGD polymer

The PLA_{8500}–PEG_{2000}–N_3 polymer was synthesized in our laboratory, as previously reported.[281] [2+3]-cycloaddition reaction was carried out for conjugating Hex-iRGD to PLA_{8500}–PEG_{2000}–N_3 polymer in our lab, as previously reported.[267] The lyophilized product was freeze-dried (yield: 50%) and characterized by circular dichroism spectroscopy (Supporting Information, Figure C2).

4.3.4. Preparation of the polymersomes encapsulating doxorubicin

The fluorescent lipid DPPE-N-lissamine rhodamine (LR, 5%), PLA_{8500}-Azo-PEG_{2000} polymer (85%), and PLA_{8500}–PEG_{2000}–iRGD (10%) were used for preparing targeted doxorubicin-encapsulated polymersomes (DOX-iPs). LR (5%) and PLA_{8500}-Azo-PEG_{2000} polymer (95%) were used to make doxorubicin-encapsulated polymersomes (non-targeted polymersomes, DOX-Ps). Doxorubicin encapsulated polymersomes were prepared using the pH gradient method.[279] The method and chemicals using to prepare polymersomes were previously reported.[258] Doxorubicin was added with a 1:5 drug/polymer molar ratio while stirring for 4 hours. The vial content was filtrated by Sephadex G100 column to collect doxorubicin-encapsulated nanoparticles.

4.3.5. Preparation of plain polymersomes

Plain (HEPES buffer-encapsulated) nanoparticles were made from the PLA_{8500}-Azo-PEG_{2000} polymer (95%) and LR dye (5%). Briefly, LR was air-dried to make a thin layer film. PLA_{8500}-Azo-PEG_{2000} polymer (100 μL) was mixed with the dried LR and added dropwise into 1000 μL HEPES buffer (pH 7.4) and evaporated for 45 minutes. Subsequently, the mixture was

sonicated for 1 hour and filtered by Sephadex G100 column. Plain polymersomes were the control for the cell cytotoxicity studies.

4.3.6. Characterization

The charge and size of the polymersomes were measured by Dynamic Light Scattering (DLS) instrument (Malvern Zetasizer). All samples were measured five times and the average of all measurements was recorded.

Nanoparticle solutions (10 μL, 1 mg/mL) were dried by nitrogen flow. A microscope (NT-MDT NTEGRA AFM) was employed for acquiring AFM images. Samples were prepared for transmission electron microscopic (TEM) images based on a reported protocol.[258]

4.3.7. Release studies

The release kinetics of the nanoparticles were carried out by preparing a mixture of targeted polymersomes, NADPH, and liver microsomes under hypoxic (2% oxygen) and normoxic (21% oxygen) conditions according to previously reported protocol in our laboratory.[258] The loading content and encapsulation efficiency of the drug in both non-targeted and targeted vesicles were calculated by measuring absorbance at 480 nm.[282]

4.3.8. Cell culture

The MDA-MB-231 cells were purchased from American Type Culture Collection (Manassas, VA). For the normoxic conditions, cells were grown in an incubator at 37 ºC containing 5% CO_2 and 21% oxygen. For the hypoxic conditions, cells were incubated in a hypoxia chamber (Biospherix C21) with 5% CO_2 and 2% oxygen at 37 ºC.

4.3.9. Neuropilin-1 protein expression

The TNBC cells were seeded (2.5 x 10^5 cells/well) in cell culture plates and incubated in normoxic conditions. When the cells reached around 40 to 50% confluence, a set of plates were

moved to the hypoxia chamber (2% oxygen). The cells were then incubated in both hypoxic and normoxic chambers, and their protein was collected after 24 hours. The whole-cell lysates were analyzed using 10% SDS polyacrylamide gel electrophoresis. Proteins were transferred on PVDF membranes before incubation with NRP-1 (Abcam) and β-Actin (Applied Biological Materials) primary antibodies. Protein bands were detected by imaging the membrane, and densitometry analysis was carried out by Image Studio v.5.2 software.

4.3.10. Cellular internalization

The cells were seeded (5,000 cells/well) in two 12-well tissue culture plates and incubated under 5% CO_2. When the cells reached 80% confluence, they were washed with 1X PBS and replenished with fresh cell culture media. Then, one of the plates was moved to the hypoxia chamber (2% oxygen) for one doubling time before starting the experiments. The cells in both plates were treated with iRGD-conjugated and non-conjugated polymersomes (targeted and non-targeted treatments, respectively, 20 μL each) for three hours. The plates were then washed three times with PBS, and the cell nuclei were stained with DAPI (NucBlue, Invitrogen). The images were taken by a Leica fluorescence microscope. The densitometry analysis was carried out by the NIH ImageJ (version: 1.52a) software.

4.3.11. Cytotoxicity in monolayer cultures

The cells were seeded (5,000cells/well) in the plates and grown 24 hours. The wells containing the cells were categorized into five treatments: HEPES-buffer encapsulated polymersomes, non-targeted polymersomes (DOX-Ps), targeted polymersomes (DOX-iPs), free DOX, and control (only HEPES buffer). 1, 2, and 4 μM of free DOX and the same amounts of drug-encapsulated polymersomes were used for 72 hours under hypoxic and normoxic conditions. For the cytotoxicity study, the cells were incubated with different concentrations of

plain polymersomes (20 to 100 μg/mL). The cytotoxicity was measured after 4 hours by recording the fluorescence (excitation at 560 nm and emission at 595 nm).

4.3.12. Three-dimensional cytotoxicity studies

The cells were cultured as spheroids using Nanoshuttle three-dimensional cell culture kit (Greiner Bio-one). The NanoShuttle nanoparticles (200 μL) were added into an 80-90% confluent MDA-MB-231 cells for magnetizing the cells overnight. The cells were dislodged, counted, and 20,000 cells were transferred into each well. The plates were laid on top of magnetic spheroid drives for 15 minutes to form spheroids and incubated for 24 hours. The wells were then categorized into five treatments and incubated for 72 hours in both hypoxia and normoxia with the same three different doxorubicin concentrations (1, 2, and 4 μM). The spheroids were then washed with PBS, transferred to new plates for growing 24 hours. Subsequently, the cytotoxicity was determined (same as monolayer cell viability assay).

4.3.13. In vivo toxicity and anti-tumor efficacy

The anti-tumor efficacy of the polymersomes was evaluated on tumor-bearing mouse models. The MDA-MB-231 cell suspension (10^6 cells per mouse) was mixed in Matrigel (Corning) at a 1:1 ratio (total 200 μL) and subcutaneously injected into the 8-week-old female athymic nude mice (Envigo). Three weeks after injection, 30 mice with a tumor volume ranging from 50-80 mm^3 were randomly divided into five treatment groups. The treatment groups were vehicle, free DOX, polymersomes, non-targeted, and targeted nanoparticles. The control and polymersome-only groups received saline and polymersomes, respectively. The other 3 groups received 5 mg DOX/kg dose. All treatments were given twice per week for four weeks. The body weights and tumor volumes were evaluated once every three days. Two weeks after the treatment

ended, all mice were euthanized, the tumors were excised, and weighed. The vital organs were dissected and fixed in 10% formalin for histological evaluation.

4.3.14. In vivo biodistribution

Tumor-bearing female athymic nude mice were i.v. injected with iRGD-polymersomes containing lissamine rhodamine fluorescent dye. The mice were then euthanized after 3 and 8 hours, the organs (lung, liver, and kidney) were excised and imaged. The fluorescence integral density of accumulated polymersomes in each organ tissue was analyzed.

4.3.15. Statistical analysis

The statistical analyses were all processed using Origin software (Origin 9.3, Northampton, Massachusetts) and presented as mean ± SEM. The significant statistical difference between normoxic and hypoxic conditions within treatment groups were evaluated by ANOVA.

4.4. Results and discussion

4.4.1. Synthesis and characterization of polymersomes

Hypoxia contributes to the overall progression, migration, and invasion of TNBC and other solid tumors.[283] We synthesized PLA_{8500}-Azo-PEG_{2000} polymer with a hypoxia-responsive diazobenzene linker (Scheme 4.1), which self-assembles into polymersomes under appropriate conditions.

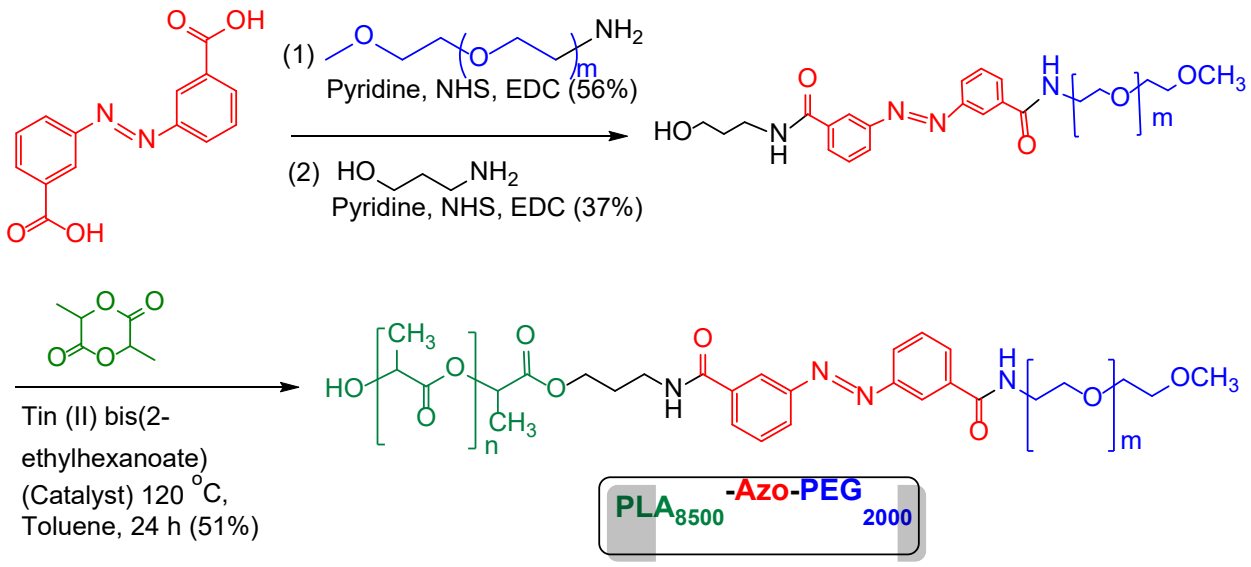

Scheme 4.1. Synthesis of the polymer with hypoxia-sensitive diazobenzene linker (green: PLA; red: hypoxia-responsive linker; blue: PEG).

The polydispersity index was calculated from Gel Permeation Chromatography to be 1.17. The surface PEG groups increase circulation time and the amount of polymersomes in cancerous tissue microenvironment by EPR effect.[266] The alkyne functional group on hexynoic acid was subsequently used for the conjugation of iRGD peptide to the azide (N_3) functional group of PLA_{8500}–PEG_{2000}–N_3 polymer (Scheme 4.2). This peptide conjugation with the polymer was evaluated by circular dichroism spectroscopy (Supporting Information, Figure C2). We actively encapsulated doxorubicin into the nanoparticles, while unencapsulated doxorubicin was separated by passing the sample through the gel filtration column. A standard curve was plotted by measuring doxorubicin absorption as a function of concentration (Supporting Information, Figure C3). The encapsulation efficiency and loading of the non-targeted polymersomes were 51% and 9 weight percent, and for the targeted polymersomes were 63% and 11 weight percent, respectively. These polymersomes were stable over 8 weeks at 4 °C (Supporting Information, Figure C4).

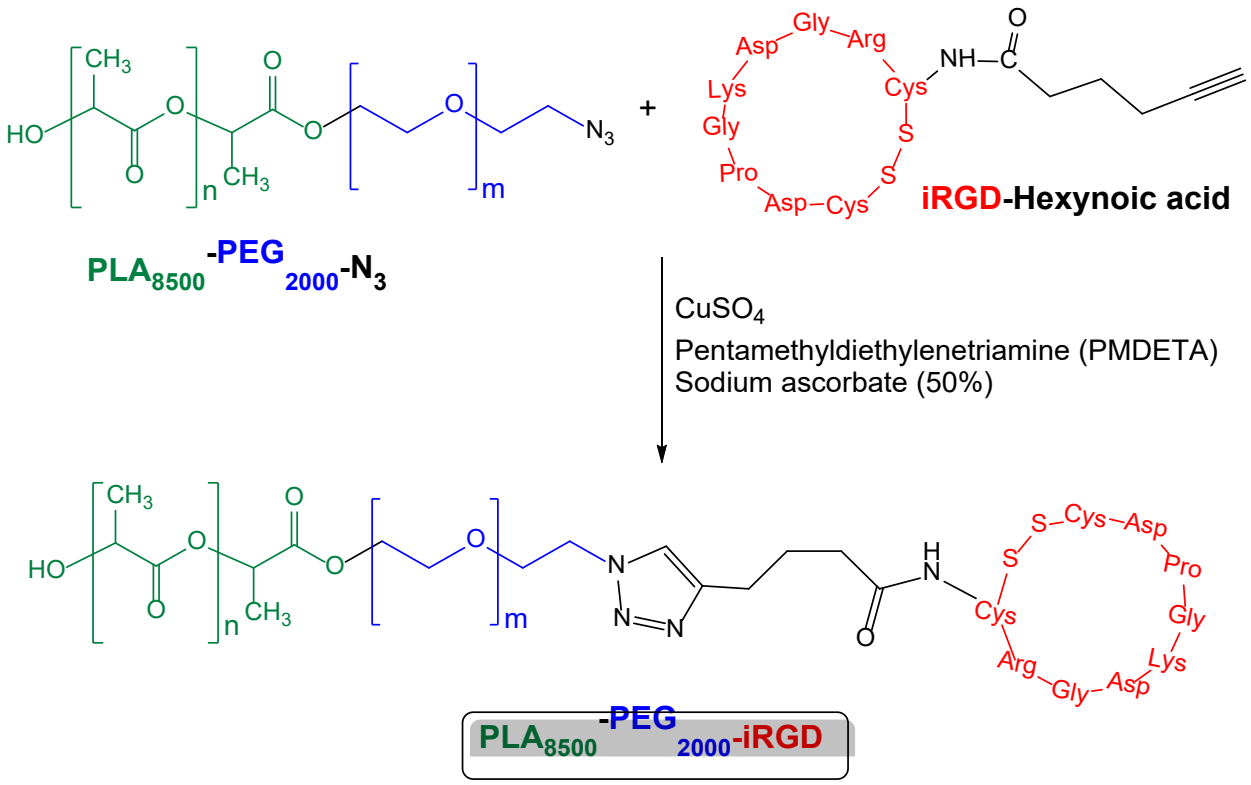

Scheme 4.2. Reaction of PLA_{8500}–PEG_{2000}–N_3 polymer and Hex-iRGD.

The synthesized PLA_{8500}–PEG_{2000}–iRGD conjugate was then incorporated into the polymeric nanoparticles to prepare doxorubicin encapsulated hypoxia-responsive iRGD-conjugated polymersomes (DOX-iPs). The iRGD peptide in the structure of polymersome first targets $\alpha_v\beta_3$ and $\alpha_v\beta_5$ integrins on the cells. Subsequent enzymatic cleavage exposes the CendR (RGDK) motif to interact with the NRP-1 receptors, cellular internalization, and endocytic transcytosis.[284] The size, charge, and polydispersity index (PDI) of the nanoparticles were calculated by dynamic light scattering, DLS (Figure 2A, 2B, Table 4.1), and the spherical shape was confirmed by atomic force microscopic (AFM) imaging (Figure 2C, 2D). The average size of the nanoparticles significantly changed in hypoxic conditions (Figure 2A, C5, Table 4.1). Targeted vesicles indicated larger diameters because of the conjugation of iRGD peptide. Figure

2B, C6, and Table 4.1). The slightly positive ζ potential almost remained consistent within all conditions for non-targeted and targeted polymersomes (Table 4.1).

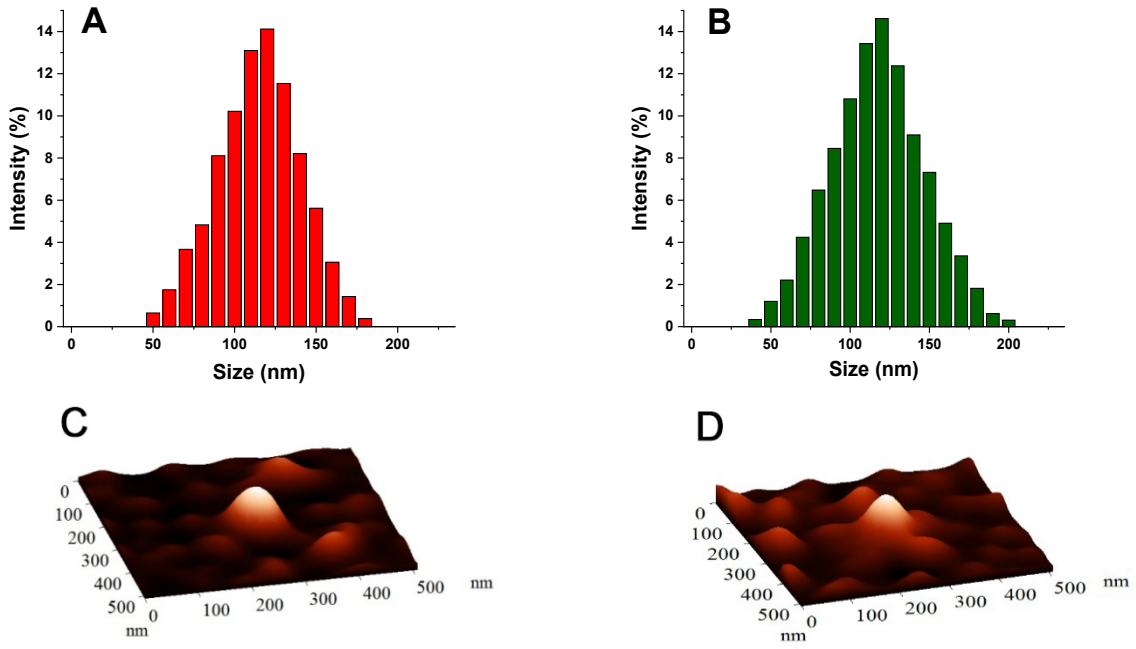

Figure 4.2. The size of non-targeted (**A**) and targeted (**B**) nanoparticles. AFM images of non-targeted (**C**) and targeted (**D**) nanoparticles.

Table 4.1. Diameter, ζ potential, and PDI of different polymersomes

Polymersome	Average diameter (nm)		ζ potential (mV)		PDI	
	Normoxia	Hypoxia	Normoxia	Hypoxia	Normoxia	Hypoxia
Non-targeted	118 ± 4	43 ± 4, 419 ± 22	0.13 ± 0.09	0.21 ± 0.11	0.13 ± 0.02	0.73 ± 0.16
Targeted	136 ± 7	51 ± 3, 574 ± 27	0.23 ± 0.12	0.31 ± 0.14	0.18 ± 0.05	0.76 0.19

4.4.2. Release studies in hypoxia and normoxia

Solid tumors have an environment that is rich in reducing agents.[285] The diazobenzene moieties in the polymers' structure undergo a four-electron reduction reaction in hypoxia which leads to disassembling of block polymers. This disintegrates the polymersomes and releasing the encapsulated drugs [286] (Figure 3A).

To check the drug release from polymersomes, targeted DOX-loaded polymersomes (DOX-iPs) were prepared. The release behavior was evaluated within hypoxic and normoxic conditions as a function of time (Figure 3B).

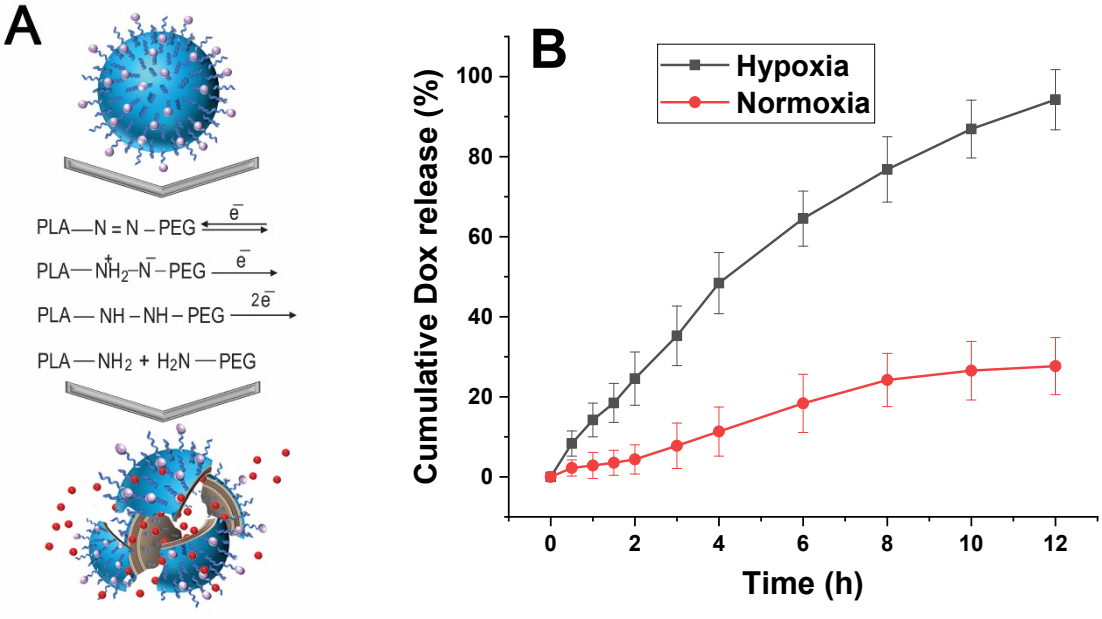

Figure 4.3. (A) Mechanism of the reduction under hypoxic environment. **(B)** DOX release within hypoxia (2% oxygen) and normoxia (21% 0xygen) (n = 3).

The polymersomes released significantly higher amount of Dox in hypoxia than normoxia. Polymersomes released about 95% of their encapsulated DOX within hypoxic conditions around 12 hours, although about 25% of DOX was released in the normoxic condition within 12 hours. This confirmed that nanoparticles released their cargo due to the reduction of diazobenzene linker in hypoxia (Figure 3A).

AFM and TEM images showed that the vesicular shape of the nanoparticles changed within hypoxia (Figure 4). Irregular morphology of the polymersomes in hypoxic conditions demonstrates possible disintegration and fusion of the polymeric vesicles (Figure 4B, 4D). We also observed that hypoxia decreased the hydrodynamic diameter and increased the vesicles' polydispersity index (Table 4.1).

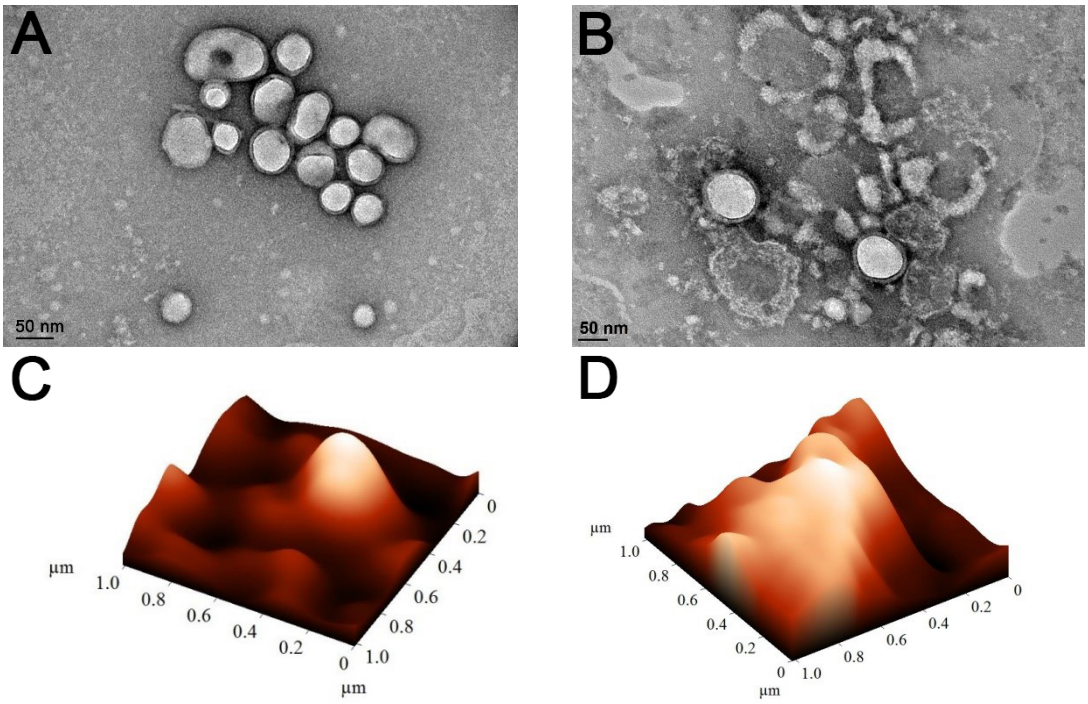

Figure 4.4. AFM and TEM images of the vesicles within normoxic (**A**, **C**) and hypoxic (**B**, **D**) conditions (scale bar: 50 nm).

4.4.3. Neuropilin-1 expression

To investigate any hypoxia-induced expression of NRP-1, the MDA-MB-231 cells grew under both normoxic (21% oxygen) and hypoxic (2% oxygen) conditions. Western blotting demonstrated a significant increase in NRP-1 protein expression within the cells cultured in hypoxia than normoxia (Figure 5). The protein β-actin used as internal control. We found that the level of NRP-1 expression significantly increased after 24 hours within hypoxia (Figure 5B). This result suggested that hypoxia might structurally and functionally induce transmembrane NRP-1 protein expression through angiogenesis in TNBC cells.

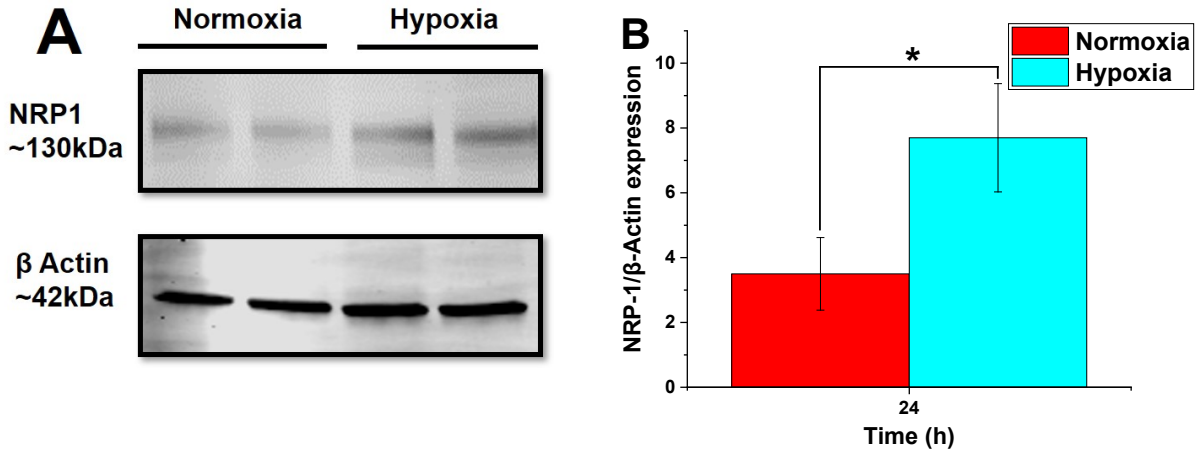

Figure 4.5. (A) NRP-1 expression in MDA-MB-231 cells with significant upregulation in hypoxic conditions (24h exposure). (**B**) The level of NRP-1/β-Actin expression (n = 3, *p < 0.05).

4.4.4. Cellular uptake

To demonstrate the nanoparticle penetration into TNBC cells, DPPE-lissamine rhodamine lipid (5%) was incorporated into the composition of polymersomes (without drug) for the ease of visualization and fluorescence microscopic imaging.[273,287] The MDA-MB-231 cells were treated for 3 hours with both targeted and non-targeted polymersomes. The red fluorescence (lissamine rhodamine dye) was observed inside the cells treated with targeted nanoparticles under hypoxia. However, the cells incubated with non-targeted vesicles (control) did not show significant intensity of the red fluorescence inside the cells (Figure 6A) either in hypoxia or normoxia. The images' quantitative fluorescence integral density indicated a significant difference between the iRGD-targeted polymersomes in hypoxia and normoxia. Also, the uptake results were significantly different for targeted and non-targeted polymersomes within hypoxia and normoxia (Figure 6B). It was found that the intensity of targeted nanoparticles were 8.5 times more than non-targeted polymersomes within hypoxic condition and 3 times more than targeted nanoparticles within normoxic condition. According to earlier studies, nanocarrier uptake in TNBC cells increases dynamically within the hypoxic condition.[288]

Since TNBC cells overexpress the NRP-1 receptor on the surface,[289] targeted iRGD-conjugated polymersomes will show increased uptake within these cells. Besides, western blotting of MDA-MB-231 cells displayed an increased expression of NRP-1 under hypoxia. Based on these findings, we concluded that exposing the MDA-MB231 cells to iRGD-conjugated polymersomes for three hours elevated the cellular uptake.

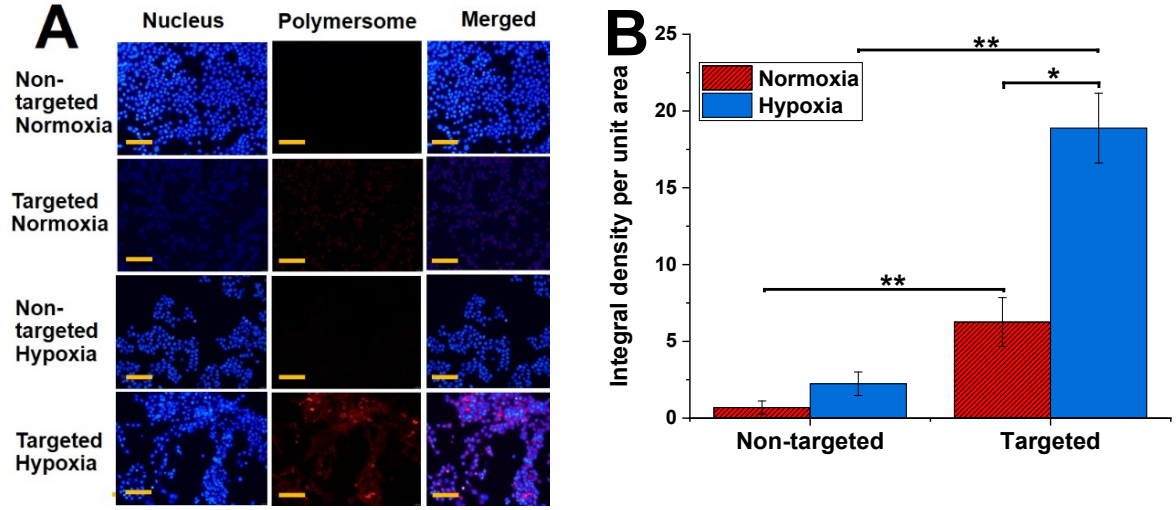

Figure 4.6. (A) Fluorescence images of non-targeted and targeted polymersome uptake within MDA-MB-231 cells in hypoxia and normoxia (scale bar: 50 µm). **(B)** fluorescence intensity of polymersome uptake (n = 3, *p < 0.05, **p < 0.01).

4.4.5. Polymer toxicity and monolayer cytotoxicity

To assess polymer toxicity, the cells were treated with different amounts of the polymersomes encapsulating HEPES buffer within hypoxia and normoxia for 3 days. The polymersomes demonstrated more than 88% cell viability with the maximumof 100 µg/mL polymer concentration (Figure 7A), indicating minimal toxicity. To demonstrate polymersomes' efficacy, the MDA-MB-231 monolayer cultures were treated for 3 days using four groups: control (no treatment, HEPES buffer only), free drug, non-targeted, and targeted nanoparticles. The results demonstrated that incubating the MDA-MB-231 cells with 4 µM DOX encapsulated within targeted polymersomes under hypoxia reduced cell viability to 28% compared to

normoxia (Figure 7B, $p < 0.05$). It was observed that targeted vesicles were more effective in contrast to non-targeted polymersomes and free DOX to kill TNBC cells under hypoxia. This is likely due to the binding of tumor-homing iRGD peptide on the targeted polymersomes with the overexpressed NRP-1 receptors on TNBC cells. According to drug release study (Figure 3B), nanoparticles released one-third (33%) of their loaded DOX within 3 h and around 79% within 8 h. Therefore, 3-day treatment will ensure enough time for the polymersomes to translocate the breast cancer cells, break open, and release their drug cargo within the cells.

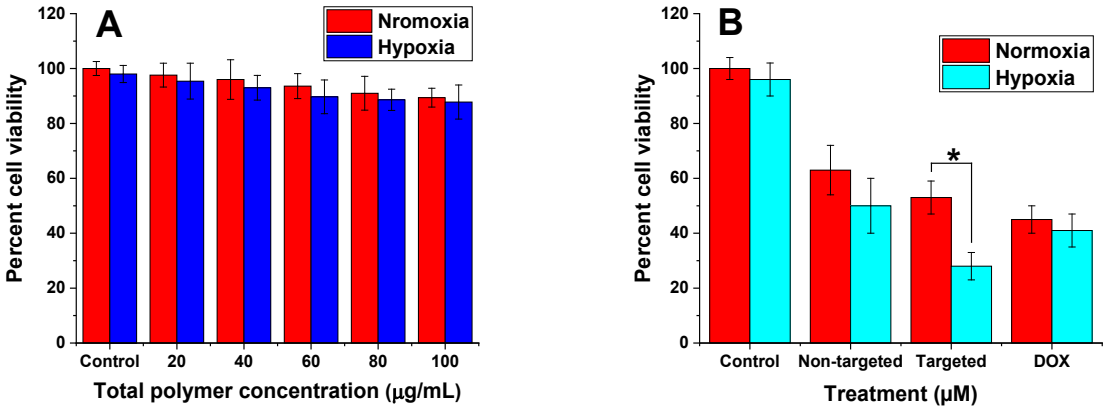

Figure 4.7. Viability of MDA-MB231 cells (monolayer) after 3-day treatment with buffer-encapsulated polymersomes (**A**, n = 6), free DOX, non-targeted, and targeted polymersomes (**B**, n = 3, * $P < 0.05$).

4.4.6. Cell viability in spheroid cultures

The MDA-MB-231 three-dimensional spheroids were cultured for 3 days in hypoxic and normoxic conditions with the same treatment groups as a monolayer cell viability study (Figure 8A). The results indicated that under hypoxia, the cell viability was significantly diminished to 36% when the spheroids were incubated with 4 µM DOX loaded within targeted vesicles in contrast to non-targeted vesicles within normoxic condition (66%) (Figure 8B). However, there was no significant difference in viability when the cells were incubated with non-targeted vesicles or free drug within hypoxic and normoxic conditions. This might reflect the slow

diffusion of non-targeted nanoparticles and DOX inside the three-dimensional cultures. Instead, targeted polymersomes showed enhanced cytotoxicity based on receptor-mediated cell penetration. Some polymersomes might release the encapsulated DOX in the extracellular regions. In this regard, the free drug penetrates to the cells via cell membrane.[290] However, passive diffusion could be less prevalent in comparison with targeted drug-encapsulated nanoparticle delivery.

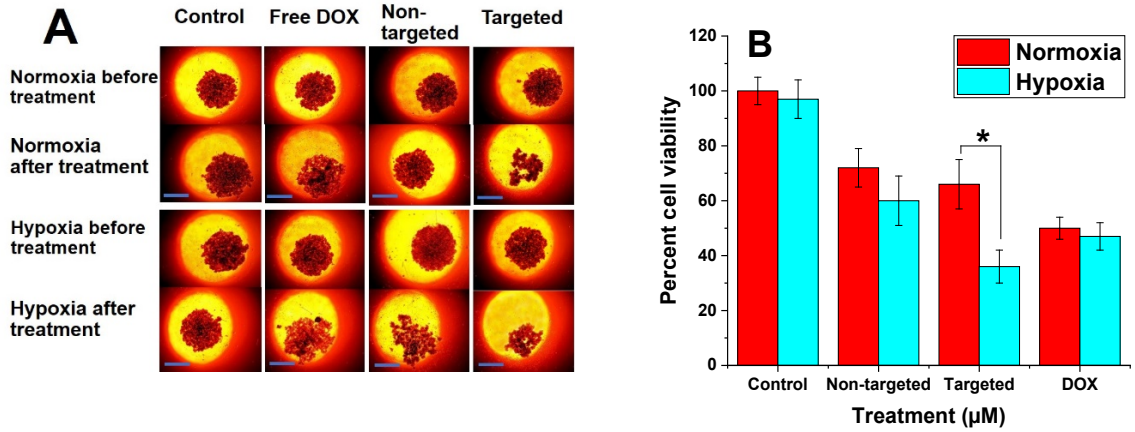

Figure 4.8. (A) Three-dimensional MDA-MB-231 spheroid images before and after incubating the cells with non-targeted and targeted vesicles under hypoxic and normoxic conditions (scale bar: 100 μm). **(B)** Viability of MDA-MB-231 cell spheroids (n = 3, * $P < 0.05$).

4.4.7. In vivo anti-tumor efficacy

To evaluate the anti-tumor efficacy, MDA-MB231 tumor-bearing female nude mice were administered through tail vein with saline (control), DOX, plain polymersomes, non-targeted, and targeted DOX-polymersomes twice per week for 4 weeks. Mice were monitored daily for potential toxicity of the drugs, and the tumor volume and body weight were calculated once every three days. The percent tumor volume growth within days was calculated (Figure 9A) and suggested tumor growth inhibition in all DOX-treated groups in comparison with the control. The tumor growth in the group treated with plain polymersomes demonstrated a slight difference compared to the saline group. Free DOX showed an increase of 337% in tumor volume. Non-

targeted polymersomes exhibited 253% increase in tumor volume that was significantly different compared to the saline group. However, targeted DOX-encapsulated nanoparticles demonstrated a much lower increase in volume of just 129%, and displayed significant a difference in comparison with non-targeted vesicles, DOX, and saline ($p < 0.05$ vs non-targeted polymersomes $p < 0.01$ vs free DOX, and $p < 0.001$ vs saline). This suggested that targeted polymersomes were the most effective nanoparticles to inhibit TNBC tumor growth. At the end of the experiment, the mice were euthanized; the tumors were excised and weighed (Figure 9B).

The plain polymersomes, free DOX, and non-targeted polymersome treatment groups revealed the average tumor weights of 0.712, 0.661, and 0.565 g, respectively. However, the targeted polymersome treatment group resulted in the lowest average tumor weight of 0.312 g, significantly different compared to DOX treated groups and saline ($p < 0.05$ vs. non-targeted, $p < 0.01$ vs. free DOX, and $p < 0.001$ vs. saline). The percent tumor growth inhibition (TGI) was determined based on DOX treated groups' tumor volume in contrast to the saline tumor volume group (Figure 9C). The free DOX and non-targeted polymersome groups presented TGI of 41% and 55.7%, respectively. However, targeted polymersome treatment groups demonstrated a TGI of 77.6% that was significantly higher than non-targeted polymersome and free DOX treatment groups. Excised tumors in all treatment groups were dissected in half and imaged (Figure 9D). Overall, the expected high anti-tumor efficacy of the targeted polymersomes might be due to the defective tumor vasculature, enhanced blood circulation and accumulation within the tumors via surface-modified tumor penetrating iRGD peptide,[286] disintegration within hypoxic niches of breast tumors based on the presence of hypoxia-responsive moiety, and liberation of the drug within the cells.

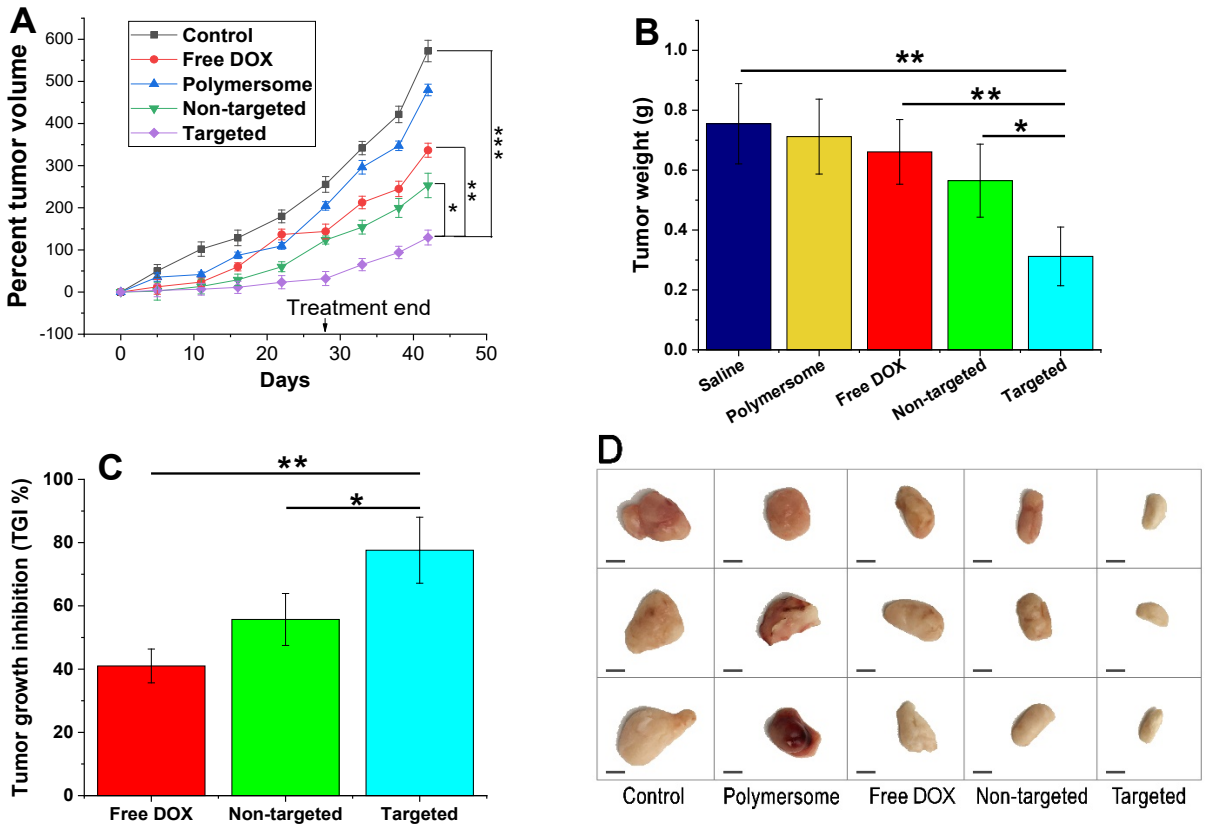

Figure 4.9. *In vivo* anti-tumor efficacy studies **(A)** Tumor volume growth of MDA-MB-231 cancer xenografts treated with saline, plain polymersomes, DOX, non-targeted and targeted polymersomes with a dose of 5 mg DOX/kg. **(B)** Average tumor weight of all treatment groups (n = 3, *p < 0.05, **p < 0.01). **(C)** Percent tumor growth inhibition (TGI) of DOX treated groups (n = 3, *p < 0.05, **p < 0.01). **(D)** Excised tumor images from outside (scale bar: 5 mm).

4.4.8. In vivo toxicity of polymersomes

To determine the polymersomes' toxicity, main organs (lung, liver, and kidney) were collected at the end of the experiment and evaluated using histological assessments (hematoxylin and eosin staining, Figure 10). Histological analyses of mice treated with saline demonstrated some metastatic lesions within the liver tissue (black arrows) due to the diffusion of neoplastic cells through the vessels. The mice treated with DOX, non-targeted, and targeted nanoparticles, did not show any metastatic lesion or toxicity. This presented substantial tumor growth inhibition and anti-tumor efficacy of the polymersome formulations and free drug. We did not evaluate

heart tissue lesions in our study. However, possible toxicity might be expected with high doses of DOX to create myocardial damaged fibers. Overall, most of the organs treated with DOX-loaded vesicles were normal with no tissue necrosis or cell lesion. The histological evaluations demonstrated that non-targeted and targeted polymersomes delivered their drug cargo into the tumor tissues, enhanced anti-tumor efficacy, and reduced off-target toxicity.

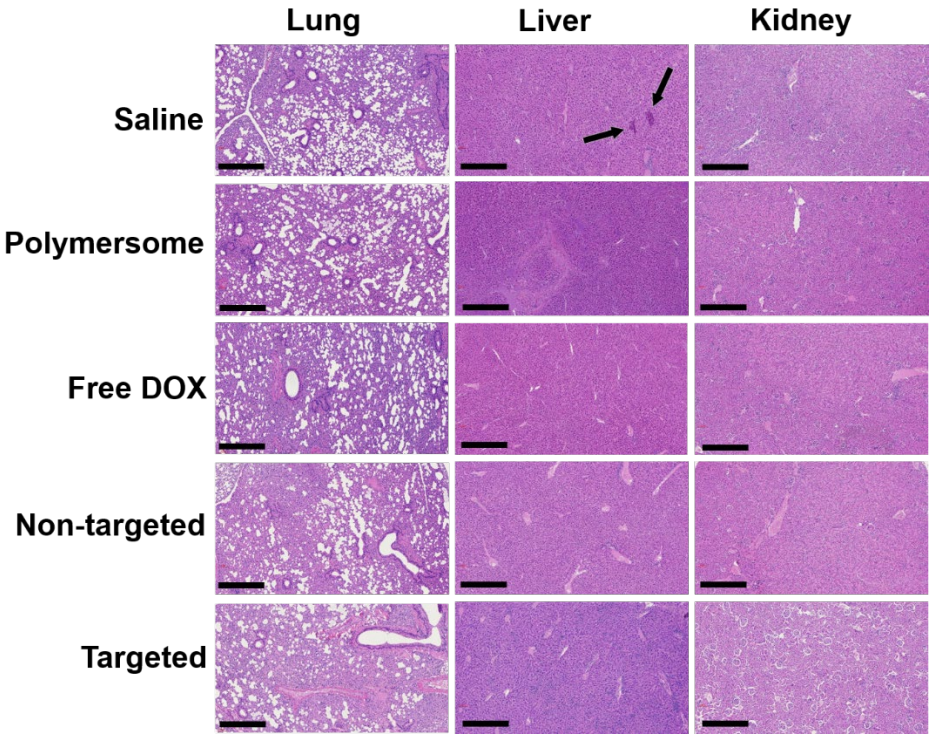

Figure 4.10. Histological assessment of lung, liver, and kidney tissues of nude mice after treating with control, free DOX, non-targeted, targeted, and plain polymersomes (scale bar: 100 μm,10x objective). In the saline-treated group, liver tissues demonstrated metastatic lesions (black arrows).

4.4.9. Biodistribution and nanoparticle accumulation

To assess the biodistribution of the targeted polymersomes, fluorescently labeled iRGD-conjugated polymersomes were injected via the tail vein into the female nude mice. The mice were euthanized at predetermined time points, and the liver, kidney, and lung were excised and imaged (Figure 11A). We did not observe any significant polymersome accumulation within organs after either 3 h or 8 h post-injection. The biodistribution study showed that targeted

nanoparticles might selectively accumulate within the tumor tissues and reduce off-target organ cytotoxicity. The fluorescence integral density of nanoparticle accumulation within organ tissues was calculated by NIH ImageJ software (Figure 11B).

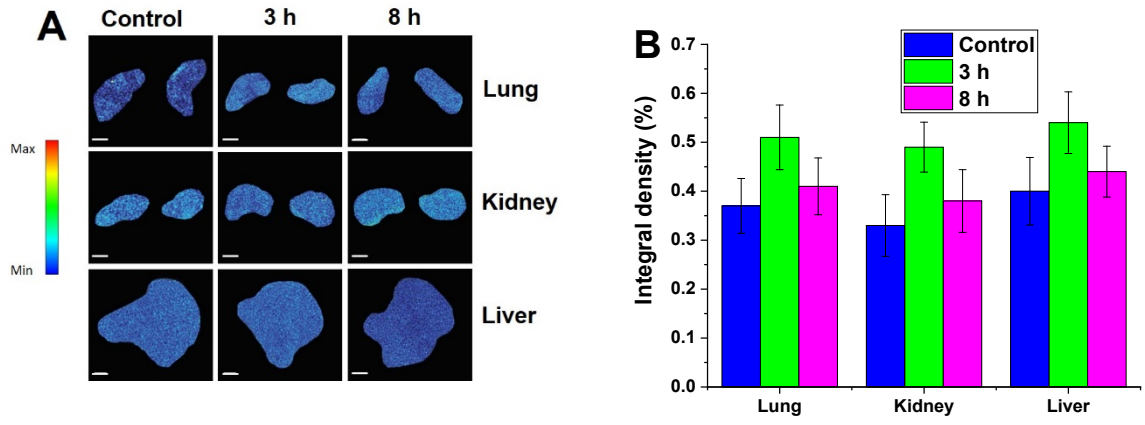

Figure 4.11. (A) Biodistribution to organs at 3 h and 8 h post-injection of indocyanine green-loaded iRGD-polymersomes (n = 3) (scale bar: 2 mm). **(B)** Accumulation of targeted Polymersomes in organs after 3 h and 8 h post-injection of polymersomes (n = 3).

There are other methods for evaluating biodistribution in animals such as radiolabeling the nanoparticles with ^{99m}Tc or ^{124}I and measuring the radioactivity of different organs.[291,292] The radiolabeling can be carried out based on Bolton-Hunter method by forming a covalent linkage between amine groups on the surface of nanoparticles and N-hydroxysuccinimide ester group (NHS) bounded with radioactive elements.[291] Biodistribution is crucial for the translational evaluation of the nanoparticles before administrating in humans. However, using radiolabels has its own limitations. For instance, radiolabels should be attached to the nanoparticles to be accurately imaged. In any case of dissociation, imaging will be resulted in wrong information. The other limitation related to exact biodistribution study is the compatibility of the materials used for nanoparticle preparation. If the structural materials used for nanoparticle are incompatible with radiolabel elements, labels can detach from the nanoparticles and make it

difficult to measure the biodistribution. The longitude of biodistribution assessment should be considered as a limiting factor due to radiolabel decay.[293]

Scanning transmission electron microscopy (STEM) of tissues is another technique to determine the biodistribution of nanoparticles within the cells and cellular organelles.[294] This technique has been used to assess the accumulation of gold nanoparticles in the liver of the mice with a high resolution. Although STEM is a quantitative approach for the biodistribution of nanoparticles within tissues, it has some limitations, including incapability to measure tissue sections thicker than 150 nm.[295] In addition, electron microscopy is expensive for evaluating nanoparticle distribution within different tissues or the whole organ. Furthermore, lipid soluble solvents are used to prepare samples which is not applicable for all nanoparticles. For instance, micelles or liposomes cannot be measures by electron microscopic imaging.[295]

4.5. Conclusion

We synthesized an amphiphilic diblock copolymer with a hypoxia-responsive diazobenzene linker capable of self-assembly into polymersomes. Doxorubicin was successfully encapsulated into the polymersomes. The tumor-targeting and penetrating iRGD peptide was conjugated into the polymersomes via click chemistry to make targeted hypoxia-responsive polymersomes. Targeted polymersomes exhibited higher cytotoxicity on TNBC cells in hypoxia compared to normoxia in both monolayer and three-dimensional spheroid cell cultures. *In vivo* studies on TNBC tumor-bearing, nude mice demonstrated that targeted polymersomes have an enhanced anti-tumor efficacy in contrast to non-targeted polymersomes and free doxorubicin. These drug-loaded polymer nanoparticles caused no toxicity in various internal organs, such as the liver, kidney, and lung. This is the first administration of hypoxia-responsive iRGD-polymersomes encapsulating doxorubicin in animal models of triple-negative breast cancer. An

earlier study has demonstrated tumor suppression by employing doxorubicin within hypoxia-responsive nanoparticles to reach the TNBC tumors via the EPR effect.[296] The nanoparticles in our study are hypoxia-responsive and iRGD-conjugated. Hence, they offer the benefit of selective delivery of doxorubicin to TNBC tumors via active receptor-mediated targeting and enhanced penetration into the cells while lowering the off-target toxicity compared to passive tumor diffusion of nanoparticles or free drugs. The inclusion of diazobenzene hypoxia-responsive moiety contributes to the selective release of chemotherapeutics within the breast tumors' hypoxic niches. The results of this study indicated that targeted hypoxia-responsive polymersomes could be effective anticancer drug delivery vehicles when administered into solid tumors of triple-negative breast cancer.

4.6. Acknowledgements

This research was supported by NIH grant 2R01GM 114080 (NIGMS) to SM and VS, and a Ready-to-Go award from the DaCCoTA Center (NIGMS U54 GM128729) to SM. SM also acknowledges partial support from the National Science Foundation under NSF EPSCoR Track-1 Cooperative Agreement OIA #1946202. Any opinions, findings, and conclusions or recommendations expressed in this material are those of the author(s) and do not necessarily reflect the views of the National Science Foundation. The authors thank Parinaz Ghanbari for designing all schematic illustrations in this manuscript. The mouse experiments were conducted in the Animal Studies Core Facility, supported by the NIGMS COBRE award 1P20 GM109024.

5. CONCLUSION AND FUTURE DIRECTIONS

Cancer is the major malignancy among men and women worldwide. Despite advances in developing various chemotherapeutics, these drugs are not effective enough to differentiate between cancer and healthy cells. Thus, systemic toxicity and adverse side-effects restrict therapeutic efficacy of anticancer drugs. The other problems related to some chemotherapeutic drugs are their low solubility, immunogenicity, and short circulation half-life which limit their further development. In addition, rapid proliferation of cancer cells along with insufficient blood supply induce low oxygen partial pressure or hypoxia in solid tumors. Hypoxia increases to the conundrum of cancer treatment by enhancing cancer cell survival through resistance to chemo- and radiation therapy. However, many of these challenges can be addressed by employing the nanotechnology which is applying the nanoscale devices to improve the chemotherapeutic efficacy. During the recent three decades, numerous drug-loaded nanoparticles have been developed for the treatment of many disorders including cancer. Nanoparticle-based drug delivery systems can increase the circulation half-life of anticancer drugs, improve the solubility of low-soluble drugs, decrease the immunogenicity, and reduce the administration of chemotherapy by producing a sustained drug release profile. The ideal nanoparticles are stable, biodegradable, easy to be prepared, and able to selectively release their chemotherapeutic cargo within target site. Among various drug-loaded nanoparticles, polymeric nanoparticles (referred to as polymersomes) have attracted countless attention due to their tunable membrane features, stability, biodegradability, biocompatibility, and ability to encapsulate a vast range of hydrophobic and hydrophilic molecules and anticancer drugs. Polymersomes are made of amphiphilic block copolymers. The common hydrophilic block copolymer is usually polyethylene glycol (PEG) which is used for increasing nanoparticle’s blood circulation.

Different kinds of hydrophobic blocks can be used in polymersome structure, including polylactic acid (PLA), polycaprolactone (PCL), polybutadiene (PBD), and polydimethylsiloxane (PDMS). Stimuli-responsive polymersomes have been developed based on incorporating sensitive moieties into the building blocks of the polymersomes for controlled release of encapsulated drugs. Stimuli-responsive polymersomes are responsive to various external or internal stimuli, including pH, hypoxia, redox, temperature, light, magnetic field, and glucose concentration. Hypoxia-responsive polymersomes have been received more attraction due to releasing their chemotherapeutic drugs within hypoxic niches of tumor microenvironment. To meet the need of targeted drug delivery to the specific tumor site, there are passive and active tumor targeting strategies. Passive tumor targeting is based on enhanced permeability and retention (EPR) effect which is due to leaky vasculature and impaired lymphatic drainage present in tumor environments. Passive tumor targeting allows for accumulation of nanoparticles within the diseased site. There are specific biochemical and biological characteristics in cancer cells which discriminate them from healthy cells. For instance, cancer cells usually express specific biomarkers on their surface which can be used for developing successful therapeutic strategies in cancer treatment. Active tumor targeting is based on an increased interaction between drug-loaded nanoparticles and cancer cells through receptor-mediated targeted drug delivery. This can be achieved by labeling nanoparticles with ligands that can selectively interact with overexpressed receptors on the surface of cancer cells. The nanoparticles then march into the tumor, disintegrate, release their anticancer drug, and destroy the tumor. Targeted drug delivery enhances the therapeutic efficacy through accumulating the chemotherapeutics within desired tumor tissues and reducing off-target side effects.

Although Doxil and Abraxane have been approved by the FDA as efficient anticancer nanoparticulate formulations to improve safety profiles compared to free drugs, numerous drug-loaded nanoparticles have not been developed to be effective in human. In addition, several drug nano-formulations have been tested successfully on animal models, but the translation of these nanoparticles in the human has been limited due to several hurdles. For instance, nanoparticles are used to reduce toxicity and side effects of drugs but the carrier systems themselves may impose risks to the patients. The toxicity of substances used for nanoparticle preparation differs from one nanoparticulate formulation to the other delivery system. Clearly, the potential interaction and toxicity of nanocarriers with the human cells and tissues greatly depends on the composition of these nanoparticle formulations.

The route of administration makes a great toxicological difference for the local drug delivery vehicles compared to systemic delivery of nanoparticles. For instance, a high exposure of inhaling drug-loaded nanoparticles can be observed in the lungs compared to the low or even insignificant exposure of these local drugs in other organs. In addition, the quantity of drugs absorbed from airway tracts influences the toxicity of inhaled nanoparticles. For the systemic administration of drug-loaded nanoparticles, the major problem would be the accumulation of nanoparticles in other healthy organs compared to the desired tumor site. This will cause off-target side effects which needs to be addressed by tumor-targeted drug delivery.

The size of nanoparticles is an important factor for the potential crossing of these particles through biological barriers such as cell membrane, nuclear pore complexes, and even blood brain barrier (BBB) for drug delivery to the brain. The size of nanoparticles also greatly affects the efficacy of drug delivery to the tumors which affects circulation, biodistribution, tumor penetration and accumulation. Nanoparticles will be cleared by mononuclear phagocytic

system (MPS) or filtered by the spleen and liver very quickly. The renal filtration happens for the particles less than 6 nm.[297] Those particles with sizes smaller than 50 nm will be absorbed by the endothelial cells and get trapped in the liver.[298] Basically, nanoparticles ranging from 150 nm to 1.2 micrometers can pass through the tumor cells.[299] Nanoparticles with larger sizes can be retained within tumor tissues for longer times.

One of the major potential challenges for preparing drug-loaded nanoparticles is the proper release of drug after transporting them to the desired tumor sites. In this case, biodegradable nanocarrier formulations are of crucial importance. The most common strategy for stimulating drug-encapsulated nanoparticles to release their cargo is the implementation of stimuli-responsive chemicals within their construction. In our research, we developed polymeric nanoparticles containing hypoxia-responsive moieties within their structure for the sustained drug release under partial low oxygen pressure within the tumors.

We prepared various targeted hypoxia-responsive polymersomes by incorporating diazobenzene responsive linker between PEG and PLA block copolymers. These nanoparticles can target overexpressed estrogen receptors on the surface of estrogen receptor positive breast cancer cells (Chapters 2 and 3) and neuropilin-1 receptors on the surface of triple negative breast cancer cells.

In Chapter 2, we incorporated estradiol into the polymersomes to prepare estradiol-conjugated, hypoxia-responsive polymersomes. These nanoparticles were characterized by various methods including transmission electron microscopic and atomic force microscopic imaging. The polymersomes encapsulated doxorubicin within their aqueous core. We demonstrated that over 90% of encapsulated doxorubicin was released after 12 hours within hypoxia. Targeted polymersomes developed here reduced the viability of MCF-7 breast cancer

cells after 72 hours to 14% and 21% in monolayer and three-dimensional spheroid cell cultures, respectively. Targeted polymersomes shrank the MCF-7 cell spheroid volume up to 68%.

In Chapter 3, we conjugated endoxifen to the surface PEG molecules and prepared targeted hypoxia-responsive, doxorubicin-encapsulated polymersomes. The particle size was calculated by dynamic light scattering, and the shape was characterized by transmission electron microscopy and atomic force microscopy. The polymersomes released over 90% of their encapsulated drug within 8 hours under hypoxic condition. The MCF-7 monolayer and three-dimensional spheroid cell cultures were treated with targeted doxorubicin-encapsulated polymersomes for 72 hours. The cell viability in monolayer and spheroid cell cultures reduced to 18% and 31%, respectively. Targeted polymersomes were toxic against MCF-7 spheroids by shrinking half of the spheroid volume.

In Chapter 4, we synthesized PEG-diazobenzene-PLA polymer along with a tumor-homing and penetrating iRGD peptide. The iRGD peptide was reacted with PLA-PEG-N_3 using copper-catalyzed azide-alkyne cycloaddition reaction. The produced PLA-PEG-iRGD polymer was then incorporated into the polymersome structure to prepare targeted iRGD-conjugated, doxorubicin-encapsulated polymersomes. These polymersomes were stable at 4 °C for 8 weeks. They released about 95% of the encapsulated doxorubicin in hypoxia after 12 hours. The triple negative breast cancer MDA-MB231 monolayer and spheroid cell cultures were treated with targeted drug-loaded polymersomes for 72 hours under hypoxia and normoxia. The viability of the cells decreased to 28% in monolayer and 36% in spheroid cell cultures. We induced triple negative breast cancer tumor-bearing mice and administered our targeted polymersome formulation through tail vein twice per week for 4 weeks. The results demonstrated that targeted doxorubicin-loaded polymersomes significantly inhibited tumor growth compared to free

doxorubicin and control groups. These polymersomes have no toxicity to other organs such as liver, kidney, or lung.

The various types of targeted drug-encapsulated polymeric nanoparticles we developed in our studies have the potential for targeted drug delivery to hypoxic estrogen receptor positive and triple negative breast solid tumors.

REFERENCES

(1) DeSantis, C. E.; Ma, J.; Gaudet, M. M.; Newman, L. A.; Miller, K. D.; Sauer, A. G.; Jemal, A.; Siegel, R. L. Breast Cancer Statistics, 2019. *CA: A Cancer Journal for Clinicians* **2019**, *69* (6), 438–451. https://doi.org/10.3322/caac.21583.

(2) Weigelt, B.; Peterse, J. L.; van't Veer, L. J. Breast Cancer Metastasis: Markers and Models. *Nature Reviews Cancer* **2005**, *5* (8), 591–602. https://doi.org/10.1038/nrc1670.

(3) Cummings, M. C.; Simpson, P. T.; Reid, L. E.; Jayanthan, J.; Skerman, J.; Song, S.; McCart Reed, A. E.; Kutasovic, J. R.; Morey, A. L.; Marquart, L.; O'Rourke, P.; Lakhani, S. R. Metastatic Progression of Breast Cancer: Insights from 50 Years of Autopsies. *J Pathol* **2014**, *232* (1), 23–31. https://doi.org/10.1002/path.4288.

(4) Henry, N. L.; Hayes, D. F. Cancer Biomarkers. *Mol Oncol* **2012**, *6* (2), 140–146. https://doi.org/10.1016/j.molonc.2012.01.010.

(5) Ulaner, G. A.; Riedl, C. C.; Dickler, M. N.; Jhaveri, K.; Pandit-Taskar, N.; Weber, W. Molecular Imaging of Biomarkers in Breast Cancer. *J Nucl Med* **2016**, *57* (Suppl 1), 53S-59S. https://doi.org/10.2967/jnumed.115.157909.

(6) Jorns, J. M. Breast Cancer Biomarkers: Challenges in Routine Estrogen Receptor, Progesterone Receptor, and HER2/Neu Evaluation. *Arch Pathol Lab Med* **2019**, *143* (12), 1444–1449. https://doi.org/10.5858/arpa.2019-0205-RA.

(7) Mamnoon, B.; Feng, L.; Froberg, J.; Choi, Y.; Sathish, V.; Mallik, S. Hypoxia-Responsive, Polymeric Nanocarriers for Targeted Drug Delivery to Estrogen Receptor-Positive Breast Cancer Cell Spheroids. *Mol. Pharmaceutics* **2020**. https://doi.org/10.1021/acs.molpharmaceut.0c00754.

(8) Nicolini, A.; Ferrari, P.; Duffy, M. J. Prognostic and Predictive Biomarkers in Breast Cancer: Past, Present and Future. *Seminars in Cancer Biology* **2018**, *52*, 56–73. https://doi.org/10.1016/j.semcancer.2017.08.010.

(9) Spitale, A.; Mazzola, P.; Soldini, D.; Mazzucchelli, L.; Bordoni, A. Breast Cancer Classification According to Immunohistochemical Markers: Clinicopathologic Features and Short-Term Survival Analysis in a Population-Based Study from the South of Switzerland. *Annals of Oncology* **2009**, *20* (4), 628–635. https://doi.org/10.1093/annonc/mdn675.

(10) Couse, J. F.; Korach, K. S. Estrogen Receptor Null Mice: What Have We Learned and Where Will They Lead Us? *Endocr Rev* **1999**, *20* (3), 358–417. https://doi.org/10.1210/edrv.20.3.0370.

(11) Ali, S.; Coombes, R. C. Estrogen Receptor Alpha in Human Breast Cancer: Occurrence and Significance. *J Mammary Gland Biol Neoplasia* **2000**, *5* (3), 271–281. https://doi.org/10.1023/A:1009594727358.

(12) Jia, M.; Dahlman-Wright, K.; Gustafsson, J.-Å. Estrogen Receptor Alpha and Beta in Health and Disease. *Best Practice & Research Clinical Endocrinology & Metabolism* **2015**, *29* (4), 557–568. https://doi.org/10.1016/j.beem.2015.04.008.

(13) Haldosén, L.-A.; Zhao, C.; Dahlman-Wright, K. Estrogen Receptor Beta in Breast Cancer. *Molecular and Cellular Endocrinology* **2014**, *382* (1), 665–672. https://doi.org/10.1016/j.mce.2013.08.005.

(14) Girault, I.; Andrieu, C.; Tozlu, S.; Spyratos, F.; Bièche, I.; Lidereau, R. Altered Expression Pattern of Alternatively Spliced Estrogen Receptor β Transcripts in Breast

Carcinoma. *Cancer Letters* **2004**, *215* (1), 101–112. https://doi.org/10.1016/j.canlet.2004.05.006.
(15) Tong, D.; Schuster, E.; Seifert, M.; Czerwenka, K.; Leodolte, S.; Zeillinger, R. Expression of Estrogen Receptor Beta Isoforms in Human Breast Cancer Tissues and Cell Lines. *Breast Cancer Res Treat* **2002**, *71* (3), 249–255. https://doi.org/10.1023/a:1014465916473.
(16) Saji, S.; Omoto, Y.; Shimizu, C.; Warner, M.; Hayashi, Y.; Horiguchi, S.; Watanabe, T.; Hayashi, S.; Gustafsson, J.-Å.; Toi, M. Expression of Estrogen Receptor (ER) Bcx Protein in ERα-Positive Breast Cancer: Specific Correlation with Progesterone Receptor. *Cancer Res* **2002**, *62* (17), 4849–4853.
(17) Davies, M. P. A.; O'Neill, P. A.; Innes, H.; Sibson, D. R.; Prime, W.; Holcombe, C.; Foster, C. S. Correlation of MRNA for Oestrogen Receptor Beta Splice Variants ERβ1, ERβ2/ERβcx and ERβ5 with Outcome in Endocrine-Treated Breast Cancer. *Journal of Molecular Endocrinology* **2004**, *33* (3), 773–782. https://doi.org/10.1677/jme.1.01574.
(18) Rakha, E. A.; El-Sayed, M. E.; Green, A. R.; Paish, E. C.; Powe, D. G.; Gee, J.; Nicholson, R. I.; Lee, A. H. S.; Robertson, J. F. R.; Ellis, I. O. Biologic and Clinical Characteristics of Breast Cancer With Single Hormone Receptor–Positive Phenotype. *JCO* **2007**, *25* (30), 4772–4778. https://doi.org/10.1200/JCO.2007.12.2747.
(19) Kastner, P.; Krust, A.; Turcotte, B.; Stropp, U.; Tora, L.; Gronemeyer, H.; Chambon, P. Two Distinct Estrogen-Regulated Promoters Generate Transcripts Encoding the Two Functionally Different Human Progesterone Receptor Forms A and B. *EMBO J* **1990**, *9* (5), 1603–1614.
(20) Graham, J. D.; Yager, M. L.; Hill, H. D.; Byth, K.; O'Neill, G. M.; Clarke, C. L. Altered Progesterone Receptor Isoform Expression Remodels Progestin Responsiveness of Breast Cancer Cells. *Mol Endocrinol* **2005**, *19* (11), 2713–2735. https://doi.org/10.1210/me.2005-0126.
(21) Boonyaratanakornkit, V.; McGowan, E.; Sherman, L.; Mancini, M. A.; Cheskis, B. J.; Edwards, D. P. The Role of Extranuclear Signaling Actions of Progesterone Receptor in Mediating Progesterone Regulation of Gene Expression and the Cell Cycle. *Mol Endocrinol* **2007**, *21* (2), 359–375. https://doi.org/10.1210/me.2006-0337.
(22) Daniel, A. R.; Knutson, T. P.; Lange, C. A. Signaling Inputs to Progesterone Receptor Gene Regulation and Promoter Selectivity. *Molecular and Cellular Endocrinology* **2009**, *308* (1), 47–52. https://doi.org/10.1016/j.mce.2009.01.004.
(23) Rugo, H. S.; Rumble, R. B.; Macrae, E.; Barton, D. L.; Connolly, H. K.; Dickler, M. N.; Fallowfield, L.; Fowble, B.; Ingle, J. N.; Jahanzeb, M.; Johnston, S. R. D.; Korde, L. A.; Khatcheressian, J. L.; Mehta, R. S.; Muss, H. B.; Burstein, H. J. Endocrine Therapy for Hormone Receptor–Positive Metastatic Breast Cancer: American Society of Clinical Oncology Guideline. *JCO* **2016**, *34* (25), 3069–3103. https://doi.org/10.1200/JCO.2016.67.1487.
(24) Mitri, Z.; Constantine, T.; O'Regan, R. The HER2 Receptor in Breast Cancer: Pathophysiology, Clinical Use, and New Advances in Therapy. *Chemother Res Pract* **2012**, *2012*. https://doi.org/10.1155/2012/743193.
(25) Meric-Bernstam, F.; Hung, M.-C. Advances in Targeting Human Epidermal Growth Factor Receptor-2 Signaling for Cancer Therapy. *Clin Cancer Res* **2006**, *12* (21), 6326–6330. https://doi.org/10.1158/1078-0432.CCR-06-1732.

(26) Slamon, D. J.; Clark, G. M.; Wong, S. G.; Levin, W. J.; Ullrich, A.; McGuire, W. L. Human Breast Cancer: Correlation of Relapse and Survival with Amplification of the HER-2/Neu Oncogene. *Science* **1987**, *235* (4785), 177–182. https://doi.org/10.1126/science.3798106.
(27) Escrivá-de-Romaní, S.; Arumí, M.; Bellet, M.; Saura, C. HER2-Positive Breast Cancer: Current and New Therapeutic Strategies. *The Breast* **2018**, *39*, 80–88. https://doi.org/10.1016/j.breast.2018.03.006.
(28) Tai, W.; Mahato, R.; Cheng, K. The Role of HER2 in Cancer Therapy and Targeted Drug Delivery. *Journal of Controlled Release* **2010**, *146* (3), 264–275. https://doi.org/10.1016/j.jconrel.2010.04.009.
(29) Ryu, D. W.; Jung, M. J.; Choi, W. S.; Lee, C. H. Clinical Significance of Morphologic Characteristics in Triple Negative Breast Cancer. *Journal of the Korean Surgical Society* **2011**, *80* (5), 301–306. https://doi.org/10.4174/jkss.2011.80.5.301.
(30) Lund, M. J.; Trivers, K. F.; Porter, P. L.; Coates, R. J.; Leyland-Jones, B.; Brawley, O. W.; Flagg, E. W.; O'Regan, R. M.; Gabram, S. G. A.; Eley, J. W. Race and Triple Negative Threats to Breast Cancer Survival: A Population-Based Study in Atlanta, GA. *Breast Cancer Res Treat* **2009**, *113* (2), 357–370. https://doi.org/10.1007/s10549-008-9926-3.
(31) Lehmann, B. D.; Pietenpol, J. A. Identification and Use of Biomarkers in Treatment Strategies for Triple Negative Breast Cancer Subtypes. *J Pathol* **2014**, *232* (2), 142–150. https://doi.org/10.1002/path.4280.
(32) Bai, Z.; Gust, R. Breast Cancer, Estrogen Receptor and Ligands. *Archiv der Pharmazie* **2009**, *342* (3), 133–149. https://doi.org/10.1002/ardp.200800174.
(33) Wang, B.; Rosano, J. M.; Cheheltani, R.; Achary, M. P.; Kiani, M. F. Towards a Targeted Multi-Drug Delivery Approach to Improve Therapeutic Efficacy in Breast Cancer. *Expert Opinion on Drug Delivery* **2010**, *7* (10), 1159–1173. https://doi.org/10.1517/17425247.2010.513968.
(34) Tacar, O.; Sriamornsak, P.; Dass, C. R. Doxorubicin: An Update on Anticancer Molecular Action, Toxicity and Novel Drug Delivery Systems. *Journal of Pharmacy and Pharmacology* **2013**, *65* (2), 157–170. https://doi.org/10.1111/j.2042-7158.2012.01567.x.
(35) Piccart-Gebhart, M. J.; Burzykowski, T.; Buyse, M.; Sledge, G.; Carmichael, J.; Lück, H.-J.; Mackey, J. R.; Nabholtz, J.-M.; Paridaens, R.; Biganzoli, L.; Jassem, J.; Bontenbal, M.; Bonneterre, J.; Chan, S.; Basaran, G. A.; Therasse, P. Taxanes Alone or in Combination With Anthracyclines As First-Line Therapy of Patients With Metastatic Breast Cancer. *JCO* **2008**, *26* (12), 1980–1986. https://doi.org/10.1200/JCO.2007.10.8399.
(36) Reichardt, P.; von Minckwitz, G.; Thuss-Patience, P. C.; Jonat, W.; Kölbl, H.; Jänicke, F.; Kieback, D. G.; Kuhn, W.; Schindler, A. E.; Mohrmann, S.; Kaufmann, M.; Lück, H. J. Multicenter Phase II Study of Oral Capecitabine (Xeloda") in Patients with Metastatic Breast Cancer Relapsing after Treatment with a Taxane-Containing Therapy. *Annals of Oncology* **2003**, *14* (8), 1227–1233. https://doi.org/10.1093/annonc/mdg346.
(37) Jones, S.; Holmes, F. A.; O'Shaughnessy, J.; Blum, J. L.; Vukelja, S. J.; McIntyre, K. J.; Pippen, J. E.; Bordelon, J. H.; Kirby, R. L.; Sandbach, J.; Hyman, W. J.; Richards, D. A.; Mennel, R. G.; Boehm, K. A.; Meyer, W. G.; Asmar, L.; Mackey, D.; Riedel, S.; Muss, H.; Savin, M. A. Docetaxel With Cyclophosphamide Is Associated With an Overall Survival Benefit Compared With Doxorubicin and Cyclophosphamide: 7-Year Follow-

Up of US Oncology Research Trial 9735. *JCO* **2009**, *27* (8), 1177–1183. https://doi.org/10.1200/JCO.2008.18.4028.
(38) Perou, C. M.; Sørlie, T.; Eisen, M. B.; van de Rijn, M.; Jeffrey, S. S.; Rees, C. A.; Pollack, J. R.; Ross, D. T.; Johnsen, H.; Akslen, L. A.; Fluge, Ø.; Pergamenschikov, A.; Williams, C.; Zhu, S. X.; Lønning, P. E.; Børresen-Dale, A.-L.; Brown, P. O.; Botstein, D. Molecular Portraits of Human Breast Tumours. *Nature* **2000**, *406* (6797), 747–752. https://doi.org/10.1038/35021093.
(39) Orlando, L.; Schiavone, P.; Fedele, P.; Calvani, N.; Nacci, A.; Rizzo, P.; Marino, A.; D'Amico, M.; Sponziello, F.; Mazzoni, E.; Cinefra, M.; Fazio, N.; Maiello, E.; Silvestris, N.; Colucci, G.; Cinieri, S. Molecularly Targeted Endocrine Therapies for Breast Cancer. *Cancer Treatment Reviews* **2010**, *36*, S67–S71. https://doi.org/10.1016/S0305-7372(10)70023-2.
(40) Lim, Y. C.; Desta, Z.; Flockhart, D. A.; Skaar, T. C. Endoxifen (4-Hydroxy-N-Desmethyl-Tamoxifen) Has Anti-Estrogenic Effects in Breast Cancer Cells with Potency Similar to 4-Hydroxy-Tamoxifen. *Cancer Chemother Pharmacol* **2005**, *55* (5), 471–478. https://doi.org/10.1007/s00280-004-0926-7.
(41) Li, F.; Dou, J.; Wei, L.; Li, S.; Liu, J. The Selective Estrogen Receptor Modulators in Breast Cancer Prevention. *Cancer Chemother Pharmacol* **2016**, *77* (5), 895–903. https://doi.org/10.1007/s00280-016-2959-0.
(42) Aihara, T.; Takatsuka, Y.; Ohsumi, S.; Aogi, K.; Hozumi, Y.; Imoto, S.; Mukai, H.; Iwata, H.; Watanabe, T.; Shimizu, C.; Nakagami, K.; Tamura, M.; Ito, T.; Masuda, N.; Ogino, N.; Hisamatsu, K.; Mitsuyama, S.; Abe, H.; Tanaka, S.; Yamaguchi, T.; Ohashi, Y. Phase III Randomized Adjuvant Study of Tamoxifen Alone versus Sequential Tamoxifen and Anastrozole in Japanese Postmenopausal Women with Hormone-Responsive Breast Cancer: N-SAS BC03 Study. *Breast Cancer Res Treat* **2010**, *121* (2), 379–387. https://doi.org/10.1007/s10549-010-0888-x.
(43) Glück, S.; Gorouhi, F. Clinical and Economic Benefits of Aromatase Inhibitor Therapy in Early-Stage Breast Cancer. *Am J Health Syst Pharm* **2011**, *68* (18), 1699–1706. https://doi.org/10.2146/ajhp100492.
(44) Slamon, D. J.; Leyland-Jones, B.; Shak, S.; Fuchs, H.; Paton, V.; Bajamonde, A.; Fleming, T.; Eiermann, W.; Wolter, J.; Pegram, M.; Baselga, J.; Norton, L. Use of Chemotherapy plus a Monoclonal Antibody against HER2 for Metastatic Breast Cancer That Overexpresses HER2. *New England Journal of Medicine* **2001**, *344* (11), 783–792. https://doi.org/10.1056/NEJM200103153441101.
(45) Gelmon, K. A.; Boyle, F. M.; Kaufman, B.; Huntsman, D. G.; Manikhas, A.; Di Leo, A.; Martin, M.; Schwartzberg, L. S.; Lemieux, J.; Aparicio, S.; Shepherd, L. E.; Dent, S.; Ellard, S. L.; Tonkin, K.; Pritchard, K. I.; Whelan, T. J.; Nomikos, D.; Nusch, A.; Coleman, R. E.; Mukai, H.; Tjulandin, S.; Khasanov, R.; Rizel, S.; Connor, A. P.; Santillana, S. L.; Chapman, J.-A. W.; Parulekar, W. R. Lapatinib or Trastuzumab Plus Taxane Therapy for Human Epidermal Growth Factor Receptor 2–Positive Advanced Breast Cancer: Final Results of NCIC CTG MA.31. *JCO* **2015**, *33* (14), 1574–1583. https://doi.org/10.1200/JCO.2014.56.9590.
(46) Pasquier, E.; Kavallaris, M. Microtubules: A Dynamic Target in Cancer Therapy. *IUBMB Life* **2008**, *60* (3), 165–170. https://doi.org/10.1002/iub.25.
(47) Patterson, D. M.; Rustin, G. J. S. Vascular Damaging Agents. *Clinical Oncology* **2007**, *19* (6), 443–456. https://doi.org/10.1016/j.clon.2007.03.014.

(48) R. Murata, M. R. H., J. Overgaard. Comparative Effects of Combretastatin A-4 Disodium Phosphate and 5,6-Dimethylxanthenone-4-Acetic Acid on Blood Perfusion in a Murine Tumour and Normal Tissues. *International Journal of Radiation Biology* **2001**, *77* (2), 195–204. https://doi.org/10.1080/09553000010007695.
(49) Shi, J.; Votruba, A. R.; Farokhzad, O. C.; Langer, R. Nanotechnology in Drug Delivery and Tissue Engineering: From Discovery to Applications. *Nano Lett.* **2010**, *10* (9), 3223–3230. https://doi.org/10.1021/nl102184c.
(50) Zhang, L.; Gu, F. X.; Chan, J. M.; Wang, A. Z.; Langer, R. S.; Farokhzad, O. C. Nanoparticles in Medicine: Therapeutic Applications and Developments. *Clinical Pharmacology & Therapeutics* **2008**, *83* (5), 761–769. https://doi.org/10.1038/sj.clpt.6100400.
(51) Amreddy, N.; Babu, A.; Muralidharan, R.; Panneerselvam, J.; Srivastava, A.; Ahmed, R.; Mehta, M.; Munshi, A.; Ramesh, R. Recent Advances in Nanoparticle-Based Cancer Drug and Gene Delivery. *Adv Cancer Res* **2018**, *137*, 115–170. https://doi.org/10.1016/bs.acr.2017.11.003.
(52) Karandish, F.; Mamnoon, B.; Feng, L.; Haldar, M. K.; Xia, L.; Gange, K. N.; You, S.; Choi, Y.; Sarkar, K.; Mallik, S. Nucleus-Targeted, Echogenic Polymersomes for Delivering a Cancer Stemness Inhibitor to Pancreatic Cancer Cells. *Biomacromolecules* **2018**, *19* (10), 4122–4132. https://doi.org/10.1021/acs.biomac.8b01133.
(53) Confeld, M. I.; Mamnoon, B.; Feng, L.; Jensen-Smith, H.; Ray, P.; Froberg, J.; Kim, J.; Hollingsworth, M. A.; Quadir, M.; Choi, Y.; Mallik, S. Targeting the Tumor Core: Hypoxia-Responsive Nanoparticles for the Delivery of Chemotherapy to Pancreatic Tumors. *Mol. Pharmaceutics* **2020**, *17* (8), 2849–2863. https://doi.org/10.1021/acs.molpharmaceut.0c00247.
(54) Liyanage, P. Y.; Hettiarachchi, S. D.; Zhou, Y.; Ouhtit, A.; Seven, E. S.; Oztan, C. Y.; Celik, E.; Leblanc, R. M. Nanoparticle-Mediated Targeted Drug Delivery for Breast Cancer Treatment. *Biochimica et Biophysica Acta (BBA) - Reviews on Cancer* **2019**, *1871* (2), 419–433. https://doi.org/10.1016/j.bbcan.2019.04.006.
(55) Peer, D.; Karp, J. M.; Hong, S.; Farokhzad, O. C.; Margalit, R.; Langer, R. Nanocarriers as an Emerging Platform for Cancer Therapy. *Nature Nanotechnology* **2007**, *2* (12), 751–760. https://doi.org/10.1038/nnano.2007.387.
(56) Gao, H.; Yang, Z.; Zhang, S.; Cao, S.; Shen, S.; Pang, Z.; Jiang, X. Ligand Modified Nanoparticles Increases Cell Uptake, Alters Endocytosis and Elevates Glioma Distribution and Internalization. *Sci Rep* **2013**, *3*. https://doi.org/10.1038/srep02534.
(57) Large, D. E.; Soucy, J. R.; Hebert, J.; Auguste, D. T. Advances in Receptor-Mediated, Tumor-Targeted Drug Delivery. *Advanced Therapeutics* **2019**, *2* (1), 1800091. https://doi.org/10.1002/adtp.201800091.
(58) Wang, M.; Li, Y.; HuangFu, M.; Xiao, Y.; Zhang, T.; Han, M.; Xu, D.; Li, F.; Ling, D.; Jin, Y.; Gao, J. Pluronic-Attached Polyamidoamine Dendrimer Conjugates Overcome Drug Resistance in Breast Cancer. *Nanomedicine* **2016**, *11* (22), 2917–2934. https://doi.org/10.2217/nnm-2016-0252.
(59) Kutty, R. V.; Feng, S.-S. Cetuximab Conjugated Vitamin E TPGS Micelles for Targeted Delivery of Docetaxel for Treatment of Triple Negative Breast Cancers. *Biomaterials* **2013**, *34* (38), 10160–10171. https://doi.org/10.1016/j.biomaterials.2013.09.043.
(60) Zhang, T.; Luo, J.; Fu, Y.; Li, H.; Ding, R.; Gong, T.; Zhang, Z. Novel Oral Administrated Paclitaxel Micelles with Enhanced Bioavailability and Antitumor Efficacy

for Resistant Breast Cancer. *Colloids and Surfaces B: Biointerfaces* **2017**, *150*, 89–97. https://doi.org/10.1016/j.colsurfb.2016.11.024.

(61) Rosch, J. G.; Winter, H.; DuRoss, A. N.; Sahay, G.; Sun, C. Inverse-Micelle Synthesis of Doxorubicin-Loaded Alginate/Chitosan Nanoparticles and in Vitro Assessment of Breast Cancer Cytotoxicity. *Colloid Interface Sci Commun* **2019**, *28*, 69–74. https://doi.org/10.1016/j.colcom.2018.12.002.

(62) Sabra, S. A.; Sheweita, S. A.; Haroun, M.; Ragab, D.; Eldemellawy, M. A.; Xia, Y.; Goodale, D.; Allan, A. L.; Elzoghby, A. O.; Rohani, S. Magnetically Guided Self-Assembled Protein Micelles for Enhanced Delivery of Dasatinib to Human Triple-Negative Breast Cancer Cells. *Journal of Pharmaceutical Sciences* **2019**, *108* (5), 1713–1725. https://doi.org/10.1016/j.xphs.2018.11.044.

(63) Esfahani, M. K. M.; Alavi, S. E.; Movahedi, F.; Alavi, F.; Akbarzadeh, A. Cytotoxicity of Liposomal Paclitaxel in Breast Cancer Cell Line MCF-7. *Indian J Clin Biochem* **2013**, *28* (4), 358–360. https://doi.org/10.1007/s12291-013-0296-1.

(64) Anders, C. K.; Adamo, B.; Karginova, O.; Deal, A. M.; Rawal, S.; Darr, D.; Schorzman, A.; Santos, C.; Bash, R.; Kafri, T.; Carey, L.; Miller, C. R.; Perou, C. M.; Sharpless, N.; Zamboni, W. C. Pharmacokinetics and Efficacy of PEGylated Liposomal Doxorubicin in an Intracranial Model of Breast Cancer. *PLoS One* **2013**, *8* (5). https://doi.org/10.1371/journal.pone.0061359.

(65) Raju, A.; Muthu, M. S.; Feng, S.-S. Trastuzumab-Conjugated Vitamin E TPGS Liposomes for Sustained and Targeted Delivery of Docetaxel. *Expert Opin Drug Deliv* **2013**, *10* (6), 747–760. https://doi.org/10.1517/17425247.2013.777425.

(66) Xu, J.; Zhao, Q.; Jin, Y.; Qiu, L. High Loading of Hydrophilic/Hydrophobic Doxorubicin into Polyphosphazene Polymersome for Breast Cancer Therapy. *Nanomedicine: Nanotechnology, Biology and Medicine* **2014**, *10* (2), 349–358. https://doi.org/10.1016/j.nano.2013.08.004.

(67) Gomari, H.; Forouzandeh Moghadam, M.; Soleimani, M. Targeted Cancer Therapy Using Engineered Exosome as a Natural Drug Delivery Vehicle. *Onco Targets Ther* **2018**, *11*, 5753–5762. https://doi.org/10.2147/OTT.S173110.

(68) Teixeira, R. A. R.; Lataliza, A. A. B.; Raposo, N. R. B.; Costa, L. A. S.; Sant'Ana, A. C. Insights on the Transport of Tamoxifen by Gold Nanoparticles for MCF-7 Breast Cancer Cells Based on SERS Spectroscopy. *Colloids and Surfaces B: Biointerfaces* **2018**, *170*, 712–717. https://doi.org/10.1016/j.colsurfb.2018.07.001.

(69) François, A.; Laroche, A.; Pinaud, N.; Salmon, L.; Ruiz, J.; Robert, J.; Astruc, D. Encapsulation of Docetaxel into PEGylated Gold Nanoparticles for Vectorization to Cancer Cells. *ChemMedChem* **2011**, *6* (11), 2003–2008. https://doi.org/10.1002/cmdc.201100311.

(70) Licciardi, M.; Li Volsi, A.; Mauro, N.; Scialabba, C.; Cavallaro, G.; Giammona, G. Preparation and Characterization of Inulin Coated Gold Nanoparticles for Selective Delivery of Doxorubicin to Breast Cancer Cells https://www.hindawi.com/journals/jnm/2016/2078315/ (accessed Dec 13, 2020). https://doi.org/10.1155/2016/2078315.

(71) Marcu, A.; Pop, S.; Dumitrache, F.; Mocanu, M.; Niculite, C. M.; Gherghiceanu, M.; Lungu, C. P.; Fleaca, C.; Ianchis, R.; Barbut, A.; Grigoriu, C.; Morjan, I. Magnetic Iron Oxide Nanoparticles as Drug Delivery System in Breast Cancer. *Applied Surface Science* **2013**, *281*, 60–65. https://doi.org/10.1016/j.apsusc.2013.02.072.

(72) Kossatz, S.; Grandke, J.; Couleaud, P.; Latorre, A.; Aires, A.; Crosbie-Staunton, K.; Ludwig, R.; Dähring, H.; Ettelt, V.; Lazaro-Carrillo, A.; Calero, M.; Sader, M.; Courty, J.; Volkov, Y.; Prina-Mello, A.; Villanueva, A.; Somoza, Á.; Cortajarena, A. L.; Miranda, R.; Hilger, I. Efficient Treatment of Breast Cancer Xenografts with Multifunctionalized Iron Oxide Nanoparticles Combining Magnetic Hyperthermia and Anti-Cancer Drug Delivery. *Breast Cancer Res* **2015**, *17* (1). https://doi.org/10.1186/s13058-015-0576-1.

(73) Nifontova, G.; Ramos-Gomes, F.; Baryshnikova, M.; Alves, F.; Nabiev, I.; Sukhanova, A. Cancer Cell Targeting With Functionalized Quantum Dot-Encoded Polyelectrolyte Microcapsules. *Front. Chem.* **2019**, *7*. https://doi.org/10.3389/fchem.2019.00034.

(74) Meng, H.; Mai, W. X.; Zhang, H.; Xue, M.; Xia, T.; Lin, S.; Wang, X.; Zhao, Y.; Ji, Z.; Zink, J. I.; Nel, A. E. Codelivery of an Optimal Drug/SiRNA Combination Using Mesoporous Silica Nanoparticles To Overcome Drug Resistance in Breast Cancer in Vitro and in Vivo. *ACS Nano* **2013**, *7* (2), 994–1005. https://doi.org/10.1021/nn3044066.

(75) Raza, K.; Thotakura, N.; Kumar, P.; Joshi, M.; Bhushan, S.; Bhatia, A.; Kumar, V.; Malik, R.; Sharma, G.; Guru, S. K.; Katare, O. P. C60-Fullerenes for Delivery of Docetaxel to Breast Cancer Cells: A Promising Approach for Enhanced Efficacy and Better Pharmacokinetic Profile. *International Journal of Pharmaceutics* **2015**, *495* (1), 551–559. https://doi.org/10.1016/j.ijpharm.2015.09.016.

(76) Al Faraj, A.; Shaik, A. P.; Shaik, A. S. Magnetic Single-Walled Carbon Nanotubes as Efficient Drug Delivery Nanocarriers in Breast Cancer Murine Model: Noninvasive Monitoring Using Diffusion-Weighted Magnetic Resonance Imaging as Sensitive Imaging Biomarker. *Int J Nanomedicine* **2014**, *10*, 157–168. https://doi.org/10.2147/IJN.S75074.

(77) Feng, T.; Ai, X.; Ong, H.; Zhao, Y. Dual-Responsive Carbon Dots for Tumor Extracellular Microenvironment Triggered Targeting and Enhanced Anticancer Drug Delivery. *ACS Appl. Mater. Interfaces* **2016**, *8* (29), 18732–18740. https://doi.org/10.1021/acsami.6b06695.

(78) Esfandiari, N.; Arzanani, M. K.; Soleimani, M.; Kohi-Habibi, M.; Svendsen, W. E. A New Application of Plant Virus Nanoparticles as Drug Delivery in Breast Cancer. *Tumor Biol.* **2016**, *37* (1), 1229–1236. https://doi.org/10.1007/s13277-015-3867-3.

(79) Le, D. H. T.; Lee, K. L.; Shukla, S.; Commandeur, U.; Steinmetz, N. F. Potato Virus X, a Filamentous Plant Viral Nanoparticle for Doxorubicin Delivery in Cancer Therapy. *Nanoscale* **2017**, *9* (6), 2348–2357. https://doi.org/10.1039/c6nr09099k.

(80) Guney Eskiler, G.; Cecener, G.; Dikmen, G.; Egeli, U.; Tunca, B. Solid Lipid Nanoparticles: Reversal of Tamoxifen Resistance in Breast Cancer. *European Journal of Pharmaceutical Sciences* **2018**, *120*, 73–88. https://doi.org/10.1016/j.ejps.2018.04.040.

(81) Xu, W.; Bae, E. J.; Lee, M.-K. Enhanced anticancer activity and intracellular uptake of paclitaxel-containing solid lipid nanoparticles in multidrug-resistant breast cancer cells https://www.dovepress.com/enhanced-anticancer-activity-and-intracellular-uptake-of-paclitaxel-co-peer-reviewed-fulltext-article-IJN (accessed Dec 13, 2020). https://doi.org/10.2147/IJN.S182621.

(82) Yuan, Q.; Han, J.; Cong, W.; Ge, Y.; Ma, D.; Dai, Z.; Li, Y.; Bi, X. Docetaxel-loaded solid lipid nanoparticles suppress breast cancer cells growth with reduced myelosuppression toxicity https://www.dovepress.com/docetaxel-loaded-solid-lipid-

nanoparticles-suppress-breast-cancer-cell-peer-reviewed-fulltext-article-IJN (accessed Dec 13, 2020).
(83) Kang, K. W.; Chun, M.-K.; Kim, O.; Subedi, R. K.; Ahn, S.-G.; Yoon, J.-H.; Choi, H.-K. Doxorubicin-Loaded Solid Lipid Nanoparticles to Overcome Multidrug Resistance in Cancer Therapy. *Nanomedicine: Nanotechnology, Biology and Medicine* **2010**, *6* (2), 210–213. https://doi.org/10.1016/j.nano.2009.12.006.
(84) Meng, F.; Zhong, Z. Polymersomes Spanning from Nano- to Microscales: Advanced Vehicles for Controlled Drug Delivery and Robust Vesicles for Virus and Cell Mimicking. *J. Phys. Chem. Lett.* **2011**, *2* (13), 1533–1539. https://doi.org/10.1021/jz200007h.
(85) Christian, D. A.; Cai, S.; Bowen, D. M.; Kim, Y.; Pajerowski, J. D.; Discher, D. E. Polymersome Carriers: From Self-Assembly to SiRNA and Protein Therapeutics. *European Journal of Pharmaceutics and Biopharmaceutics* **2009**, *71* (3), 463–474. https://doi.org/10.1016/j.ejpb.2008.09.025.
(86) Discher, D. E.; Ahmed, F. Polymersomes. *Annu. Rev. Biomed. Eng.* **2006**, *8* (1), 323–341. https://doi.org/10.1146/annurev.bioeng.8.061505.095838.
(87) Won, Y.-Y.; Brannan, A. K.; Davis, H. T.; Bates, F. S. Cryogenic Transmission Electron Microscopy (Cryo-TEM) of Micelles and Vesicles Formed in Water by Poly(Ethylene Oxide)-Based Block Copolymers. *J. Phys. Chem. B* **2002**, *106* (13), 3354–3364. https://doi.org/10.1021/jp013639d.
(88) Meng, F.; Engbers, G. H. M.; Gessner, A.; Müller, R. H.; Feijen, J. Pegylated Polystyrene Particles as a Model System for Artificial Cells. *Journal of Biomedical Materials Research Part A* **2004**, *70A* (1), 97–106. https://doi.org/10.1002/jbm.a.30068.
(89) Du, J.; O'Reilly, R. K. Advances and Challenges in Smart and Functional Polymer Vesicles. *Soft Matter* **2009**, *5* (19), 3544–3561. https://doi.org/10.1039/B905635A.
(90) Luo, L.; Eisenberg, A. Thermodynamic Stabilization Mechanism of Block Copolymer Vesicles. *J. Am. Chem. Soc.* **2001**, *123* (5), 1012–1013. https://doi.org/10.1021/ja005824v.
(91) Kita-Tokarczyk, K.; Grumelard, J.; Haefele, T.; Meier, W. Block Copolymer Vesicles—Using Concepts from Polymer Chemistry to Mimic Biomembranes. *Polymer* **2005**, *46* (11), 3540–3563. https://doi.org/10.1016/j.polymer.2005.02.083.
(92) Lee, J. S.; Feijen, J. Polymersomes for Drug Delivery: Design, Formation and Characterization. *Journal of Controlled Release* **2012**, *161* (2), 473–483. https://doi.org/10.1016/j.jconrel.2011.10.005.
(93) Kukula, H.; Schlaad, H.; Antonietti, M.; Förster, S. The Formation of Polymer Vesicles or "Peptosomes" by Polybutadiene-Block-Poly(l-Glutamate)s in Dilute Aqueous Solution. *J. Am. Chem. Soc.* **2002**, *124* (8), 1658–1663. https://doi.org/10.1021/ja0120911.
(94) Shen, H.; Eisenberg, A. Morphological Phase Diagram for a Ternary System of Block Copolymer PS310-b-PAA52/Dioxane/H2O. *J. Phys. Chem. B* **1999**, *103* (44), 9473–9487. https://doi.org/10.1021/jp991365c.
(95) Lee, J. S.; Ankone, M.; Pieters, E.; Schiffelers, R. M.; Hennink, W. E.; Feijen, J. Circulation Kinetics and Biodistribution of Dual-Labeled Polymersomes with Modulated Surface Charge in Tumor-Bearing Mice: Comparison with Stealth Liposomes. *Journal of Controlled Release* **2011**, *155* (2), 282–288. https://doi.org/10.1016/j.jconrel.2011.07.028.

(96) Nardin, C.; Hirt, T.; Leukel, J.; Meier, W. Polymerized ABA Triblock Copolymer Vesicles. *Langmuir* **2000**, *16* (3), 1035–1041. https://doi.org/10.1021/la990951u.
(97) Meng, F.; Hiemstra, C.; Engbers, G. H. M.; Feijen, J. Biodegradable Polymersomes. *Macromolecules* **2003**, *36* (9), 3004–3006. https://doi.org/10.1021/ma034040+.
(98) Patel, D. V.; McGhee, C. N. Contemporary in Vivo Confocal Microscopy of the Living Human Cornea Using White Light and Laser Scanning Techniques: A Major Review. *Clinical & Experimental Ophthalmology* **2007**, *35* (1), 71–88. https://doi.org/10.1111/j.1442-9071.2007.01423.x.
(99) Habel, J.; Ogbonna, A.; Larsen, N.; Cherré, S.; Kynde, S.; Midtgaard, S. R.; Kinoshita, K.; Krabbe, S.; Jensen, G. V.; Hansen, J. S.; Almdal, K.; Hèlix-Nielsen, C. Selecting Analytical Tools for Characterization of Polymersomes in Aqueous Solution. *RSC Adv.* **2015**, *5* (97), 79924–79946. https://doi.org/10.1039/C5RA16403F.
(100) Battaglia, G.; Ryan, A. J. Bilayers and Interdigitation in Block Copolymer Vesicles. *J. Am. Chem. Soc.* **2005**, *127* (24), 8757–8764. https://doi.org/10.1021/ja050742y.
(101) Stoenescu, R.; Graff, A.; Meier, W. Asymmetric ABC-Triblock Copolymer Membranes Induce a Directed Insertion of Membrane Proteins. *Macromolecular Bioscience* **2004**, *4* (10), 930–935. https://doi.org/10.1002/mabi.200400065.
(102) Mayer, L. D.; Bally, M. B.; Cullis, P. R. Uptake of Adriamycin into Large Unilamellar Vesicles in Response to a PH Gradient. *Biochimica et Biophysica Acta (BBA) - Biomembranes* **1986**, *857* (1), 123–126. https://doi.org/10.1016/0005-2736(86)90105-7.
(103) Matoori, S.; Leroux, J.-C. Twenty-Five Years of Polymersomes: Lost in Translation? *Mater. Horiz.* **2020**, *7* (5), 1297–1309. https://doi.org/10.1039/C9MH01669D.
(104) Mamnoon, B.; Loganathan, J.; Confeld, M. I.; De Fonseka, N.; Feng, L.; Froberg, J.; Choi, Y.; Tuvin, D. M.; Sathish, V.; Mallik, S. Targeted Polymeric Nanoparticles for Drug Delivery to Hypoxic, Triple-Negative Breast Tumors. *ACS Appl. Bio Mater.* **2020**. https://doi.org/10.1021/acsabm.0c01336.
(105) Xu, J.; Zhao, Q.; Jin, Y.; Qiu, L. High Loading of Hydrophilic/Hydrophobic Doxorubicin into Polyphosphazene Polymersome for Breast Cancer Therapy. *Nanomedicine: Nanotechnology, Biology and Medicine* **2014**, *10* (2), 349–358. https://doi.org/10.1016/j.nano.2013.08.004.
(106) Son, Y. J.; Jang, J.-S.; Cho, Y. W.; Chung, H.; Park, R.-W.; Kwon, I. C.; Kim, I.-S.; Park, J. Y.; Seo, S. B.; Park, C. R.; Jeong, S. Y. Biodistribution and Anti-Tumor Efficacy of Doxorubicin Loaded Glycol-Chitosan Nanoaggregates by EPR Effect. *Journal of Controlled Release* **2003**, *91* (1), 135–145. https://doi.org/10.1016/S0168-3659(03)00231-1.
(107) Dos Santos, N.; Cox, K. A.; McKenzie, C. A.; van Baarda, F.; Gallagher, R. C.; Karlsson, G.; Edwards, K.; Mayer, L. D.; Allen, C.; Bally, M. B. PH Gradient Loading of Anthracyclines into Cholesterol-Free Liposomes: Enhancing Drug Loading Rates through Use of Ethanol. *Biochimica et Biophysica Acta (BBA) - Biomembranes* **2004**, *1661* (1), 47–60. https://doi.org/10.1016/j.bbamem.2003.11.016.
(108) Saylor, D. M.; Kim, C.-S.; Patwardhan, D. V.; Warren, J. A. Diffuse-Interface Theory for Structure Formation and Release Behavior in Controlled Drug Release Systems. *Acta Biomaterialia* **2007**, *3* (6), 851–864. https://doi.org/10.1016/j.actbio.2007.03.011.
(109) Siepmann, J.; Faisant, N.; Akiki, J.; Richard, J.; Benoit, J. P. Effect of the Size of Biodegradable Microparticles on Drug Release: Experiment and Theory. *Journal of Controlled Release* **2004**, *96* (1), 123–134. https://doi.org/10.1016/j.jconrel.2004.01.011.

(110) Mecke, A.; Dittrich, C.; Meier, W. Biomimetic Membranes Designed from Amphiphilic Block Copolymers. *Soft Matter* **2006**, *2* (9), 751–759. https://doi.org/10.1039/B605165K.
(111) Hu, X.; Zhang, Y.; Xie, Z.; Jing, X.; Bellotti, A.; Gu, Z. Stimuli-Responsive Polymersomes for Biomedical Applications. *Biomacromolecules* **2017**, *18* (3), 649–673. https://doi.org/10.1021/acs.biomac.6b01704.
(112) Thambi, T.; Park, J. H.; Lee, D. S. Stimuli-Responsive Polymersomes for Cancer Therapy. *Biomater. Sci.* **2015**, *4* (1), 55–69. https://doi.org/10.1039/C5BM00268K.
(113) Babin, J.; Pelletier, M.; Lepage, M.; Allard, J.-F.; Morris, D.; Zhao, Y. A New Two-Photon-Sensitive Block Copolymer Nanocarrier. *Angewandte Chemie International Edition* **2009**, *48* (18), 3329–3332. https://doi.org/10.1002/anie.200900255.
(114) McCarley, R. L. Redox-Responsive Delivery Systems. *Annual Rev. Anal. Chem.* **2012**, *5* (1), 391–411. https://doi.org/10.1146/annurev-anchem-062011-143157.
(115) Liu, J.; Huang, Y.; Kumar, A.; Tan, A.; Jin, S.; Mozhi, A.; Liang, X.-J. PH-Sensitive Nano-Systems for Drug Delivery in Cancer Therapy. *Biotechnology Advances* **2014**, *32* (4), 693–710. https://doi.org/10.1016/j.biotechadv.2013.11.009.
(116) Thambi, T.; Deepagan, V. G.; Yoon, H. Y.; Han, H. S.; Kim, S.-H.; Son, S.; Jo, D.-G.; Ahn, C.-H.; Suh, Y. D.; Kim, K.; Chan Kwon, I.; Lee, D. S.; Park, J. H. Hypoxia-Responsive Polymeric Nanoparticles for Tumor-Targeted Drug Delivery. *Biomaterials* **2014**, *35* (5), 1735–1743. https://doi.org/10.1016/j.biomaterials.2013.11.022.
(117) Kulkarni, P.; Haldar, M. K.; You, S.; Choi, Y.; Mallik, S. Hypoxia-Responsive Polymersomes for Drug Delivery to Hypoxic Pancreatic Cancer Cells. *Biomacromolecules* **2016**, *17* (8), 2507–2513. https://doi.org/10.1021/acs.biomac.6b00350.
(118) Khorsand, B.; Lapointe, G.; Brett, C.; Oh, J. K. Intracellular Drug Delivery Nanocarriers of Glutathione-Responsive Degradable Block Copolymers Having Pendant Disulfide Linkages. *Biomacromolecules* **2013**, *14* (6), 2103–2111. https://doi.org/10.1021/bm4004805.
(119) Liu, G.; Liu, W.; Dong, C.-M. UV- and NIR-Responsive Polymeric Nanomedicines for on-Demand Drug Delivery. *Polym. Chem.* **2013**, *4* (12), 3431–3443. https://doi.org/10.1039/C3PY21121E.
(120) Qin, S.; Geng, Y.; Discher, D. E.; Yang, S. Temperature-Controlled Assembly and Release from Polymer Vesicles of Poly(Ethylene Oxide)-Block- Poly(N-Isopropylacrylamide). *Advanced Materials* **2006**, *18* (21), 2905–2909. https://doi.org/10.1002/adma.200601019.
(121) Oliveira, H.; Pérez-Andrés, E.; Thevenot, J.; Sandre, O.; Berra, E.; Lecommandoux, S. Magnetic Field Triggered Drug Release from Polymersomes for Cancer Therapeutics. *Journal of Controlled Release* **2013**, *169* (3), 165–170. https://doi.org/10.1016/j.jconrel.2013.01.013.
(122) Ding, Y.; Kang, Y.; Zhang, X. Enzyme-Responsive Polymer Assemblies Constructed through Covalent Synthesis and Supramolecular Strategy. *Chem. Commun.* **2014**, *51* (6), 996–1003. https://doi.org/10.1039/C4CC05878J.
(123) Lee, J. S.; Groothuis, T.; Cusan, C.; Mink, D.; Feijen, J. Lysosomally Cleavable Peptide-Containing Polymersomes Modified with Anti-EGFR Antibody for Systemic Cancer Chemotherapy. *Biomaterials* **2011**, *32* (34), 9144–9153. https://doi.org/10.1016/j.biomaterials.2011.08.036.

(124) Yu, J.; Zhang, Y.; Ye, Y.; DiSanto, R.; Sun, W.; Ranson, D.; Ligler, F. S.; Buse, J. B.; Gu, Z. Microneedle-Array Patches Loaded with Hypoxia-Sensitive Vesicles Provide Fast Glucose-Responsive Insulin Delivery. *PNAS* **2015**, *112* (27), 8260–8265. https://doi.org/10.1073/pnas.1505405112.
(125) Cambre, J. N.; Sumerlin, B. S. Biomedical Applications of Boronic Acid Polymers. *Polymer* **2011**, *52* (21), 4631–4643. https://doi.org/10.1016/j.polymer.2011.07.057.
(126) Matsumoto, A.; Ikeda, S.; Harada, A.; Kataoka, K. Glucose-Responsive Polymer Bearing a Novel Phenylborate Derivative as a Glucose-Sensing Moiety Operating at Physiological PH Conditions. *Biomacromolecules* **2003**, *4* (5), 1410–1416. https://doi.org/10.1021/bm034139o.
(127) Attia, M. F.; Anton, N.; Wallyn, J.; Omran, Z.; Vandamme, T. F. An Overview of Active and Passive Targeting Strategies to Improve the Nanocarriers Efficiency to Tumour Sites. *Journal of Pharmacy and Pharmacology* **2019**, *71* (8), 1185–1198. https://doi.org/10.1111/jphp.13098.
(128) Wang, A. Z.; Langer, R.; Farokhzad, O. C. Nanoparticle Delivery of Cancer Drugs. *Annu. Rev. Med.* **2012**, *63* (1), 185–198. https://doi.org/10.1146/annurev-med-040210-162544.
(129) Maeda, H.; Wu, J.; Sawa, T.; Matsumura, Y.; Hori, K. Tumor Vascular Permeability and the EPR Effect in Macromolecular Therapeutics: A Review. *Journal of Controlled Release* **2000**, *65* (1), 271–284. https://doi.org/10.1016/S0168-3659(99)00248-5.
(130) Yoo, J.; Park, C.; Yi, G.; Lee, D.; Koo, H. Active Targeting Strategies Using Biological Ligands for Nanoparticle Drug Delivery Systems. *Cancers (Basel)* **2019**, *11* (5). https://doi.org/10.3390/cancers11050640.
(131) Pourtau, L.; Oliveira, H.; Thevenot, J.; Wan, Y.; Brisson, A. R.; Sandre, O.; Miraux, S.; Thiaudiere, E.; Lecommandoux, S. Antibody-Functionalized Magnetic Polymersomes: In Vivo Targeting and Imaging of Bone Metastases Using High Resolution MRI. *Adv Healthc Mater* **2013**, *2* (11), 1420–1424. https://doi.org/10.1002/adhm.201300061.
(132) Preparation and Brain Delivery Property of Biodegradable Polymersomes Conjugated with OX26. *Journal of Controlled Release* **2008**, *128* (2), 120–127. https://doi.org/10.1016/j.jconrel.2008.03.007.
(133) Demirgöz, D.; O. Pangburn, T.; P. Davis, K.; Lee, S.; S. Bates, F.; Kokkoli, E. PR_b-Targeted Delivery of Tumor Necrosis Factor-α by Polymersomes for the Treatment of Prostate Cancer. *Soft Matter* **2009**, *5* (10), 2011–2019. https://doi.org/10.1039/B814217C.
(134) Farokhzad, O. C.; Cheng, J.; Teply, B. A.; Sherifi, I.; Jon, S.; Kantoff, P. W.; Richie, J. P.; Langer, R. Targeted Nanoparticle-Aptamer Bioconjugates for Cancer Chemotherapy in Vivo. *PNAS* **2006**, *103* (16), 6315–6320. https://doi.org/10.1073/pnas.0601755103.
(135) Yassin, M. A.; Appelhans, D.; Wiedemuth, R.; Formanek, P.; Boye, S.; Lederer, A.; Temme, A.; Voit, B. Overcoming Concealment Effects of Targeting Moieties in the PEG Corona: Controlled Permeable Polymersomes Decorated with Folate-Antennae for Selective Targeting of Tumor Cells. *Small* **2015**, *11* (13), 1580–1591. https://doi.org/10.1002/smll.201402581.
(136) Yang, Y.; Zhang, Y.-M.; Chen, Y.; Chen, J.-T.; Liu, Y. Targeted Polysaccharide Nanoparticle for Adamplatin Prodrug Delivery. *J. Med. Chem.* **2013**, *56* (23), 9725–9736. https://doi.org/10.1021/jm4014168.

(137) Awasthi, V. D.; Garcia, D.; Klipper, R.; Goins, B. A.; Phillips, W. T. Neutral and Anionic Liposome-Encapsulated Hemoglobin: Effect of Postinserted Poly(Ethylene Glycol)-Distearoylphosphatidylethanolamine on Distribution and Circulation Kinetics. *J Pharmacol Exp Ther* **2004**, *309* (1), 241–248. https://doi.org/10.1124/jpet.103.060228.
(138) The Role of Surface Charge and Hydrophilic Groups on Liposome Clearance in Vivo. *Biochimica et Biophysica Acta (BBA) - Biomembranes* **1992**, *1103* (1), 94–100. https://doi.org/10.1016/0005-2736(92)90061-P.
(139) Long Circulating Microparticulate Drug Carriers. *Advanced Drug Delivery Reviews* **1995**, *16* (2–3), 195–214. https://doi.org/10.1016/0169-409X(95)00025-3.
(140) Polymer Vesicles in Vivo: Correlations with PEG Molecular Weight. *Journal of Controlled Release* **2003**, *90* (3), 323–334. https://doi.org/10.1016/S0168-3659(03)00201-3.
(141) Long-Circulating Poly(Ethylene Glycol)–Poly(d,l-Lactide) Block Copolymer Micelles with Modulated Surface Charge. *Journal of Controlled Release* **2001**, *77* (1–2), 27–38. https://doi.org/10.1016/S0168-3659(01)00451-5.
(142) Effects of Positive Charge Density on the Liposomal Surface on Disposition Kinetics of Liposomes in Rats. *International Journal of Pharmaceutics* **1997**, *156* (2), 163–174. https://doi.org/10.1016/S0378-5173(97)00184-1.
(143) An Investigation of the Filtration Capacity and the Fate of Large Filtered Sterically-Stabilized Microspheres in Rat Spleen. *Biochimica et Biophysica Acta (BBA) - General Subjects* **1993**, *1157* (2), 233–240. https://doi.org/10.1016/0304-4165(93)90105-H.
(144) Effect of Liposome Size on the Circulation Time and Intraorgan Distribution of Amphipathic Poly(Ethylene Glycol)-Containing Liposomes. *Biochimica et Biophysica Acta (BBA) - Biomembranes* **1994**, *1190* (1), 99–107. https://doi.org/10.1016/0005-2736(94)90038-8.
(145) Ayen, W. Y.; Kumar, N. In Vivo Evaluation of Doxorubicin-Loaded (PEG)3-PLA Nanopolymersomes (PolyDoxSome) Using DMBA-Induced Mammary Carcinoma Rat Model and Comparison with Marketed LipoDox™. *Pharm Res* **2012**, *29* (9), 2522–2533. https://doi.org/10.1007/s11095-012-0783-8.
(146) Au, J. L.-S.; Jang, S. H.; Wientjes, M. G. Clinical Aspects of Drug Delivery to Tumors. *Journal of Controlled Release* **2002**, *78* (1), 81–95. https://doi.org/10.1016/S0168-3659(01)00488-6.
(147) Gabizon, A. A. Pegylated Liposomal Doxorubicin: Metamorphosis of an Old Drug into a New Form of Chemotherapy. *Cancer Investigation* **2001**, *19* (4), 424–436. https://doi.org/10.1081/CNV-100103136.
(148) Mordente, A.; Meucci, E.; Silvestrini, A.; Martorana, G. E.; Giardina, B. New Developments in Anthracycline-Induced Cardiotoxicity. *Curr Med Chem* **2009**, *16* (13), 1656–1672. https://doi.org/10.2174/092986709788186228.
(149) Minotti, G. Reactions of Adriamycin with Microsomal Iron and Lipids. *Free Radic Res Commun* **1989**, *7* (3–6), 143–148. https://doi.org/10.3109/10715768909087936.
(150) Licata, S.; Saponiero, A.; Mordente, A.; Minotti, G. Doxorubicin Metabolism and Toxicity in Human Myocardium: Role of Cytoplasmic Deglycosidation and Carbonyl Reduction. *Chem. Res. Toxicol.* **2000**, *13* (5), 414–420. https://doi.org/10.1021/tx000013q.

(151) Wilkinson, P. M.; Israel, M.; Pegg, W. J.; Frei, E. Comparative Metabolism and Excretion of Adriamycin in Man, Monkey, and Rat. *Cancer Chemother. Pharmacol.* **1979**, *2* (2), 121–125. https://doi.org/10.1007/BF00254084.
(152) Speth, P. A. J.; van Hoesel, Q. G. C. M.; Haanen, C. Clinical Pharmacokinetics of Doxorubicin. *Clin-Pharmacokinet* **1988**, *15* (1), 15–31. https://doi.org/10.2165/00003088-198815010-00002.
(153) Pérez-Blanco, J. S.; Santos-Buelga, D.; Gatta, M. del M. F. de; Hernández-Rivas, J. M.; Martín, A.; García, M. J. Population Pharmacokinetics of Doxorubicin and Doxorubicinol in Patients Diagnosed with Non-Hodgkin's Lymphoma. *British Journal of Clinical Pharmacology* **2016**, *82* (6), 1517–1527. https://doi.org/10.1111/bcp.13070.
(154) Benjamin, R. S.; Riggs, C. E.; Bachur, N. R. Plasma Pharmacokinetics of Adriamycin and Its Metabolites in Humans with Normal Hepatic and Renal Function. *Cancer Res* **1977**, *37* (5), 1416–1420.
(155) Pippa, L. F.; Oliveira, M. L. de; Rocha, A.; de Andrade, J. M.; Lanchote, V. L. Total, Renal and Hepatic Clearances of Doxorubicin and Formation Clearance of Doxorubicinol in Patients with Breast Cancer: Estimation of Doxorubicin Hepatic Extraction Ratio. *Journal of Pharmaceutical and Biomedical Analysis* **2020**, *185*, 113231. https://doi.org/10.1016/j.jpba.2020.113231.
(156) Hoffmann, M.; Bergner, R.; Stützle, M.; Uppenkamp, M. J.; Foerster, R. Pharmacokinetics of Doxorubicin In Normal Weight and Obese Lymphoma Patients. *Blood* **2010**, *116* (21), 4935–4935. https://doi.org/10.1182/blood.V116.21.4935.4935.
(157) DeSantis, C. E.; Ma, J.; Gaudet, M. M.; Newman, L. A.; Miller, K. D.; Sauer, A. G.; Jemal, A.; Siegel, R. L. Breast Cancer Statistics, 2019. *CA: A Cancer Journal for Clinicians* **2019**, *69* (6), 438–451. https://doi.org/10.3322/caac.21583.
(158) Sørlie, T.; Perou, C. M.; Tibshirani, R.; Aas, T.; Geisler, S.; Johnsen, H.; Hastie, T.; Eisen, M. B.; van de Rijn, M.; Jeffrey, S. S.; Thorsen, T.; Quist, H.; Matese, J. C.; Brown, P. O.; Botstein, D.; Lønning, P. E.; Børresen-Dale, A.-L. Gene Expression Patterns of Breast Carcinomas Distinguish Tumor Subclasses with Clinical Implications. *Proc Natl Acad Sci U S A* **2001**, *98* (19), 10869–10874. https://doi.org/10.1073/pnas.191367098.
(159) Dai, X.; Li, T.; Bai, Z.; Yang, Y.; Liu, X.; Zhan, J.; Shi, B. Breast Cancer Intrinsic Subtype Classification, Clinical Use and Future Trends. *Am J Cancer Res* **2015**, *5* (10), 2929–2943.
(160) Street, W. Breast Cancer Facts & Figures 2019-2020. 44.
(161) Brinkhuis, R. P.; Rutjes, F. P. J. T.; Hest, J. C. M. van. Polymeric Vesicles in Biomedical Applications. *Polym. Chem.* **2011**, *2* (7), 1449–1462. https://doi.org/10.1039/C1PY00061F.
(162) Discher, B. M.; Won, Y.-Y.; Ege, D. S.; Lee, J. C.-M.; Bates, F. S.; Discher, D. E.; Hammer, D. A. Polymersomes: Tough Vesicles Made from Diblock Copolymers. *Science* **1999**, *284* (5417), 1143–1146. https://doi.org/10.1126/science.284.5417.1143.
(163) Confeld, M. I.; Mamnoon, B.; Feng, L.; Jensen-Smith, H.; Ray, P.; Froberg, J.; Kim, J.; Hollingsworth, M. A.; Quadir, M.; Choi, Y.; Mallik, S. Targeting the Tumor Core: Hypoxia-Responsive Nanoparticles for Delivery of Chemotherapy to Pancreatic Tumors. *Mol. Pharm.* **2020**. https://doi.org/10.1021/acs.molpharmaceut.0c00247.

(164) Chen, W.; Meng, F.; Cheng, R.; Zhong, Z. PH-Sensitive Degradable Polymersomes for Triggered Release of Anticancer Drugs: A Comparative Study with Micelles. *Journal of Controlled Release* **2010**, *142* (1), 40–46. https://doi.org/10.1016/j.jconrel.2009.09.023.
(165) Lomas, H.; Canton, I.; MacNeil, S.; Du, J.; Armes, S. P.; Ryan, A. J.; Lewis, A. L.; Battaglia, G. Biomimetic PH Sensitive Polymersomes for Efficient DNA Encapsulation and Delivery. *Advanced Materials* **2007**, *19* (23), 4238–4243. https://doi.org/10.1002/adma.200700941.
(166) Nahire, R.; Haldar, M. K.; Paul, S.; Ambre, A. H.; Meghnani, V.; Layek, B.; Katti, K. S.; Gange, K. N.; Singh, J.; Sarkar, K.; Mallik, S. Multifunctional Polymersomes for Cytosolic Delivery of Gemcitabine and Doxorubicin to Cancer Cells. *Biomaterials* **2014**, *35* (24), 6482–6497. https://doi.org/10.1016/j.biomaterials.2014.04.026.
(167) Karandish, F.; Mamnoon, B.; Feng, L.; Haldar, M. K.; Xia, L.; Gange, K. N.; You, S.; Choi, Y.; Sarkar, K.; Mallik, S. Nucleus-Targeted, Echogenic Polymersomes for Delivering a Cancer Stemness Inhibitor to Pancreatic Cancer Cells. *Biomacromolecules* **2018**, *19* (10), 4122–4132. https://doi.org/10.1021/acs.biomac.8b01133.
(168) Christian, D. A.; Cai, S.; Bowen, D. M.; Kim, Y.; Pajerowski, J. D.; Discher, D. E. Polymersome Carriers: From Self-Assembly to SiRNA and Protein Therapeutics. *European Journal of Pharmaceutics and Biopharmaceutics* **2009**, *71* (3), 463–474. https://doi.org/10.1016/j.ejpb.2008.09.025.
(169) Anajafi, T.; Mallik, S. Polymersome-Based Drug-Delivery Strategies for Cancer Therapeutics. *Ther Deliv* **2015**, *6* (4), 521–534. https://doi.org/10.4155/tde.14.125.
(170) Lee, J. S.; Feijen, J. Polymersomes for Drug Delivery: Design, Formation and Characterization. *Journal of Controlled Release* **2012**, *161* (2), 473–483. https://doi.org/10.1016/j.jconrel.2011.10.005.
(171) Liu, G.; Ma, S.; Li, S.; Cheng, R.; Meng, F.; Liu, H.; Zhong, Z. The Highly Efficient Delivery of Exogenous Proteins into Cells Mediated by Biodegradable Chimaeric Polymersomes. *Biomaterials* **2010**, *31* (29), 7575–7585. https://doi.org/10.1016/j.biomaterials.2010.06.021.
(172) Ahmed, F.; Pakunlu, R. I.; Brannan, A.; Bates, F.; Minko, T.; Discher, D. E. Biodegradable Polymersomes Loaded with Both Paclitaxel and Doxorubicin Permeate and Shrink Tumors, Inducing Apoptosis in Proportion to Accumulated Drug. *Journal of Controlled Release* **2006**, *116* (2), 150–158. https://doi.org/10.1016/j.jconrel.2006.07.012.
(173) Photos, P. J.; Bacakova, L.; Discher, B.; Bates, F. S.; Discher, D. E. Polymer Vesicles in Vivo: Correlations with PEG Molecular Weight. *Journal of Controlled Release* **2003**, *90* (3), 323–334. https://doi.org/10.1016/S0168-3659(03)00201-3.
(174) Yotnda, P.; Wu, D.; Swanson, A. M. Hypoxic Tumors and Their Effect on Immune Cells and Cancer Therapy. In *Immunotherapy of Cancer: Methods and Protocols*; Yotnda, P., Ed.; Methods in Molecular Biology; Humana Press: Totowa, NJ, 2010; pp 1–29. https://doi.org/10.1007/978-1-60761-786-0_1.
(175) Lu, X.; Kang, Y. Hypoxia and Hypoxia-Inducible Factors: Master Regulators of Metastasis. *Clin Cancer Res* **2010**, *16* (24), 5928–5935. https://doi.org/10.1158/1078-0432.CCR-10-1360.
(176) Wilson, W. R.; Hay, M. P. Targeting Hypoxia in Cancer Therapy. *Nat Rev Cancer* **2011**, *11* (6), 393–410. https://doi.org/10.1038/nrc3064.

(177) Ding, Y.; Kang, Y.; Zhang, X. Enzyme-Responsive Polymer Assemblies Constructed through Covalent Synthesis and Supramolecular Strategy. *Chem. Commun.* **2014**, *51* (6), 996–1003. https://doi.org/10.1039/C4CC05878J.
(178) Kulkarni, P.; Haldar, M. K.; You, S.; Choi, Y.; Mallik, S. Hypoxia-Responsive Polymersomes for Drug Delivery to Hypoxic Pancreatic Cancer Cells. *Biomacromolecules* **2016**, *17* (8), 2507–2513. https://doi.org/10.1021/acs.biomac.6b00350.
(179) Liu, J.; Huang, Y.; Kumar, A.; Tan, A.; Jin, S.; Mozhi, A.; Liang, X.-J. PH-Sensitive Nano-Systems for Drug Delivery in Cancer Therapy. *Biotechnology Advances* **2014**, *32* (4), 693–710. https://doi.org/10.1016/j.biotechadv.2013.11.009.
(180) Karandish, F.; Froberg, J.; Borowicz, P.; Wilkinson, J. C.; Choi, Y.; Mallik, S. Peptide-Targeted, Stimuli-Responsive Polymersomes for Delivering a Cancer Stemness Inhibitor to Cancer Stem Cell Microtumors. *Colloids and Surfaces B: Biointerfaces* **2018**, *163*, 225–235. https://doi.org/10.1016/j.colsurfb.2017.12.036.
(181) Thambi, T.; Park, J. H.; Lee, D. S. Stimuli-Responsive Polymersomes for Cancer Therapy. *Biomater. Sci.* **2015**, *4* (1), 55–69. https://doi.org/10.1039/C5BM00268K.
(182) Vaupel, P.; Höckel, M.; Mayer, A. Detection and Characterization of Tumor Hypoxia Using PO2 Histography. *Antioxid. Redox Signal.* **2007**, *9* (8), 1221–1235. https://doi.org/10.1089/ars.2007.1628.
(183) Mechanisms for estrogen receptor expression in human cancer | Experimental Hematology & Oncology | Full Text https://ehoonline.biomedcentral.com/articles/10.1186/s40164-018-0116-7 (accessed Jan 11, 2020).
(184) Estrogen synthesis and signaling pathways during aging: from periphery to brain - ScienceDirect https://www.sciencedirect.com/science/article/pii/S1471491412002444?via%3Dihub (accessed Jan 11, 2020).
(185) Differential expression of estrogen receptor α, β1, and β2 in lobular and ductal breast cancer | PNAS https://www.pnas.org/content/111/5/1933 (accessed Jan 11, 2020).
(186) Estrogen-Anchored pH-Sensitive Liposomes as Nanomodule Designed for Site-Specific Delivery of Doxorubicin in Breast Cancer Therapy | Molecular Pharmaceutics https://pubs.acs.org/doi/full/10.1021/mp200439z (accessed Jan 11, 2020).
(187) Estrogen-functionalized liposomes grafted with glutathione-responsive sheddable chotooligosaccharides for the therapy of osteosarcoma: Drug Delivery: Vol 25, No 1 https://www.tandfonline.com/doi/full/10.1080/10717544.2018.1458920 (accessed Jan 11, 2020).
(188) 17β-Estradiol-Associated Stealth-Liposomal Delivery of Anticancer Gene to Breast Cancer Cells - Reddy - 2005 - Angewandte Chemie International Edition - Wiley Online Library https://onlinelibrary.wiley.com/doi/full/10.1002/anie.200501793 (accessed Jan 11, 2020).
(189) Chevalier, A.; Piao, W.; Hanaoka, K.; Nagano, T.; Renard, P.-Y.; Romieu, A. Azobenzene-Caged Sulforhodamine Dyes: A Novel Class of `turn-on' Reactive Probes for Hypoxic Tumor Cell Imaging. *Methods Appl. Fluoresc.* **2015**, *3* (4), 044004. https://doi.org/10.1088/2050-6120/3/4/044004.
(190) Letchford, K.; Burt, H. A Review of the Formation and Classification of Amphiphilic Block Copolymer Nanoparticulate Structures: Micelles, Nanospheres, Nanocapsules and

Polymersomes. *European Journal of Pharmaceutics and Biopharmaceutics* **2007**, *65* (3), 259–269. https://doi.org/10.1016/j.ejpb.2006.11.009.
(191) Discher, B. M.; Won, Y.-Y.; Ege, D. S.; Lee, J. C.-M.; Bates, F. S.; Discher, D. E.; Hammer, D. A. Polymersomes: Tough Vesicles Made from Diblock Copolymers. *Science* **1999**, *284* (5417), 1143–1146. https://doi.org/10.1126/science.284.5417.1143.
(192) Patel, A.; Sant, S. Hypoxic Tumor Microenvironment: Opportunities to Develop Targeted Therapies. *Biotechnol Adv* **2016**, *34* (5), 803–812. https://doi.org/10.1016/j.biotechadv.2016.04.005.
(193) Kiyose, K.; Hanaoka, K.; Oushiki, D.; Nakamura, T.; Kajimura, M.; Suematsu, M.; Nishimatsu, H.; Yamane, T.; Terai, T.; Hirata, Y.; Nagano, T. Hypoxia-Sensitive Fluorescent Probes for in Vivo Real-Time Fluorescence Imaging of Acute Ischemia. *J. Am. Chem. Soc.* **2010**, *132* (45), 15846–15848. https://doi.org/10.1021/ja105937q.
(194) Zbaida, S.; Levine, W. G. A Novel Application of Cyclic Voltammetry for Direct Investigation of Metabolic Intermediates in Microsomal Azo Reduction. *Chem. Res. Toxicol.* **1991**, *4* (1), 82–88. https://doi.org/10.1021/tx00019a011.
(195) Confeld, M. I.; Mamnoon, B.; Feng, L.; Jensen-Smith, H.; Ray, P.; Froberg, J.; Kim, J.; Hollingsworth, M. A.; Quadir, M.; Choi, Y.; Mallik, S. Targeting the Tumor Core: Hypoxia-Responsive Nanoparticles for the Delivery of Chemotherapy to Pancreatic Tumors. *Mol. Pharmaceutics* **2020**, *17* (8), 2849–2863. https://doi.org/10.1021/acs.molpharmaceut.0c00247.
(196) Brownlee, W. J.; Seib, F. P. Impact of the Hypoxic Phenotype on the Uptake and Efflux of Nanoparticles by Human Breast Cancer Cells. *Scientific Reports* **2018**, *8* (1), 12318. https://doi.org/10.1038/s41598-018-30517-3.
(197) Neshatian, M.; Chung, S.; Yohan, D.; Yang, C.; Chithrani, D. B. Determining the Size Dependence of Colloidal Gold Nanoparticle Uptake in a Tumor-like Interface (Hypoxic). *Colloids and Interface Science Communications* **2014**, *1*, 57–61. https://doi.org/10.1016/j.colcom.2014.07.004.
(198) Jain, A. S.; Goel, P. N.; Shah, S. M.; Dhawan, V. V.; Nikam, Y.; Gude, R. P.; Nagarsenker, M. S. Tamoxifen Guided Liposomes for Targeting Encapsulated Anticancer Agent to Estrogen Receptor Positive Breast Cancer Cells: In Vitro and in Vivo Evaluation. *Biomedicine & Pharmacotherapy* **2014**, *68* (4), 429–438. https://doi.org/10.1016/j.biopha.2014.03.004.
(199) Das, R. P.; Gandhi, V. V.; Singh, B. G.; Kunwar, A. Passive and Active Drug Targeting: Role of Nanocarriers in Rational Design of Anticancer Formulations. *CPD* **2019**, *25* (28), 3034–3056. https://doi.org/10.2174/1381612825666190830155319.
(200) Dalmark, M. The Physicochemical Properties and Transmembraneous Transport of Doxorubicin. In *Anthracycline Antibiotics in Cancer Therapy: Proceedings of the International Symposium on Anthracycline Antibiotics in Cancer Therapy, New York, New York, 16–18 September 1981*; Muggia, F. M., Young, C. W., Carter, S. K., Eds.; Developments in Oncology; Springer Netherlands: Dordrecht, 1982; pp 165–172. https://doi.org/10.1007/978-94-009-7630-6_15.
(201) Müller, A.; Homey, B.; Soto, H.; Ge, N.; Catron, D.; Buchanan, M. E.; McClanahan, T.; Murphy, E.; Yuan, W.; Wagner, S. N.; Barrera, J. L.; Mohar, A.; Verástegui, E.; Zlotnik, A. Involvement of Chemokine Receptors in Breast Cancer Metastasis. *Nature* **2001**, *410* (6824), 50–56. https://doi.org/10.1038/35065016.

(202) Pérez-Herrero, E.; Fernández-Medarde, A. Advanced Targeted Therapies in Cancer: Drug Nanocarriers, the Future of Chemotherapy. *European Journal of Pharmaceutics and Biopharmaceutics* **2015**, *93*, 52–79. https://doi.org/10.1016/j.ejpb.2015.03.018.
(203) Keklikoglou, I.; Cianciaruso, C.; Güç, E.; Squadrito, M. L.; Spring, L. M.; Tazzyman, S.; Lambein, L.; Poissonnier, A.; Ferraro, G. B.; Baer, C.; Cassará, A.; Guichard, A.; Iruela-Arispe, M. L.; Lewis, C. E.; Coussens, L. M.; Bardia, A.; Jain, R. K.; Pollard, J. W.; De Palma, M. Chemotherapy Elicits Pro-Metastatic Extracellular Vesicles in Breast Cancer Models. *Nature Cell Biology* **2019**, *21* (2), 190–202. https://doi.org/10.1038/s41556-018-0256-3.
(204) Liu, H.; Lee, J. I.; Ahn, T.-G. Effect of Quercetin on the Anti-Tumor Activity of Cisplatin in EMT6 Breast Tumor-Bearing Mice. *Obstet Gynecol Sci* **2019**, *62* (4), 242–248. https://doi.org/10.5468/ogs.2019.62.4.242.
(205) Vakilinezhad, M. A.; Amini, A.; Dara, T.; Alipour, S. Methotrexate and Curcumin Co-Encapsulated PLGA Nanoparticles as a Potential Breast Cancer Therapeutic System: In Vitro and in Vivo Evaluation. *Colloids and Surfaces B: Biointerfaces* **2019**, *184*, 110515. https://doi.org/10.1016/j.colsurfb.2019.110515.
(206) Cai, F.; Luis, M. A. F.; Lin, X.; Wang, M.; Cai, L.; Cen, C.; Biskup, E. Anthracycline-Induced Cardiotoxicity in the Chemotherapy Treatment of Breast Cancer: Preventive Strategies and Treatment. *Mol Clin Oncol* **2019**, *11* (1), 15–23. https://doi.org/10.3892/mco.2019.1854.
(207) Perumalsamy, H.; Sankarapandian, K.; Kandaswamy, N.; Balusamy, S. R.; Periyathambi, D.; Raveendiran, N. Cellular Effect of Styrene Substituted Biscoumarin Caused Cellular Apoptosis and Cell Cycle Arrest in Human Breast Cancer Cells. *The International Journal of Biochemistry & Cell Biology* **2017**, *92*, 104–114. https://doi.org/10.1016/j.biocel.2017.09.019.
(208) Orive, G.; Hernández, R. M.; Gascón, A. R.; Domínguez-Gil, A.; Pedraz, J. L. Drug Delivery in Biotechnology: Present and Future. *Current Opinion in Biotechnology* **2003**, *14* (6), 659–664. https://doi.org/10.1016/j.copbio.2003.10.007.
(209) Xu, J.; Zhao, Q.; Jin, Y.; Qiu, L. High Loading of Hydrophilic/Hydrophobic Doxorubicin into Polyphosphazene Polymersome for Breast Cancer Therapy. *Nanomedicine: Nanotechnology, Biology and Medicine* **2014**, *10* (2), 349–358. https://doi.org/10.1016/j.nano.2013.08.004.
(210) Confeld, M. I.; Mamnoon, B.; Feng, L.; Jensen-Smith, H.; Ray, P.; Froberg, J.; Kim, J.; Hollingsworth, M. A.; Quadir, M.; Choi, Y.; Mallik, S. Targeting the Tumor Core: Hypoxia-Responsive Nanoparticles for the Delivery of Chemotherapy to Pancreatic Tumors. *Mol. Pharmaceutics* **2020**, *17* (8), 2849–2863. https://doi.org/10.1021/acs.molpharmaceut.0c00247.
(211) Kulkarni, P.; Haldar, M. K.; You, S.; Choi, Y.; Mallik, S. Hypoxia-Responsive Polymersomes for Drug Delivery to Hypoxic Pancreatic Cancer Cells. *Biomacromolecules* **2016**, *17* (8), 2507–2513. https://doi.org/10.1021/acs.biomac.6b00350.
(212) Mamnoon, B.; Feng, L.; Froberg, J.; Choi, Y.; Sathish, V.; Mallik, S. Hypoxia-Responsive, Polymeric Nanocarriers for Targeted Drug Delivery to Estrogen Receptor-Positive Breast Cancer Cell Spheroids. *Mol. Pharmaceutics* **2020**, *17* (11), 4312–4322. https://doi.org/10.1021/acs.molpharmaceut.0c00754.

(213) Thambi, T.; Deepagan, V. G.; Yoon, H. Y.; Han, H. S.; Kim, S.-H.; Son, S.; Jo, D.-G.; Ahn, C.-H.; Suh, Y. D.; Kim, K.; Chan Kwon, I.; Lee, D. S.; Park, J. H. Hypoxia-Responsive Polymeric Nanoparticles for Tumor-Targeted Drug Delivery. *Biomaterials* **2014**, *35* (5), 1735–1743. https://doi.org/10.1016/j.biomaterials.2013.11.022.

(214) Mamnoon, B.; Loganathan, J.; Confeld, M. I.; De Fonseka, N.; Feng, L.; Froberg, J.; Choi, Y.; Tuvin, D. M.; Sathish, V.; Mallik, S. Targeted Polymeric Nanoparticles for Drug Delivery to Hypoxic, Triple-Negative Breast Tumors. *ACS Appl. Bio Mater.* **2020**. https://doi.org/10.1021/acsabm.0c01336.

(215) Wilson, W. R.; Hay, M. P. Targeting Hypoxia in Cancer Therapy. *Nature Reviews Cancer* **2011**, *11* (6), 393–410. https://doi.org/10.1038/nrc3064.

(216) Peer, D.; Karp, J. M.; Hong, S.; Farokhzad, O. C.; Margalit, R.; Langer, R. Nanocarriers as an Emerging Platform for Cancer Therapy. *Nature Nanotechnology* **2007**, *2* (12), 751–760. https://doi.org/10.1038/nnano.2007.387.

(217) Shi, J.; Votruba, A. R.; Farokhzad, O. C.; Langer, R. Nanotechnology in Drug Delivery and Tissue Engineering: From Discovery to Applications. *Nano Lett.* **2010**, *10* (9), 3223–3230. https://doi.org/10.1021/nl102184c.

(218) Kearney, C. J.; Mooney, D. J. Macroscale Delivery Systems for Molecular and Cellular Payloads. *Nature Materials* **2013**, *12* (11), 1004–1017. https://doi.org/10.1038/nmat3758.

(219) Cuenca, A. G.; Jiang, H.; Hochwald, S. N.; Delano, M.; Cance, W. G.; Grobmyer, S. R. Emerging Implications of Nanotechnology on Cancer Diagnostics and Therapeutics. *Cancer* **2006**, *107* (3), 459–466. https://doi.org/10.1002/cncr.22035.

(220) Shi, J.; Kantoff, P. W.; Wooster, R.; Farokhzad, O. C. Cancer Nanomedicine: Progress, Challenges and Opportunities. *Nature Reviews Cancer* **2017**, *17* (1), 20–37. https://doi.org/10.1038/nrc.2016.108.

(221) Davis, M. E.; Chen, Z. (Georgia); Shin, D. M. Nanoparticle Therapeutics: An Emerging Treatment Modality for Cancer. *Nature Reviews Drug Discovery* **2008**, *7* (9), 771–782. https://doi.org/10.1038/nrd2614.

(222) Anajafi, T.; Mallik, S. Polymersome-Based Drug-Delivery Strategies for Cancer Therapeutics. *Ther Deliv* **2015**, *6* (4), 521–534. https://doi.org/10.4155/tde.14.125.

(223) Discher, D. E.; Ahmed, F. Polymersomes. *Annu. Rev. Biomed. Eng.* **2006**, *8* (1), 323–341. https://doi.org/10.1146/annurev.bioeng.8.061505.095838.

(224) Discher, B. M.; Won, Y.-Y.; Ege, D. S.; Lee, J. C.-M.; Bates, F. S.; Discher, D. E.; Hammer, D. A. Polymersomes: Tough Vesicles Made from Diblock Copolymers. *Science* **1999**, *284* (5417), 1143–1146. https://doi.org/10.1126/science.284.5417.1143.

(225) Nahire, R.; Haldar, M. K.; Paul, S.; Ambre, A. H.; Meghnani, V.; Layek, B.; Katti, K. S.; Gange, K. N.; Singh, J.; Sarkar, K.; Mallik, S. Multifunctional Polymersomes for Cytosolic Delivery of Gemcitabine and Doxorubicin to Cancer Cells. *Biomaterials* **2014**, *35* (24), 6482–6497. https://doi.org/10.1016/j.biomaterials.2014.04.026.

(226) Karandish, F.; Mamnoon, B.; Feng, L.; Haldar, M. K.; Xia, L.; Gange, K. N.; You, S.; Choi, Y.; Sarkar, K.; Mallik, S. Nucleus-Targeted, Echogenic Polymersomes for Delivering a Cancer Stemness Inhibitor to Pancreatic Cancer Cells. *Biomacromolecules* **2018**, *19* (10), 4122–4132. https://doi.org/10.1021/acs.biomac.8b01133.

(227) Meng, F.; Zhong, Z.; Feijen, J. Stimuli-Responsive Polymersomes for Programmed Drug Delivery. *Biomacromolecules* **2009**, *10* (2), 197–209. https://doi.org/10.1021/bm801127d.

(228) Thambi, T.; Park, J. H.; Lee, D. S. Stimuli-Responsive Polymersomes for Cancer Therapy. *Biomater. Sci.* **2015**, *4* (1), 55–69. https://doi.org/10.1039/C5BM00268K.
(229) Liu, J.; Huang, Y.; Kumar, A.; Tan, A.; Jin, S.; Mozhi, A.; Liang, X.-J. PH-Sensitive Nano-Systems for Drug Delivery in Cancer Therapy. *Biotechnology Advances* **2014**, *32* (4), 693–710. https://doi.org/10.1016/j.biotechadv.2013.11.009.
(230) McCarley, R. L. Redox-Responsive Delivery Systems. *Annual Rev. Anal. Chem.* **2012**, *5* (1), 391–411. https://doi.org/10.1146/annurev-anchem-062011-143157.
(231) Ding, Y.; Kang, Y.; Zhang, X. Enzyme-Responsive Polymer Assemblies Constructed through Covalent Synthesis and Supramolecular Strategy. *Chem. Commun.* **2014**, *51* (6), 996–1003. https://doi.org/10.1039/C4CC05878J.
(232) Oliveira, H.; Pérez-Andrés, E.; Thevenot, J.; Sandre, O.; Berra, E.; Lecommandoux, S. Magnetic Field Triggered Drug Release from Polymersomes for Cancer Therapeutics. *Journal of Controlled Release* **2013**, *169* (3), 165–170. https://doi.org/10.1016/j.jconrel.2013.01.013.
(233) Egli, S.; Nussbaumer, M. G.; Balasubramanian, V.; Chami, M.; Bruns, N.; Palivan, C.; Meier, W. Biocompatible Functionalization of Polymersome Surfaces: A New Approach to Surface Immobilization and Cell Targeting Using Polymersomes. *J. Am. Chem. Soc.* **2011**, *133* (12), 4476–4483. https://doi.org/10.1021/ja110275f.
(234) Lale, S. V.; Kumar, A.; Prasad, S.; Bharti, A. C.; Koul, V. Folic Acid and Trastuzumab Functionalized Redox Responsive Polymersomes for Intracellular Doxorubicin Delivery in Breast Cancer. *Biomacromolecules* **2015**, *16* (6), 1736–1752. https://doi.org/10.1021/acs.biomac.5b00244.
(235) Zhong, Y.; Meng, F.; Deng, C.; Zhong, Z. Ligand-Directed Active Tumor-Targeting Polymeric Nanoparticles for Cancer Chemotherapy. *Biomacromolecules* **2014**, *15* (6), 1955–1969. https://doi.org/10.1021/bm5003009.
(236) Akhtar, M. J.; Ahamed, M.; Alhadlaq, H. A.; Alrokayan, S. A.; Kumar, S. Targeted Anticancer Therapy: Overexpressed Receptors and Nanotechnology. *Clinica Chimica Acta* **2014**, *436*, 78–92. https://doi.org/10.1016/j.cca.2014.05.004.
(237) Elledge, R. M.; Green, S.; Pugh, R.; Allred, D. C.; Clark, G. M.; Hill, J.; Ravdin, P.; Martino, S.; Osborne, C. K. Estrogen Receptor (ER) and Progesterone Receptor (PgR), by Ligand-Binding Assay Compared with ER, PgR and PS2, by Immuno-Histochemistry in Predicting Response to Tamoxifen in Metastatic Breast Cancer: A Southwest Oncology Group Study. *International Journal of Cancer* **2000**, *89* (2), 111–117. https://doi.org/10.1002/(SICI)1097-0215(20000320)89:2<111::AID-IJC2>3.0.CO;2-W.
(238) Zhang, Z.; Maier, B.; Santen, R. J.; Song, R. X.-D. Membrane Association of Estrogen Receptor α Mediates Estrogen Effect on MAPK Activation. *Biochemical and Biophysical Research Communications* **2002**, *294* (5), 926–933. https://doi.org/10.1016/S0006-291X(02)00348-0.
(239) Yang, G.; Nowsheen, S.; Aziz, K.; Georgakilas, A. G. Toxicity and Adverse Effects of Tamoxifen and Other Anti-Estrogen Drugs. *Pharmacology & Therapeutics* **2013**, *139* (3), 392–404. https://doi.org/10.1016/j.pharmthera.2013.05.005.
(240) Chang, M. Tamoxifen Resistance in Breast Cancer. *Biomol Ther (Seoul)* **2012**, *20* (3), 256–267. https://doi.org/10.4062/biomolther.2012.20.3.256.
(241) Jain, A. S.; Goel, P. N.; Shah, S. M.; Dhawan, V. V.; Nikam, Y.; Gude, R. P.; Nagarsenker, M. S. Tamoxifen Guided Liposomes for Targeting Encapsulated Anticancer Agent to Estrogen Receptor Positive Breast Cancer Cells: In Vitro and in

Vivo Evaluation. *Biomedicine & Pharmacotherapy* **2014**, *68* (4), 429–438. https://doi.org/10.1016/j.biopha.2014.03.004.
(242) Ahmad, A.; Ali, S. M.; Ahmad, M. U.; Sheikh, S.; Ahmad, I. Orally Administered Endoxifen Is a New Therapeutic Agent for Breast Cancer. *Breast Cancer Res Treat* **2010**, *122* (2), 579–584. https://doi.org/10.1007/s10549-009-0704-7.
(243) Holmes, F. A.; Liticker, J. D. Pharmacogenomics of Tamoxifen in a Nutshell—And Who Broke the Nutcracker? *J Oncol Pract* **2005**, *1* (4), 155–159.
(244) Letchford, K.; Burt, H. A Review of the Formation and Classification of Amphiphilic Block Copolymer Nanoparticulate Structures: Micelles, Nanospheres, Nanocapsules and Polymersomes. *European Journal of Pharmaceutics and Biopharmaceutics* **2007**, *65* (3), 259–269. https://doi.org/10.1016/j.ejpb.2006.11.009.
(245) Kiyose, K.; Hanaoka, K.; Oushiki, D.; Nakamura, T.; Kajimura, M.; Suematsu, M.; Nishimatsu, H.; Yamane, T.; Terai, T.; Hirata, Y.; Nagano, T. Hypoxia-Sensitive Fluorescent Probes for in Vivo Real-Time Fluorescence Imaging of Acute Ischemia. *J. Am. Chem. Soc.* **2010**, *132* (45), 15846–15848. https://doi.org/10.1021/ja105937q.
(246) Patel, A.; Sant, S. Hypoxic Tumor Microenvironment: Opportunities to Develop Targeted Therapies. *Biotechnology Advances* **2016**, *34* (5), 803–812. https://doi.org/10.1016/j.biotechadv.2016.04.005.
(247) Perche, F.; Biswas, S.; Wang, T.; Zhu, L.; Torchilin, V. P. Hypoxia-Targeted SiRNA Delivery. *Angewandte Chemie International Edition* **2014**, *53* (13), 3362–3366. https://doi.org/10.1002/anie.201308368.
(248) Brownlee, W. J.; Seib, F. P. Impact of the Hypoxic Phenotype on the Uptake and Efflux of Nanoparticles by Human Breast Cancer Cells. *Scientific Reports* **2018**, *8* (1), 12318. https://doi.org/10.1038/s41598-018-30517-3.
(249) Neshatian, M.; Chung, S.; Yohan, D.; Yang, C.; Chithrani, D. B. Determining the Size Dependence of Colloidal Gold Nanoparticle Uptake in a Tumor-like Interface (Hypoxic). *Colloids and Interface Science Communications* **2014**, *1*, 57–61. https://doi.org/10.1016/j.colcom.2014.07.004.
(250) Stoner, M.; Saville, B.; Wormke, M.; Dean, D.; Burghardt, R.; Safe, S. Hypoxia Induces Proteasome-Dependent Degradation of Estrogen Receptor α in ZR-75 Breast Cancer Cells. *Molecular Endocrinology* **2002**, *16* (10), 2231–2242. https://doi.org/10.1210/me.2001-0347.
(251) Yan, J.; Liu, Z.; Du, S.; Li, J.; Ma, L.; Li, L. Diagnosis and Treatment of Breast Cancer in the Precision Medicine Era. *Methods Mol Biol* **2020**, *2204*, 53–61. https://doi.org/10.1007/978-1-0716-0904-0_5.
(252) Grobmyer, S. R.; Zhou, G.; Gutwein, L. G.; Iwakuma, N.; Sharma, P.; Hochwald, S. N. Nanoparticle Delivery for Metastatic Breast Cancer. *Nanomedicine: Nanotechnology, Biology and Medicine* **2012**, *8*, S21–S30. https://doi.org/10.1016/j.nano.2012.05.011.
(253) Gold, J.; Winer, E. P. Chemotherapy for Metastatic Breast Cancer. *The Breast: Comprehensive Management of Benign and Malignant Disease* **2009**, 1233–1261.
(254) Mehanna, J.; Haddad, F. G.; Eid, R.; Lambertini, M.; Kourie, H. R. Triple-Negative Breast Cancer: Current Perspective on the Evolving Therapeutic Landscape. *Int J Womens Health* **2019**, *11*, 431–437. https://doi.org/10.2147/IJWH.S178349.
(255) Dawson, S. J.; Provenzano, E.; Caldas, C. Triple Negative Breast Cancers: Clinical and Prognostic Implications. *European Journal of Cancer* **2009**, *45*, 27–40. https://doi.org/10.1016/S0959-8049(09)70013-9.

(256) Lehmann, B. D.; Bauer, J. A.; Chen, X.; Sanders, M. E.; Chakravarthy, A. B.; Shyr, Y.; Pietenpol, J. A. Identification of Human Triple-Negative Breast Cancer Subtypes and Preclinical Models for Selection of Targeted Therapies. *J Clin Invest* **2011**, *121* (7), 2750–2767. https://doi.org/10.1172/JCI45014.
(257) Lebert, J. M.; Lester, R.; Powell, E.; Seal, M.; McCarthy, J. Advances in the Systemic Treatment of Triple-Negative Breast Cancer. *Curr Oncol* **2018**, *25* (Suppl 1), S142–S150. https://doi.org/10.3747/co.25.3954.
(258) Mamnoon, B.; Feng, L.; Froberg, J.; Choi, Y.; Sathish, V.; Mallik, S. Hypoxia-Responsive, Polymeric Nanocarriers for Targeted Drug Delivery to Estrogen Receptor-Positive Breast Cancer Cell Spheroids. *Mol. Pharmaceutics* **2020**, *17* (11), 4312–4322. https://doi.org/10.1021/acs.molpharmaceut.0c00754.
(259) Gilkes, D. M.; Semenza, G. L.; Wirtz, D. Hypoxia and the Extracellular Matrix: Drivers of Tumour Metastasis. *Nat Rev Cancer* **2014**, *14* (6), 430–439. https://doi.org/10.1038/nrc3726.
(260) Hoffmann, C.; Mao, X.; Brown-Clay, J.; Moreau, F.; Absi, A. A.; Wurzer, H.; Sousa, B.; Schmitt, F.; Berchem, G.; Janji, B.; Thomas, C. Hypoxia Promotes Breast Cancer Cell Invasion through HIF-1α-Mediated up-Regulation of the Invadopodial Actin Bundling Protein CSRP2. *Sci Rep* **2018**, *8* (1), 1–14. https://doi.org/10.1038/s41598-018-28637-x.
(261) Semenza, G. L. The Hypoxic Tumor Microenvironment: A Driving Force for Breast Cancer Progression. *Biochimica et Biophysica Acta (BBA) - Molecular Cell Research* **2016**, *1863* (3), 382–391. https://doi.org/10.1016/j.bbamcr.2015.05.036.
(262) Liu, J.; Guo, X.; Luo, Z.; Zhang, J.; Li, M.; Cai, K. Hierarchically Stimuli-Responsive Nanovectors for Improved Tumor Penetration and Programed Tumor Therapy. *Nanoscale* **2018**, *10* (28), 13737–13750. https://doi.org/10.1039/C8NR02971G.
(263) Cuenca, A. G.; Jiang, H.; Hochwald, S. N.; Delano, M.; Cance, W. G.; Grobmyer, S. R. Emerging Implications of Nanotechnology on Cancer Diagnostics and Therapeutics. *Cancer* **2006**, *107* (3), 459–466. https://doi.org/10.1002/cncr.22035.
(264) Shi, J.; Kantoff, P. W.; Wooster, R.; Farokhzad, O. C. Cancer Nanomedicine: Progress, Challenges and Opportunities. *Nature Reviews Cancer* **2017**, *17* (1), 20–37. https://doi.org/10.1038/nrc.2016.108.
(265) Thambi, T.; Deepagan, V. G.; Yoon, H. Y.; Han, H. S.; Kim, S.-H.; Son, S.; Jo, D.-G.; Ahn, C.-H.; Suh, Y. D.; Kim, K.; Chan Kwon, I.; Lee, D. S.; Park, J. H. Hypoxia-Responsive Polymeric Nanoparticles for Tumor-Targeted Drug Delivery. *Biomaterials* **2014**, *35* (5), 1735–1743. https://doi.org/10.1016/j.biomaterials.2013.11.022.
(266) Kozlovskaya, V.; Liu, F.; Xue, B.; Ahmad, F.; Alford, A.; Saeed, M.; Kharlampieva, E. Polyphenolic Polymersomes of Temperature-Sensitive Poly(N-Vinylcaprolactam)-Block-Poly(N-Vinylpyrrolidone) for Anticancer Therapy. *Biomacromolecules* **2017**, *18* (8), 2552–2563. https://doi.org/10.1021/acs.biomac.7b00687.
(267) Confeld, M. I.; Mamnoon, B.; Feng, L.; Jensen-Smith, H.; Ray, P.; Froberg, J.; Kim, J.; Hollingsworth, M. A.; Quadir, M.; Choi, Y.; Mallik, S. Targeting the Tumor Core: Hypoxia-Responsive Nanoparticles for the Delivery of Chemotherapy to Pancreatic Tumors. *Mol. Pharmaceutics* **2020**, *17* (8), 2849–2863. https://doi.org/10.1021/acs.molpharmaceut.0c00247.
(268) Kulkarni, P.; Haldar, M. K.; You, S.; Choi, Y.; Mallik, S. Hypoxia-Responsive Polymersomes for Drug Delivery to Hypoxic Pancreatic Cancer Cells.

Biomacromolecules **2016**, *17* (8), 2507–2513. https://doi.org/10.1021/acs.biomac.6b00350.
(269) Golombek, S. K.; May, J.-N.; Theek, B.; Appold, L.; Drude, N.; Kiessling, F.; Lammers, T. Tumor Targeting via EPR: Strategies to Enhance Patient Responses. *Adv Drug Deliv Rev* **2018**, *130*, 17–38. https://doi.org/10.1016/j.addr.2018.07.007.
(270) Kulkarni, P.; Haldar, M. K.; Katti, P.; Dawes, C.; You, S.; Choi, Y.; Mallik, S. Hypoxia Responsive, Tumor Penetrating Lipid Nanoparticles for Delivery of Chemotherapeutics to Pancreatic Cancer Cell Spheroids. *Bioconjugate Chem.* **2016**, *27* (8), 1830–1838. https://doi.org/10.1021/acs.bioconjchem.6b00241.
(271) Niu, S.; Bremner, D. H.; Wu, J.; Wu, J.; Wang, H.; Li, H.; Qian, Q.; Zheng, H.; Zhu, L. L-Peptide Functionalized Dual-Responsive Nanoparticles for Controlled Paclitaxel Release and Enhanced Apoptosis in Breast Cancer Cells. *Drug Delivery* **2018**, *25* (1), 1275–1288. https://doi.org/10.1080/10717544.2018.1477863.
(272) Miller-Kleinhenz, J. M.; Bozeman, E. N.; Yang, L. Targeted Nanoparticles for Image-Guided Treatment of Triple Negative Breast Cancer: Clinical Significance and Technological Advances. *Wiley Interdiscip Rev Nanomed Nanobiotechnol* **2015**, *7* (6), 797–816. https://doi.org/10.1002/wnan.1343.
(273) Karandish, F.; Mamnoon, B.; Feng, L.; Haldar, M. K.; Xia, L.; Gange, K. N.; You, S.; Choi, Y.; Sarkar, K.; Mallik, S. Nucleus-Targeted, Echogenic Polymersomes for Delivering a Cancer Stemness Inhibitor to Pancreatic Cancer Cells. *Biomacromolecules* **2018**, *19* (10), 4122–4132. https://doi.org/10.1021/acs.biomac.8b01133.
(274) Guan, L.; Rizzello, L.; Battaglia, G. Polymersomes and Their Applications in Cancer Delivery and Therapy. *Nanomedicine* **2015**, *10* (17), 2757–2780. https://doi.org/10.2217/nnm.15.110.
(275) Martin, C.; Aibani, N.; Callan, J. F.; Callan, B. Recent Advances in Amphiphilic Polymers for Simultaneous Delivery of Hydrophobic and Hydrophilic Drugs. *Therapeutic Delivery* **2015**, *7* (1), 15–31. https://doi.org/10.4155/tde.15.84.
(276) Teesalu, T.; Sugahara, K. N.; Ruoslahti, E. Tumor-Penetrating Peptides. *Front Oncol* **2013**, *3*. https://doi.org/10.3389/fonc.2013.00216.
(277) Kulkarni, P.; Haldar, M. K.; Karandish, F.; Confeld, M.; Hossain, R.; Borowicz, P.; Gange, K.; Xia, L.; Sarkar, K.; Mallik, S. Tissue-Penetrating, Hypoxia-Responsive Echogenic Polymersomes For Drug Delivery To Solid Tumors. *Chemistry – A European Journal* **2018**, *24* (48), 12490–12494. https://doi.org/10.1002/chem.201802229.
(278) Sugahara, K. N.; Teesalu, T.; Karmali, P. P.; Kotamraju, V. R.; Agemy, L.; Girard, O. M.; Hanahan, D.; Mattrey, R. F.; Ruoslahti, E. Tissue-Penetrating Delivery of Compounds and Nanoparticles into Tumors. *Cancer Cell* **2009**, *16* (6), 510–520. https://doi.org/10.1016/j.ccr.2009.10.013.
(279) Krausz, A. E.; Adler, B. L.; Makdisi, J.; Schairer, D.; Rosen, J.; Landriscina, A.; Navati, M.; Alfieri, A.; Friedman, J. M.; Nosanchuk, J. D.; Rodriguez-Gabin, A.; Ye, K. Q.; McDaid, H. M.; Friedman, A. J. Nanoparticle-Encapsulated Doxorubicin Demonstrates Superior Tumor Cell Kill in Triple Negative Breast Cancer Subtypes Intrinsically Resistant to Doxorubicin. *Precis Nanomed* **2018**, *1* (3), 173–182. https://doi.org/10.33218/prnano1(3).181029.1.
(280) Gref, R.; Minamitake, Y.; Peracchia, M. T.; Trubetskoy, V.; Torchilin, V.; Langer, R. Biodegradable Long-Circulating Polymeric Nanospheres. *Science* **1994**, *263* (5153), 1600–1603. https://doi.org/10.1126/science.8128245.

(281) Anajafi, T.; Yu, J.; Sedigh, A.; Haldar, M. K.; Muhonen, W. W.; Oberlander, S.; Wasness, H.; Froberg, J.; Molla, M. S.; Katti, K. S.; Choi, Y.; Shabb, J. B.; Srivastava, D. K.; Mallik, S. Nuclear Localizing Peptide-Conjugated, Redox-Sensitive Polymersomes for Delivering Curcumin and Doxorubicin to Pancreatic Cancer Microtumors. *Mol. Pharmaceutics* **2017**, *14* (6), 1916–1928. https://doi.org/10.1021/acs.molpharmaceut.7b00014.

(282) Du, Y.; Chen, W.; Zheng, M.; Meng, F.; Zhong, Z. PH-Sensitive Degradable Chimaeric Polymersomes for the Intracellular Release of Doxorubicin Hydrochloride. *Biomaterials* **2012**, *33* (29), 7291–7299. https://doi.org/10.1016/j.biomaterials.2012.06.034.

(283) Krishnamachary, B.; Penet, M.-F.; Nimmagadda, S.; Mironchik, Y.; Raman, V.; Solaiyappan, M.; Semenza, G. L.; Pomper, M. G.; Bhujwalla, Z. M. Hypoxia Regulates CD44 and Its Variant Isoforms through HIF-1α in Triple Negative Breast Cancer. *PLOS ONE* **2012**, *7* (8), e44078. https://doi.org/10.1371/journal.pone.0044078.

(284) Liu, X.; Jiang, J.; Ji, Y.; Lu, J.; Chan, R.; Meng, H. Targeted Drug Delivery Using IRGD Peptide for Solid Cancer Treatment. *Mol. Syst. Des. Eng.* **2017**, *2* (4), 370–379. https://doi.org/10.1039/C7ME00050B.

(285) Patel, A.; Sant, S. Hypoxic Tumor Microenvironment: Opportunities to Develop Targeted Therapies. *Biotechnology Advances* **2016**, *34* (5), 803–812. https://doi.org/10.1016/j.biotechadv.2016.04.005.

(286) Confeld, M. I.; Mamnoon, B.; Feng, L.; Jensen-Smith, H.; Ray, P.; Froberg, J.; Kim, J.; Hollingsworth, M. A.; Quadir, M.; Choi, Y.; Mallik, S. Targeting the Tumor Core: Hypoxia-Responsive Nanoparticles for Delivery of Chemotherapy to Pancreatic Tumors. *Mol. Pharmaceutics* **2020**. https://doi.org/10.1021/acs.molpharmaceut.0c00247.

(287) Mamnoon, B.; Feng, L.; Froberg, J.; Choi, Y.; Sathish, V.; Mallik, S. Hypoxia-Responsive, Polymeric Nanocarriers for Targeted Drug Delivery to Estrogen Receptor-Positive Breast Cancer Cell Spheroids. *Mol. Pharmaceutics* **2020**, *17* (11), 4312–4322. https://doi.org/10.1021/acs.molpharmaceut.0c00754.

(288) Brownlee, W. J.; Seib, F. P. Impact of the Hypoxic Phenotype on the Uptake and Efflux of Nanoparticles by Human Breast Cancer Cells. *Scientific Reports* **2018**, *8* (1), 12318. https://doi.org/10.1038/s41598-018-30517-3.

(289) Cano-Cortes, M. V.; Navarro-Marchal, S. A.; Ruiz-Blas, M. P.; Diaz-Mochon, J. J.; Marchal, J. A.; Sanchez-Martin, R. M. A Versatile Theranostic Nanodevice Based on an Orthogonal Bioconjugation Strategy for Efficient Targeted Treatment and Monitoring of Triple Negative Breast Cancer. *Nanomedicine: Nanotechnology, Biology and Medicine* **2020**, *24*, 102120. https://doi.org/10.1016/j.nano.2019.102120.

(290) Dalmark, M. The Physicochemical Properties and Transmembraneous Transport of Doxorubicin. In *Anthracycline Antibiotics in Cancer Therapy: Proceedings of the International Symposium on Anthracycline Antibiotics in Cancer Therapy, New York, New York, 16–18 September 1981*; Muggia, F. M., Young, C. W., Carter, S. K., Eds.; Developments in Oncology; Springer Netherlands: Dordrecht, 1982; pp 165–172. https://doi.org/10.1007/978-94-009-7630-6_15.

(291) Kumar, R.; Roy, I.; Ohulchanskky, T. Y.; Vathy, L. A.; Bergey, E. J.; Sajjad, M.; Prasad, P. N. In Vivo Biodistribution and Clearance Studies Using Multimodal ORMOSIL Nanoparticles. *ACS Nano* **2010**, *4* (2), 699–708. https://doi.org/10.1021/nn901146y.

(292) Sánchez-Martínez, M.; da Costa Martins, R.; Quincoces, G.; Gamazo, C.; Caicedo, C.; Irache, J. M.; Peñuelas, I. [Radiolabeling and biodistribution studies of polymeric

nanoparticles as adjuvants for ocular vaccination against brucellosis]. *Rev Esp Med Nucl Imagen Mol* **2013**, *32* (2), 92–97. https://doi.org/10.1016/j.remn.2012.11.005.
(293) Arms, L.; Smith, D. W.; Flynn, J.; Palmer, W.; Martin, A.; Woldu, A.; Hua, S. Advantages and Limitations of Current Techniques for Analyzing the Biodistribution of Nanoparticles. *Front. Pharmacol.* **2018**, *9*. https://doi.org/10.3389/fphar.2018.00802.
(294) García-Negrete, C. A.; Haro, M. C. J. de; Blasco, J.; Soto, M.; Fernández, A. STEM-in-SEM High Resolution Imaging of Gold Nanoparticles and Bivalve Tissues in Bioaccumulation Experiments. *Analyst* **2015**, *140* (9), 3082–3089. https://doi.org/10.1039/C4AN01643B.
(295) Kempen, P. J.; Thakor, A. S.; Zavaleta, C.; Gambhir, S. S.; Sinclair, R. A Scanning Transmission Electron Microscopy Approach to Analyzing Large Volumes of Tissue to Detect Nanoparticles. *Microscopy and Microanalysis* **2013**, *19* (5), 1290–1297. https://doi.org/10.1017/S143192761300192X.
(296) Zhang, P.; Yang, H.; Shen, W.; Liu, W.; Chen, L.; Xiao, C. Hypoxia-Responsive Polypeptide Nanoparticles Loaded with Doxorubicin for Breast Cancer Therapy. *ACS Biomater. Sci. Eng.* **2020**, *6* (4), 2167–2174. https://doi.org/10.1021/acsbiomaterials.0c00125.
(297) Choi, H. S.; Liu, W.; Misra, P.; Tanaka, E.; Zimmer, J. P.; Ipe, B. I.; Bawendi, M. G.; Frangioni, J. V. Renal Clearance of Nanoparticles. *Nat Biotechnol* **2007**, *25* (10), 1165–1170. https://doi.org/10.1038/nbt1340.
(298) Liu, D.; Mori, A.; Huang, L. Role of Liposome Size and RES Blockade in Controlling Biodistribution and Tumor Uptake of GM1-Containing Liposomes. *Biochimica et Biophysica Acta (BBA) - Biomembranes* **1992**, *1104* (1), 95–101. https://doi.org/10.1016/0005-2736(92)90136-A.
(299) Hobbs, S. K.; Monsky, W. L.; Yuan, F.; Roberts, W. G.; Griffith, L.; Torchilin, V. P.; Jain, R. K. Regulation of Transport Pathways in Tumor Vessels: Role of Tumor Type and Microenvironment. *PNAS* **1998**, *95* (8), 4607–4612. https://doi.org/10.1073/pnas.95.8.4607.

APPENDIX A. SUPPORTING INFORMATION FOR CHAPTER 2

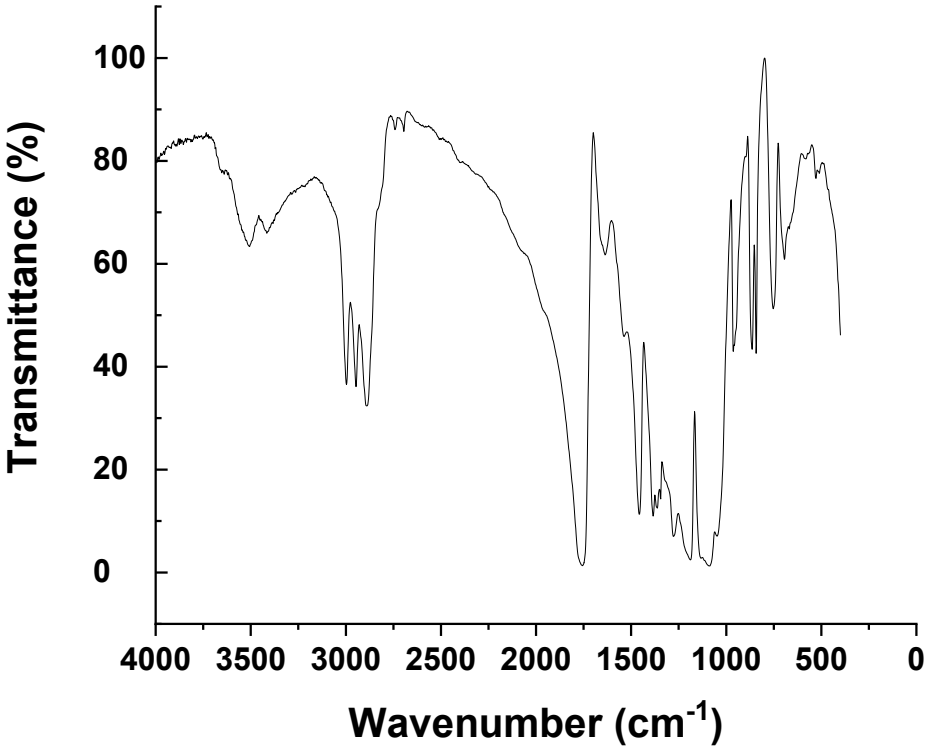

Figure A1. Infrared spectrum of PLA8500–diazobenzene–PEG2000.

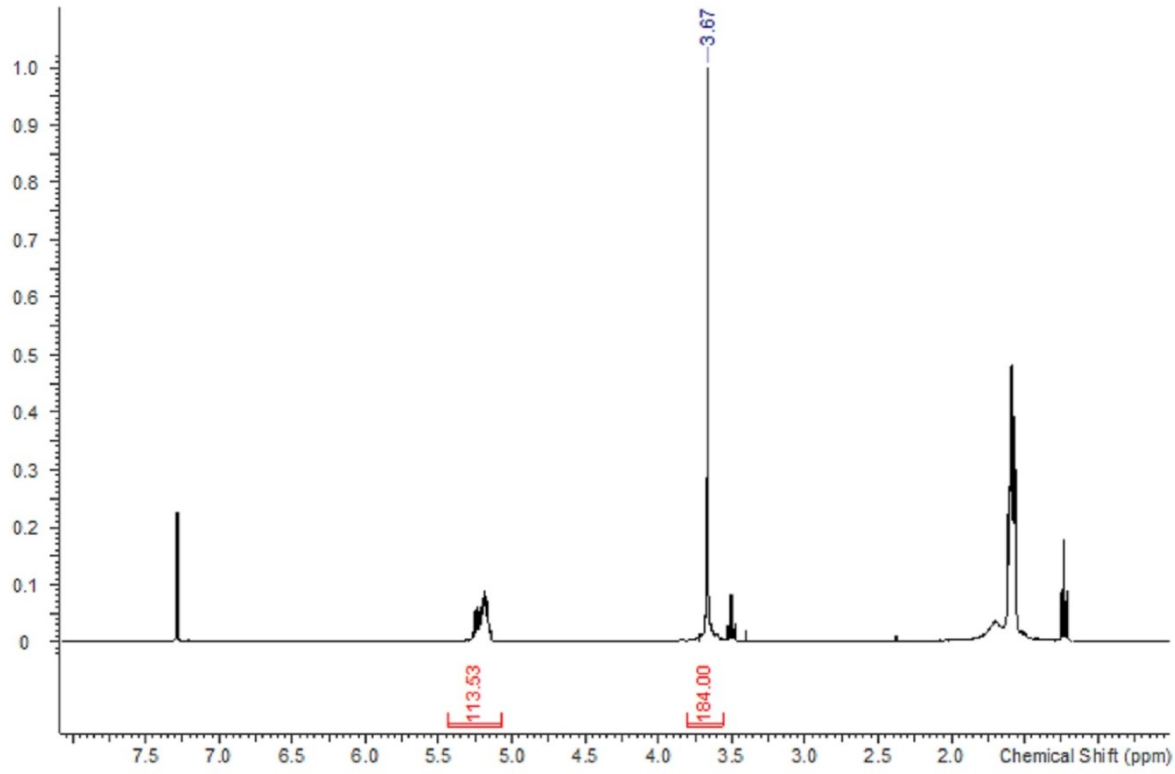

Figure A2. ^{1}H NMR spectrum (CDCl3) of the hypoxia-responsive polymer PLA8500–diazobenzene–PEG2000

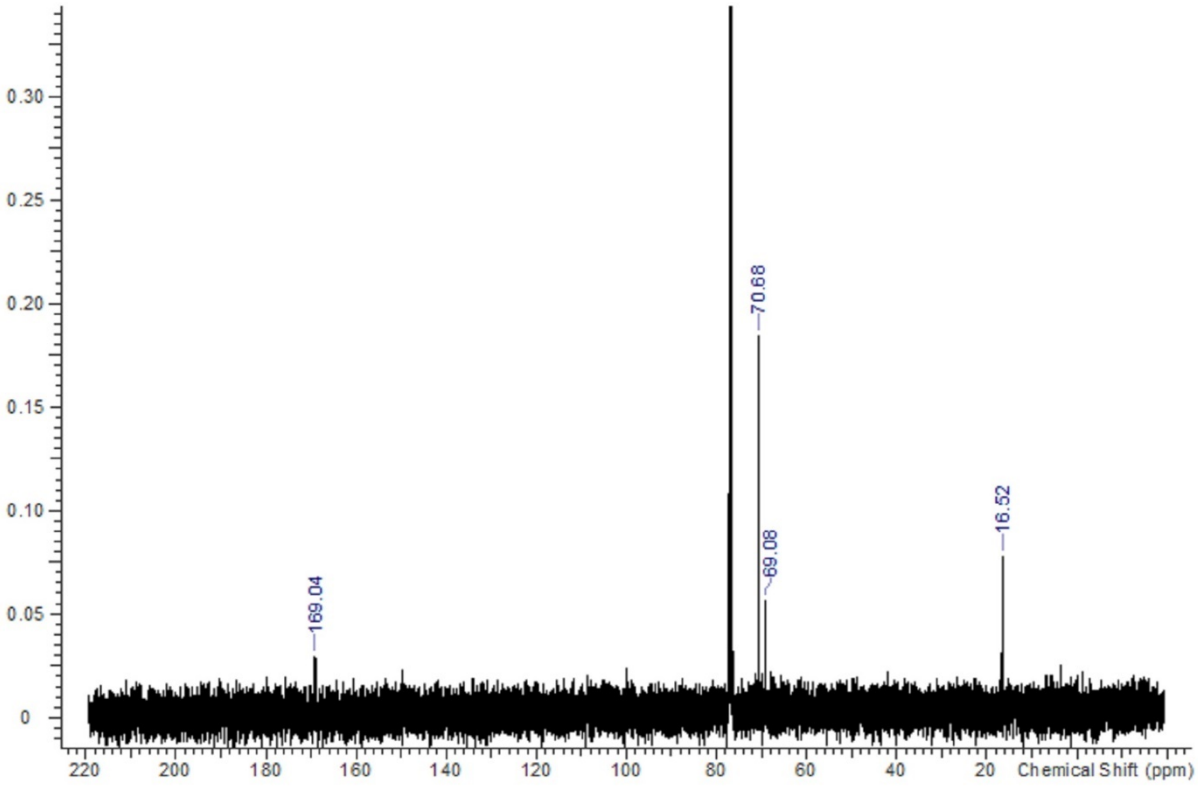

Figure A3. ^{13}C NMR (CDCl3) of the hypoxia-responsive polymer PLA8500–azobenzene–PEG2000

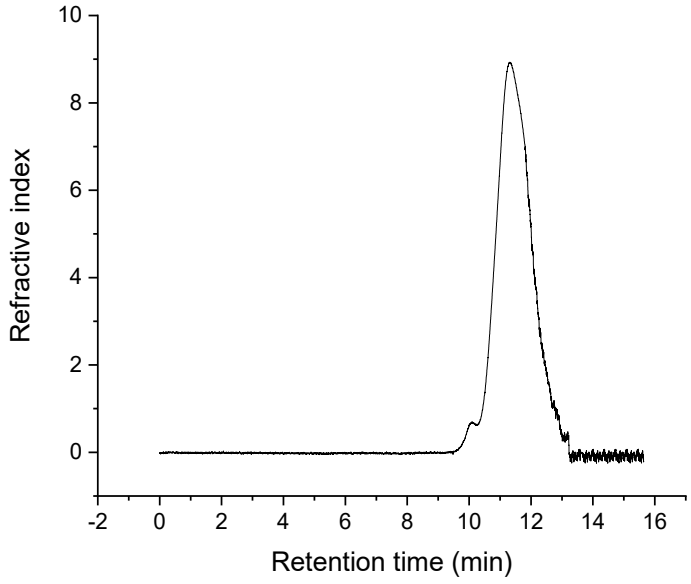

Figure A4. GPC in THF of the hypoxia-responsive polymer PLA8500–diazobenzene–PEG2000

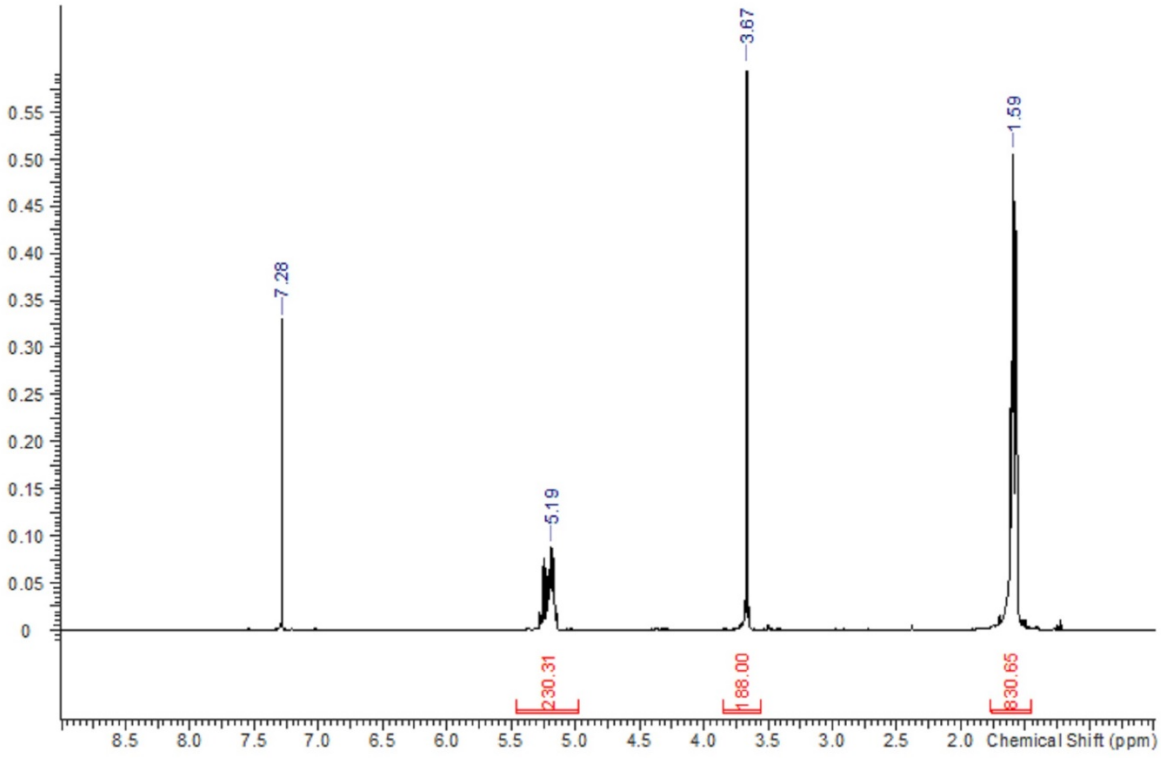

Figure A5. ^{1}H NMR spectrum (CDCl3) of the polymer PLA17000–PEG2000-N3

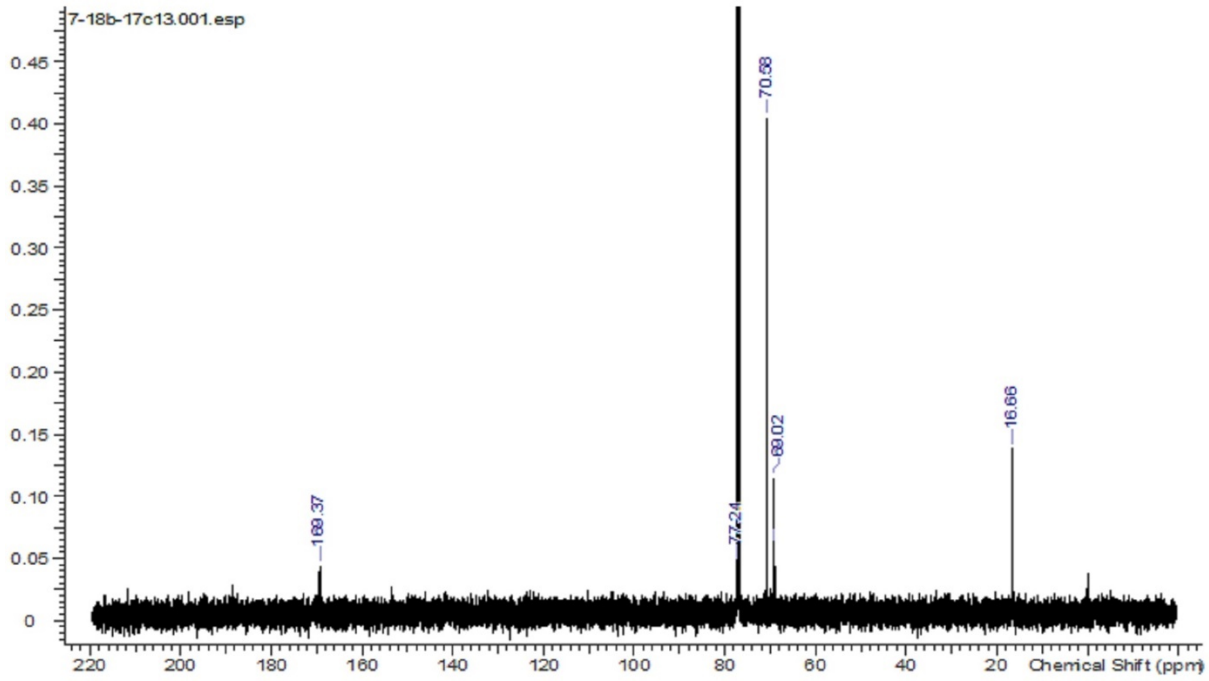

Figure A6. ^{13}C NMR spectrum (CDCl3) of the polymer PLA17000–PEG2000-N3

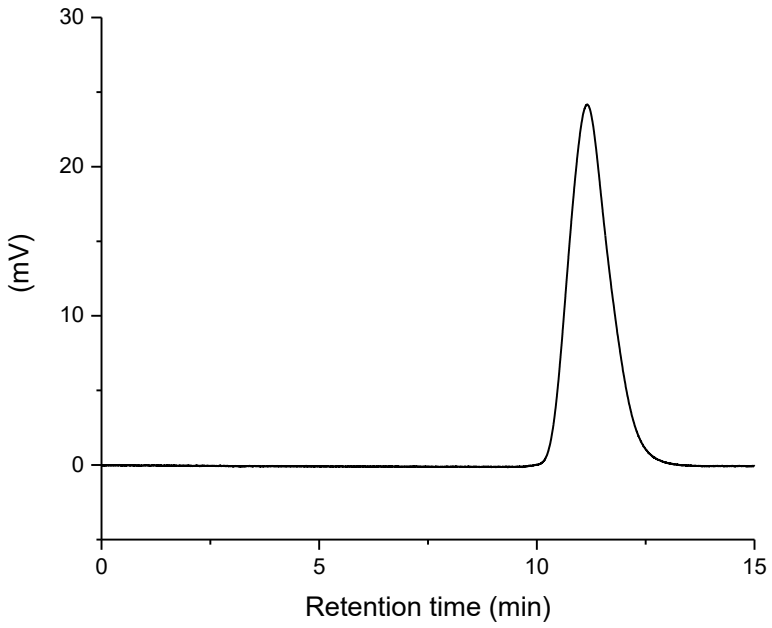

Figure A7. GPC in THF of the polymer PLA17000–PEG2000-Estradiol

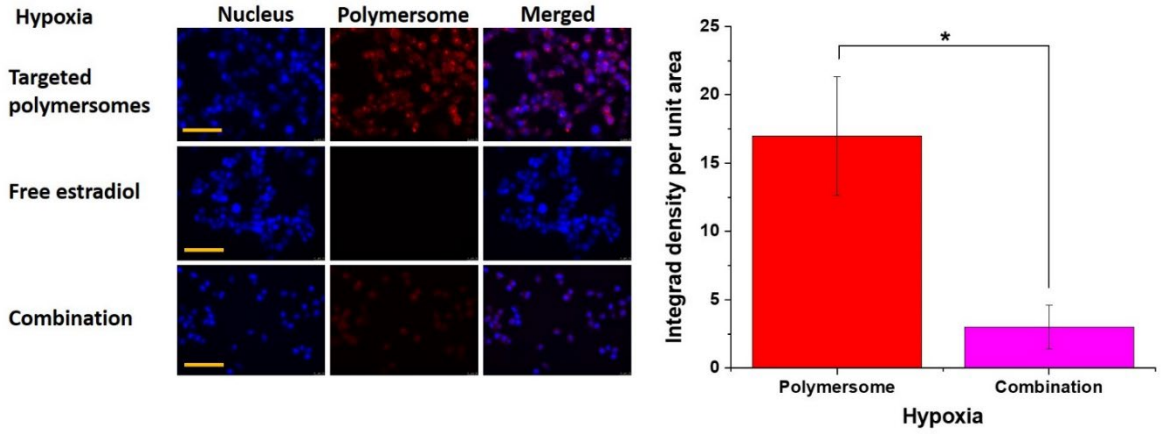

Figure A8. Fluorescence microscopic images and integral density of cellular uptake using targeted poymersomes, free estradiol, and the combination of targeted polymersomes and free estradiol under hypoxia

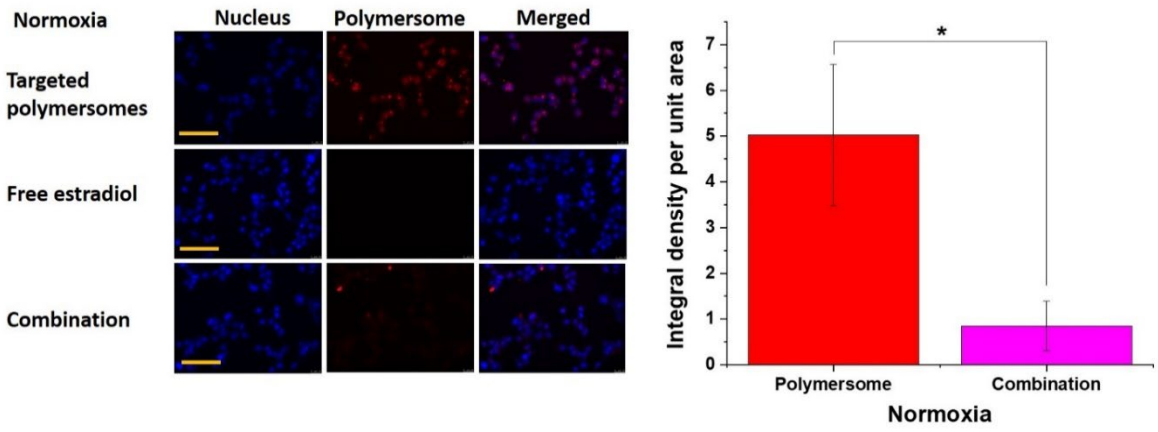

Figure A9. Fluorescence microscopic images and integral density of cellular uptake using targeted poymersomes, free estradiol, and the combination of targeted polymersomes and free estradiol under normoxia

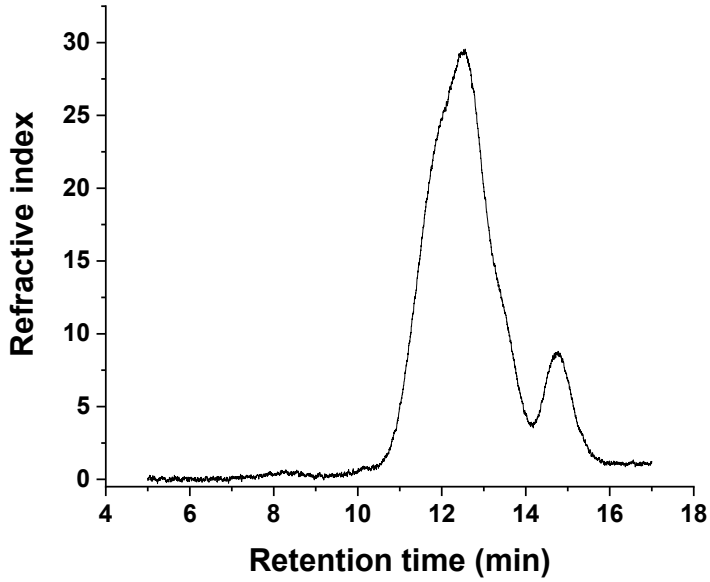

Figure A10. GPC in THF of the polymer PLA8500–azobenzene-PEG2000 before exposure to hypoxia

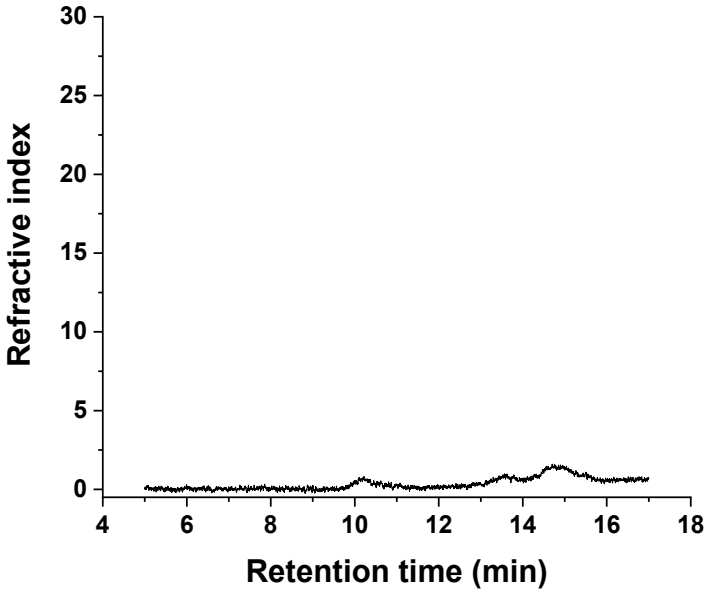

Figure A11. GPC in THF of the polymer PLA8500–azobenzene-PEG2000 after exposure to hypoxia

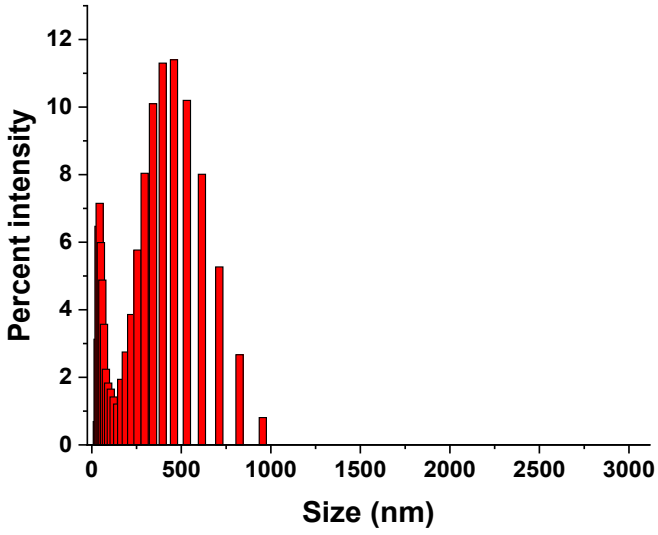

Figure A12. Hydrodynamic diameter of non-targeted polymersomes in hypoxia

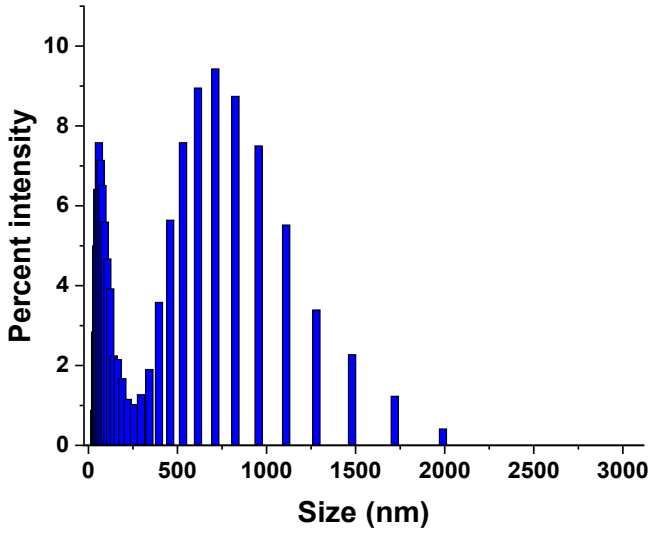

Figure A13. Hydrodynamic diameter of targeted E_2-polymersomes in hypoxia

APPENDIX B. SUPPORTING INFORMATION FOR CHAPTER 3

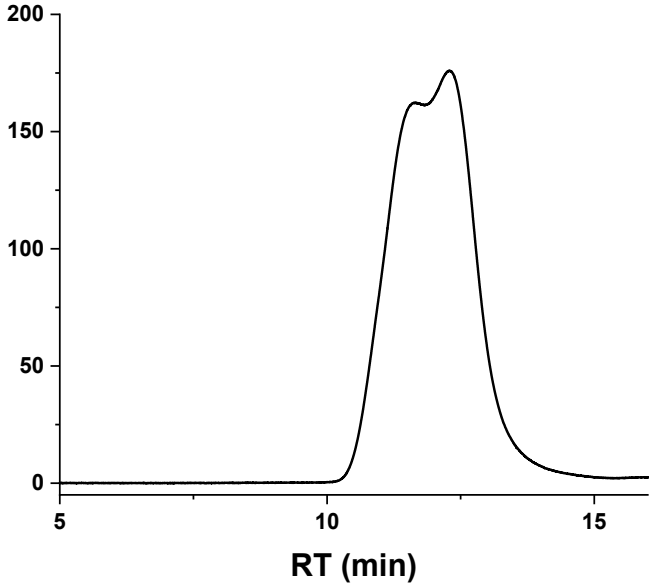

Peak 1; Mn = 16,640, Mw = 17,900, PDI = 1.076
Peak 2; Mn = 7,078, Mw = 7,802, PDI = 1.102

Figure B1. GPC in THF of the polymer PLA17000–PEG2000-Endoxifen

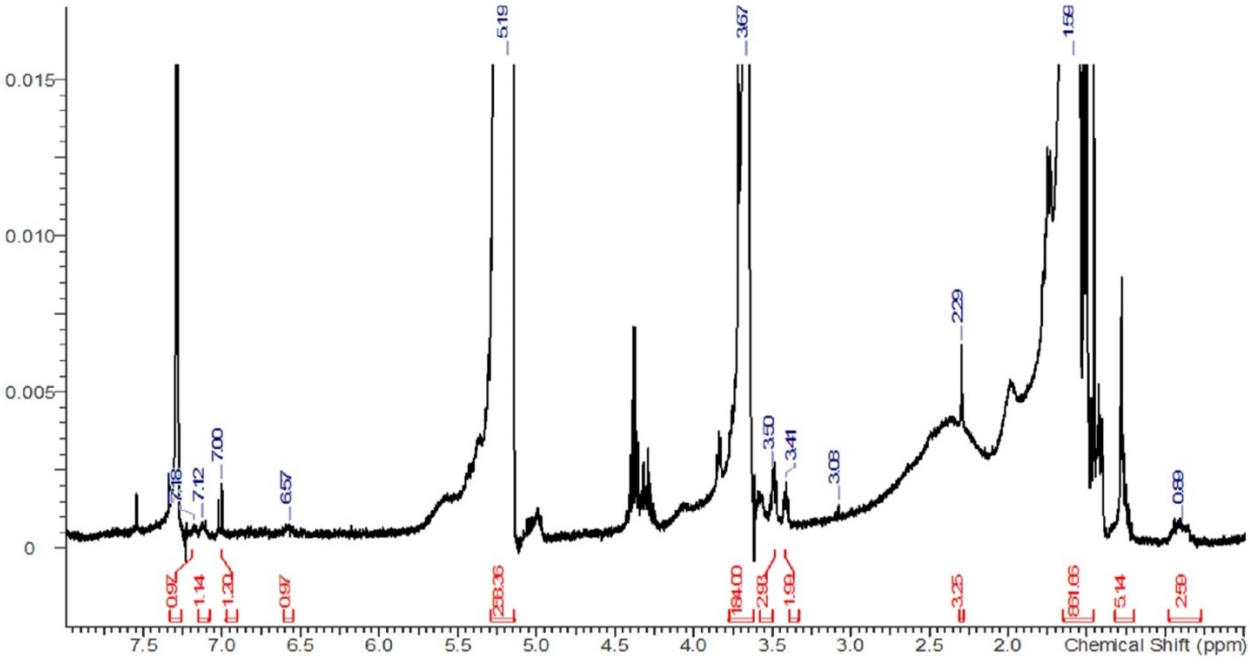

Figure B2. ^{1}H NMR spectrum (CDCl3) of the polymer PLA17000-PEG2000-Endoxifen

APPENDIX C. SUPPORTING INFORMATION FOR CHAPTER 4

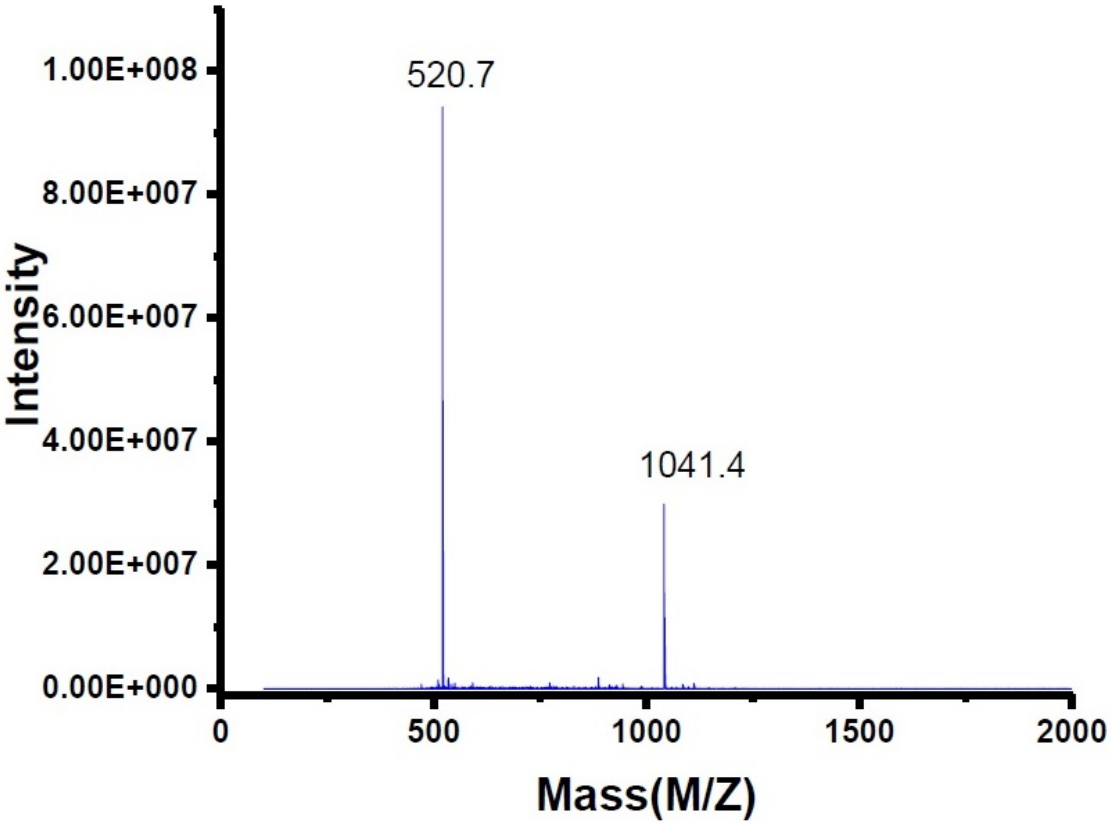

Figure C1. MALDI-TOF mass spectrum of the synthesized iRGD peptide

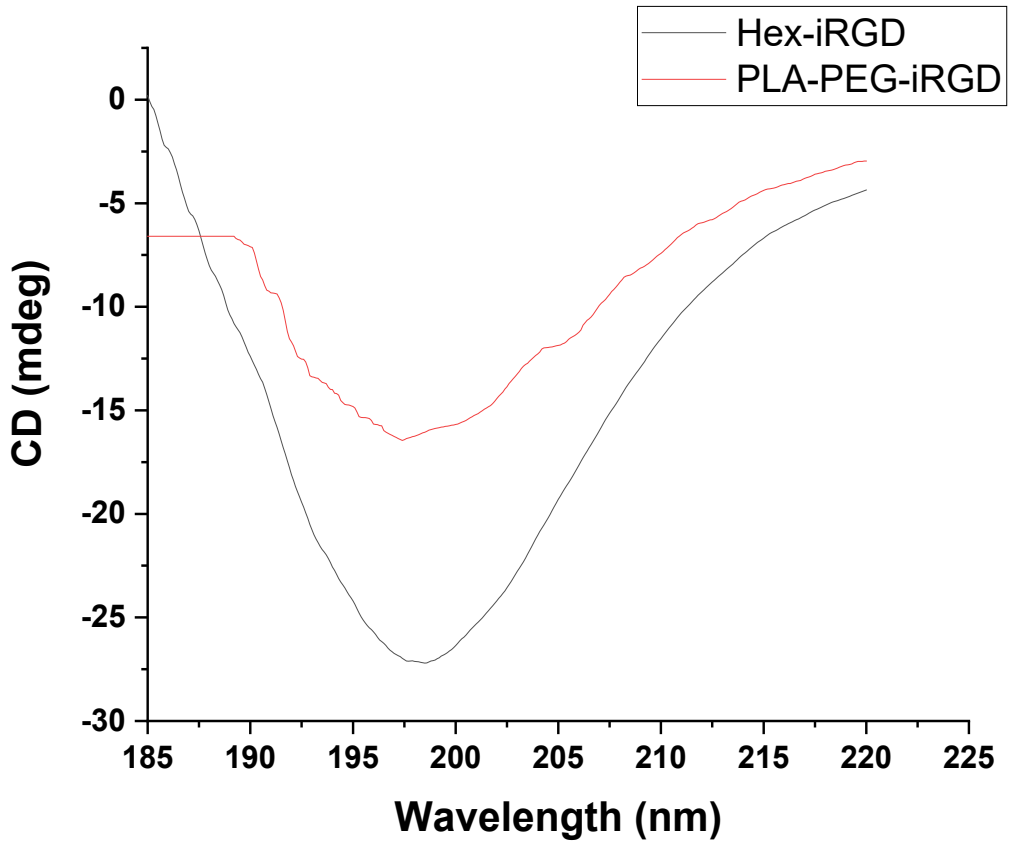

Figure C2. Circular dichroism (CD) spectrum of the synthesized iRGD peptide

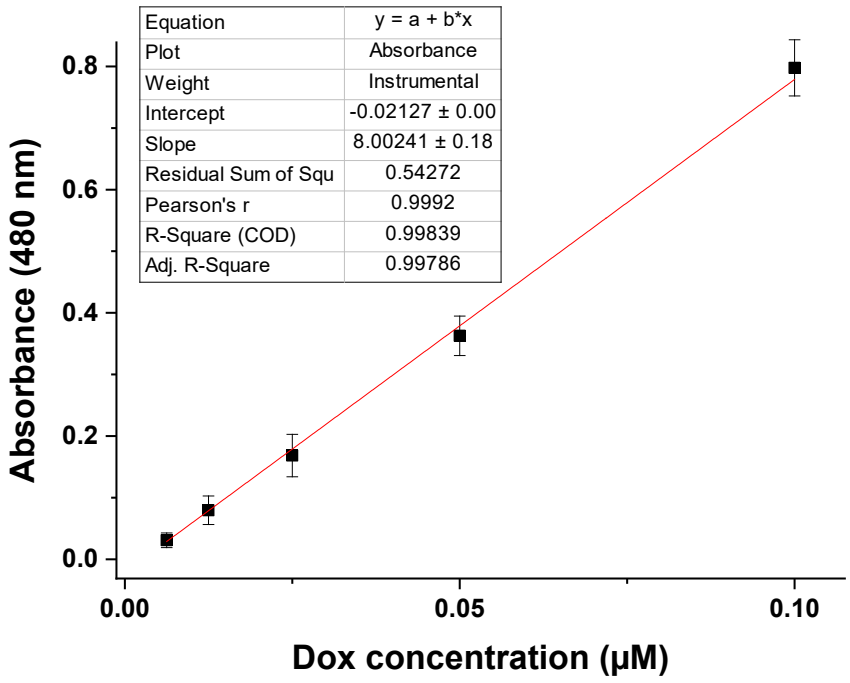

Figure C3. Calibration curve of doxorubicin hydrochloride solution

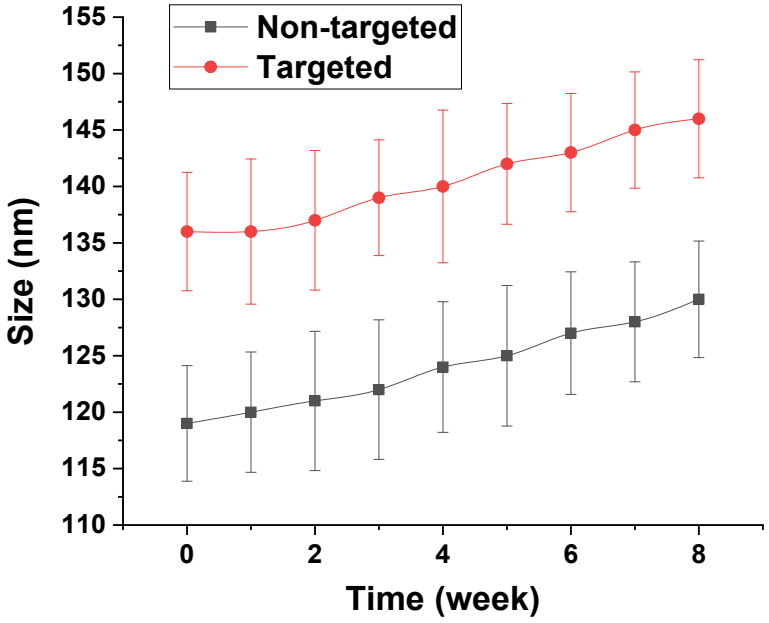

Figure C4. Polymersome stability at 4 °C

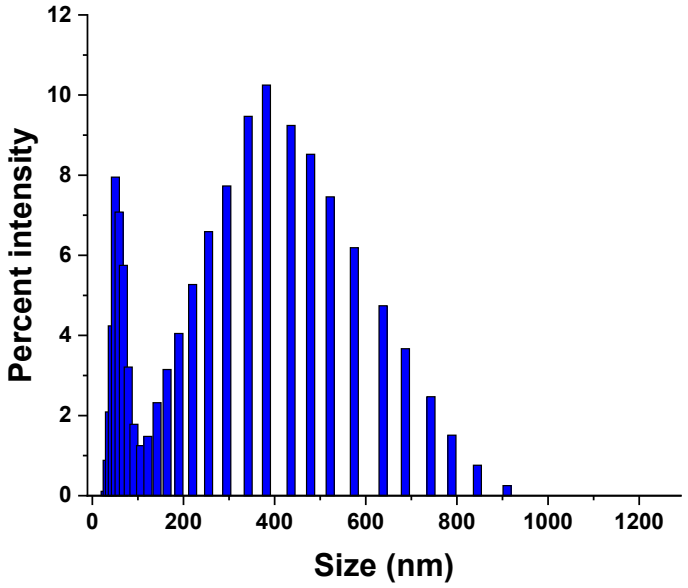

Figure C5. Hydrodynamic diameter of non-targeted polymersomes in hypoxia

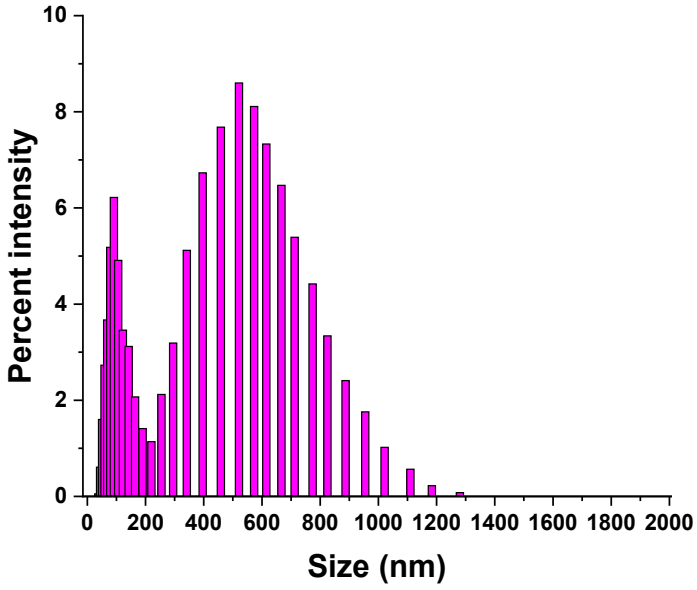

Figure C6. Hydrodynamic diameter of targeted polymersomes in hypoxia